Thiacalix[4]arene macrocycles as versatile building blocks for the rational design of high-nuclearity metallic clusters, metallamacrocycles, porous coordination cages and containers

Ivan Khariushin, Véronique Bulach, Svetlana Solovieva, Igor Antipin, Alexander Ovsyannikov, Sylvie Ferlay

Thiacalix[4]arene macrocycles as versatile building blocks for the rational design of high-nuclearity metallic clusters, metallamacrocycles, porous coordination cages and containers

Ivan V. Khariushin,[a] Véronique Bulach,[a] Svetlana E. Solovieva,[b] Igor S. Antipin,[b] Alexander S. Ovsyannikov,[c] and Sylvie Ferlay[a*]

[a] Université de Strasbourg, CNRS, CMC UMR 7140, F-67000 Strasbourg, France,
[b] Kazan Federal University, Kremlevskaya str. 18, Kazan 420008, Russian Federation
[c] A. E. Arbuzov Institute of Organic and Physical Chemistry, FRC Kazan Scientific Centre, Russian Academy of Sciences, Arbuzova 8 str., 420088 Kazan, Russian Federation
email: ferlay@unistra.fr

Abstract

The preparation and rational design of nanosized clusters (M_n) and cages based on the macrocyclic thiacalix[4]arene backbone in *cone* conformation has been analysed in the presence/absence of O and N donor atoms of different additional ligands. The coordination abilities of this class of macrocyclic ligands is reviewed leading to supramolecular species like: (1) metallic (Ag, Au) core Nanoparticles decorated with an organic thiacalix[4]arene derivatives shell; (2) different types of high nuclearity clusters (up to M_{32}); (3) metallamacrocycles (up to M_{30}); (4) the formation of pocket-like (M_6 or M_8) or square-like species (M_{16}) presenting internal and external porosity (5) the formation of octahedral cages involving 8 or 12 external ligands paving the faces or edges of the octahedron (6) species of higher nuclearity (up to M_{72}). For the pocket-like, square-like and octahedral species, their formation has been rationalized by the use of judiciously chosen organic ligands, as shown by the systematic analysis. A special attention has been drawn to the structure/properties relationships of these finite species: magnetic, luminescence, gas sorption, molecular recognition and catalytic properties. Perspectives and future challenges in this emerging field are also discussed.

Keywords: ThiaCalix[4]Arene; TetraSulfonylThiaCalix[4]Arene; TetraMercaptoThiaCalix[4]Arene; Clusters; Coordination Cages; Metal Organic Polyhedra; Metallamacrocycles; Properties.

1. INTRODUCTION: Thiacalix[4]arene and different metallic clusters

1.1 The nanoworld of clusters and cages

The term "metallic clusters" relates to a concentration of metallic atoms in a minimum of space, at the nanometric level. In the field of supramolecular chemistry [1], one can cite the metallic nanoclusters [2] and some of them present a purely metallic core (metallic Nanoparticles), involving metal-metal interactions, "protected" by an organic shell [3]. It is illustrated by the case of Au or Ag NPs held by strong Au-Au or Ag-Ag interactions, that can behave as quantum metallic **N**ano**P**article**s** (NPs), with a size range of 1-100 nm, and present applications in the fields of medicine or materials [4]. Beside the presence of metal-metal interactions within the clusters, it is also interesting to consider the formation of μ-oxo- and/or hydroxo-bridged polyoxometallate-type compounds, because of their chemical and physical properties in nanochemistry especially [5]. Going to more sophisticated molecular species, the role of small organic linkers is crucial. These species, **M**etal **O**rganic **C**oordination cages (**MOC**s) or metal-organic polyhedra (MOPs), resulting from the molecular recognition between the active coordination species are attracting attention, due to their intriguing architectures and properties that can be tuned by a judicious choice of their constituents: metal ions or clusters and linkers [6]. This field is of particular interest, depending of the shape and electronic structure of the ligands that they are built from. The obtained species demonstrate the ability to perform efficient catalytical activity or/and high selectivity in specific guests trapping inside their cavities [7], for example.

Due to infinite possibilities to design these coordination compounds, molecular engineering offers new opportunities to develop appealing and functional species and in this review, we intend to demonstrate the diversity of the nano-sized supramolecular architectures (NPs, high nuclearity clusters and cages) that can be generated using only one type of macrocyclic ligands: **thiacalix[4]arene** derivatives.

1.2 Generalities concerning calix[4]arene family of compounds

Calix[4]arene (figure 1) is a cyclic tetrameric polyphenolic compound with an **upper rim** generally decorated by *tert*-butyl or H groups (leading to *p-tert*-butyl calix[4]arene or *p*-H-calix[4]arene) or other chemical groups, whereas the **lower rim** presents phenolic OH or thiophenolic SH groups that can also be further functionalised. Among many macrocyclic calix[4]arene ligands already explored for coordination with metals, one can mention macrocyclic backbones such as **C**alix[4]**A**rene **(CA)**, **T**hia**C**alix[4]**A**rene **(TCA)** for which four CH_2 bridges, connecting the phenolic moieties, are replaced by four S atoms [8], and **T**etra**M**ercapto**T**hia**C**alix[4]**A**rene **(TMTCA)** where the phenoxy groups have been replaced by thioether groups [9] (Figure 1 a).

Owing to the rotation around C-C_{Ar} or S-C_{Ar} bonds, these macrocycles can adopt different conformations (*cone*, *partial cone*, *1,2-Alternate* and *1,3-Alternate* for calix[4]arene, Figure 1 b).

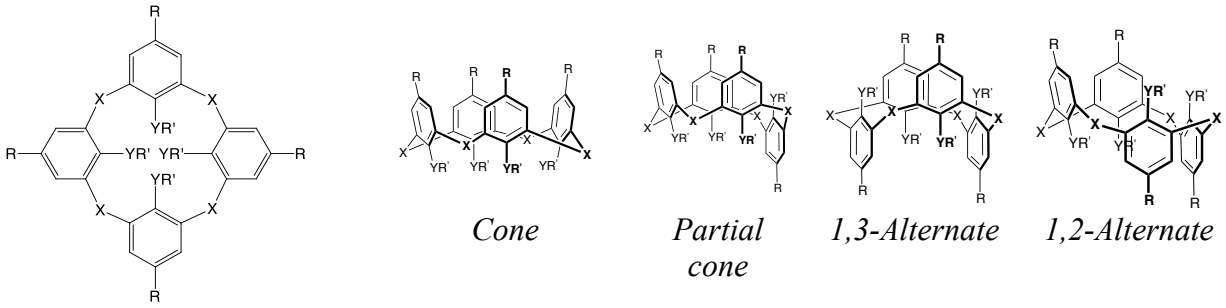

Figure 1: (a) General representation of a calix[4]arene with R=upper rim organic substituent and R'=low rim organic substituent: **C**alix[4]**A**rene, **CA** (X=CH_2, Y=O, R=*p-tert*-butyl and R'=H) and **T**hia**C**alix[4]**A**rene, **TCA**, (X=S, Y=O, R=*p-tert*-butyl and R'=H) and **T**etra**M**ercapto**T**hia**C**alix[4]**A**rene, **TMTCA** (X=S, Y=S R=*p-tert*-butyl and R'=H) and (b) the different conformations of the calix[4]arene unit.

It is interesting to note that, for the formation of discrete species discussed in this review, only the ***cone* conformation** will be considered.

Over the last decades, a huge variety of architectures using calix[4]arene and especially thiacalix[4]arene backbone have been provided, and thus, new supramolecular systems, based on the principles of molecular recognition and host-guest chemistry emerged [10, 11]. In 2006, the chemical modifications of thiacalix[4]arenes, together with the beginning of its coordination abilities were reviewed by Miyano and Iki *et al.* [12]. Thiacalix[4]arene derivatives (without metals) present the ability to easily form crystals in the solid state, which is crucial for structural investigations, and the peculiar shape of the molecules allows them to be involved in several interactions with guests in the solid state [13].

1.3 Coordination abilities of classical Calix[4]arene and Thiacalix[4]arenes

The formation of coordination compounds based on the calix[4]arene family has been discussed in the literature for *ca*. two decades, as already mentioned [12]. The possibility of anchoring up to eight or more coordinating sites by functionalization of the lower and/or upper rims of classical Calix[4]arenes, and also of varying the nature of the connecting groups between the phenolic units (-CH_2- or -S bridges) make these compounds attractive candidates to form coordination assemblies.

To illustrate this, we have reviewed in 2017 the formation of extended coordination polymers using (thia)calix[4]arene derivatives [14].

Concerning the formation of finite species, one can briefly notice the generation of complexes/clusters using less coordinating classical calix[4]arene derivatives, presenting few donor atoms around their cavities. Vanadium clusters have been reported [15], also Cu_9 [16], Mn_4 [17], Mn_5 [18], Mn_{10} [19], Ti [20], Sc [21] and concerning *4f* metals, Ln_6 (Ln = Gd, Tb, Dy and Ho) [22] or mixed 3d/4f [23] have also been described in the literature; in 2009, Brechin *et al.* reviewed the calix[4]arene coordination abilities for the formation of Single Molecules Magnets [24] and also Fuller *et al*. in 2020 [25]. In addition, an uranyl based coordination cage has also been described using carboxylate derivatives of calix[4]arene [26].

In contrast, the use of thiacalix[4]arene revealed an access to a larger variety of compounds, due to additional coordination possibilities (S and O atoms), and among them, high nuclearity clusters.

In 2007 Iki *et al.* discussed the different transition metal and lanthanide clusters and complexes based on the highly coordinating thiacalix[n]arene ligands [27], due to the presence of the coordinating sulfur atoms, and one can mention the first homometallic *3d* tetranuclear M_4 (or M_3) species ("**shuttlecock-like" species**), of different formulas $[M^{II}_4(\mu_4\text{-}X)YTCA]^{3+}$ (X = Cl, OH), $[M^{II}_4(\mu_4\text{-}H_2O)YTCA]^{4+}$ or $[M^{II}_3(\mu_4\text{-}X)YTCA]^{+}$ (X = Cl, OH), $[M^{II}_3(\mu_4\text{-}H_2O)YTCA]^{3+}$ (Y = -, D, P, SO_2, see figure 3), as shown in Figure 2, that are the basis of the building blocks of clusters and cages [28]. Higher nuclearities like M_6 [28b] or M_8 [29] thiacalix[4]arene based species have also been reported. Concerning homometallic lanthanide thiacalix[4]arene based complexes, one can mention Ln_4 [30], Ln_5 [31], Ln_8 [32] or Ln_9 [33] complexes. In addition, heterometallic low nuclearity nd/4f [34] or ns/4f [32] complexes/clusters have been also reported.

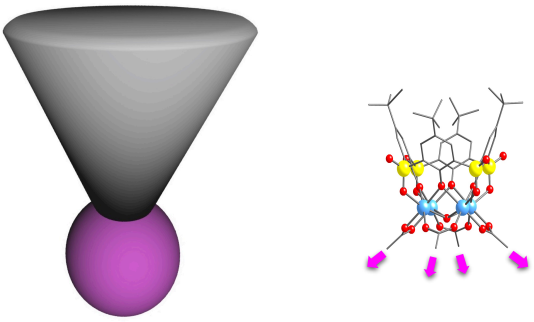

"Shuttlecock-like" building block

Figure 2: Schematic representation of the "shuttlecock-like" M_4 or M_3 species involving CA or TCA in *cone* conformation.

In this review, we will focus on coordination species formed by the thiacalix[4]arene derivatives in *cone* conformation: **H_4TCA** (*p-tert*-butylThiacalix[4]arene), **H_4DTCA** (*p*-H-Thiacalix[4]arene), **H_4PTCA** (*p*-phenylThiacalix[4]arene), **H_4SO_2TCA** (*p-tert*-butylsulfonylCalix[4]arene) and **H_4TMTCA** (TetramercaptoThiacalix[4]Arene), as shown in Figure 3. Some additional derivatives are also presented on Figure 35. These compounds have be chosen for their additional coordination abilities, compared to the one of the classical calix[4]arene, and caused by the propensity of bridging -S- or -SO_2- groups to be involved in co-coordination with metal ions.

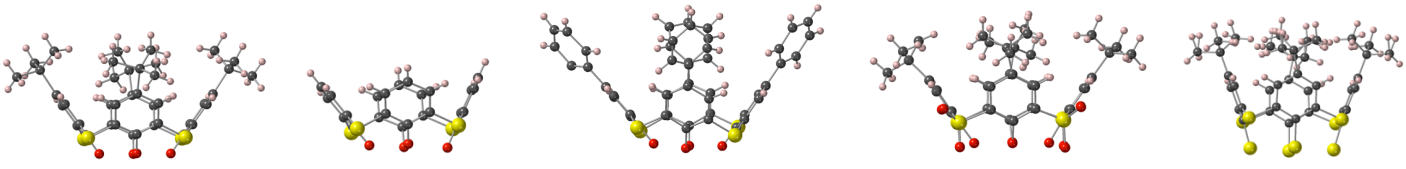

H_4TCA **H_4DTCA** **H_4PTCA** **H_4SO_2TCA** **H_4TMTCA**

Figure 3: Schematic representation of the TCA derivatives mainly used in this review (other examples will be provided in Figure 34).

We focus on the description of discrete species involving thiacalix[4]arene ligands, such as

high nuclearity metallic NPs; clusters, containing the metallic core composed of more than 10 metal ions, and porous coordination cages (MOCs) are targeted. All structures of presented compounds are established using XRD analysis on single crystal. The formula of the core only is provided in the text. For all compounds, the *3d* metals are at the oxidation state +2, while *4f* metals are in the oxidation state +3. The disordered atoms around the clusters are generally not represented. The choice for the atom colour is the following: C = grey, N = blue, O = red, S = yellow, Cl = green, Br = dark brown, Ag= black, Au = orange, Co = dark blue, Ni = green, Zn = light grey, Cr = pink, Fe = brown, Mo = violet, Mn = purple and Cu = light blue. For coordination cages the space-filling model presentation has been applied whereas the clusters are shown in polyhedral mode.

In addition, various application of such high nuclear species will be provided and gathered at the end of this review.

2. Formation of metallic NPs and high nuclearity oxo-clusters decorated with thiacalix[4]arenes

In this part, the clusters and oxoclusters containing thiacalix[4]arene, going from decorated metallic NPs, to oxo-clusters involving organic ligands, will be reviewed.

2.1. Thiacalix[4]arene decorated metallic NPs

Calix[4]arenes have been already used for the stabilization of metallic NPs [35], based on a limited number of metallic atoms, with applications in the field of catalysis for example, for gold and silver NPs. The functionalisation of NPs by organic ligands is a promising approach in order to tune the electronic surface of the NPs and thus change their properties. It has been shown that calix[4]arene macrocycles bearing phosphines [36] or thiol [37] coordinating groups, have been used for the stabilization of gold or silver NPs, leading thus to inorganic/organic core-shell NPs.

Based on these observations, H_4TCA derivatives, which presents a good affinity towards gold or silver atoms, have been used for the formation of the following clusters: Ag_{21} ($[Ag_{21}(TCA)_3(O_2PPh_2)_6]SbF_6$) [38] Ag_{35} ($[Ag_{35}(H_2TCA)_2(TCA)(C{\equiv}CBu^t)_{16}](SbF_6)_3$) [39] or isostructural Ag_{34} and $Ag_{33}Ag$ ($[Ag_{34}(TCA)_3(C{\equiv}CBu^t)_9(tfa)_4(CH_3OH)_3]SbF_6$ and $[Ag_{33}Au(TCA)_3(C{\equiv}CBu^t)_9(tfa)_4(CH_3OH)_3]SbF_6$) [40], involving the presence of ancillary alkynyl ligand or diphenylphosphonate (Figure 4 a, b, c and d respectively) have been reported. The TCA macrocycle is acting as a shell, together with other organic ligands, tuning the surface around the metallic core, held by strong Ag-Ag or Au-Au interactions (represented as dashed lines in the corresponding figures). For some of the compounds the light absorption properties have been studied (§ 6. 1. 2.). Smaller nuclearity of Thiacalix[4]arene decorated polynuclear metallic NPs have also been reported [41] and are not discussed here.

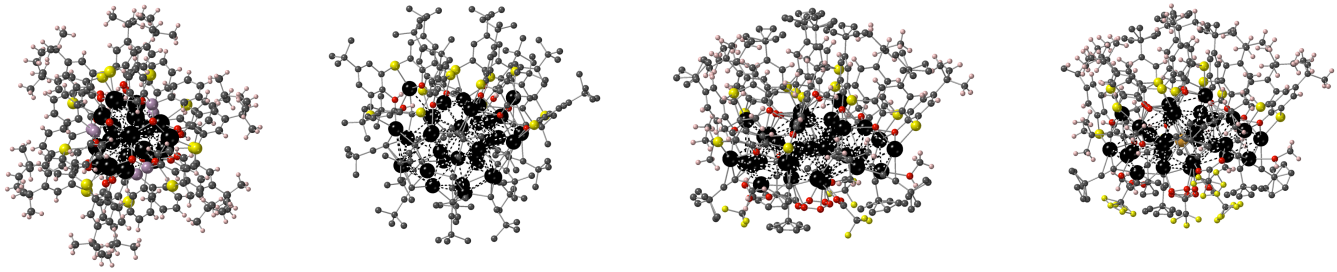

a b c d

Figure 4: A portion of the X-ray structure showing the cationic high nuclearity metallic clusters capped by calix[4]arene ligands (a) $[Ag_{21}\text{-}(TCA)_3(O_2PPh_2)_6]SbF_6$, (b) $[Ag_{35}(H_2TCA)_2(TCA)(C{\equiv}CBu^t)_{16}](SbF_6)_3$, (c) $([Ag_{34}(TCA)_3(C{\equiv}CBu^t)_9(tfa)_4(CH_3OH)_3]SbF_6$ and (d) isostructural $[Ag_{33}Au(TCA)_3(C{\equiv}CBu^t)_9(tfa)_4(CH_3OH)_3]SbF_6$. Solvent molecules are not presented for the sake of clarity. Ag-Ag or Au-Au interactions are represented as dashed lines. Adapted from Ref. [38], [39] and [40].

Using a different thiacalix[4]arene derivative, *p*-phenylthiacalix[4]arene H_4PTCA (figure 3), cationic clusters of other nuclearity, involving CrO_4^{2-} or Cl^- were obtained: Ag_{37} ($[Cl_7@Ag_{37}Na(PTCA)_5(iPrS)_{10}(DMF)_4(CH_3CN)_2]$), and Ag_{46} ($[(CrO_4)_2Cl_6@Ag_{46}(PTCA)_6(iPrS)_{12}(CH_3CN)_6]$) [42] (Figure 5a and b).

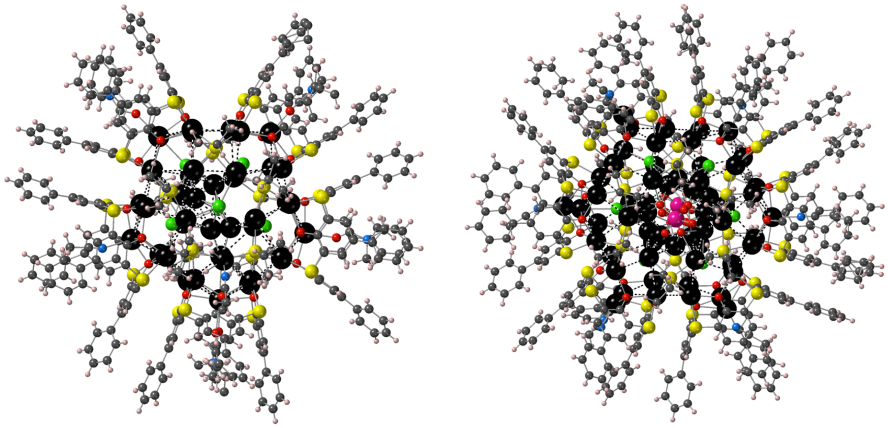

a b

Figure 5: A portion of the X-ray structure showing the cationic high nuclearity metallic clusters involving *p*-phenyl-thiacalix[4]arene ligands (a) $([Cl_7@Ag_{37}Na(PTCA)_5(iPrS)_{10}(DMF)_4(CH_3CN)_2]$, (b) $[(CrO_4)_2Cl_6@Ag_{46}(PTCA)_6(iPrS)_{12}(CH_3CN)_6]$. Ag-Ag interactions are represented as dashed lines. Solvent molecules are not presented for the sake of clarity. Adapted from Ref. [42].

The clusters are generally prepared by reduction of a $AgC{\equiv}CBu^t$ (or AgO_2PPh_2) and $AgSbF_6$ solution containing also TCA by $NaBH_4$. Their crystalline structure revealed the formation of cationic clusters capped by deprotonated TCA ligands leading to NPs, adopting a deformed shape and presenting short Ag-Ag (or Au) distances (2.76-3.37 Å).

The number of metallic species has been seriously increased with the report and structural description of cationic Ag_{88} and Ag_{155} clusters; Ag_{88} ($Ag_{88}(TCA)_8(EtS)_{32}(OAc)_8$] [43] appears as a metallic wheel protected by 8 TCA deprotonated TCA ligands and encircling CrO_4^{2-} units, and Ag_{155} ($Ag_{155}(CyS)_{40}(TCA)_5Cl_2$), that exhibits a pseudo 5-fold spherical symmetry [44] (Figure 6 a and b).

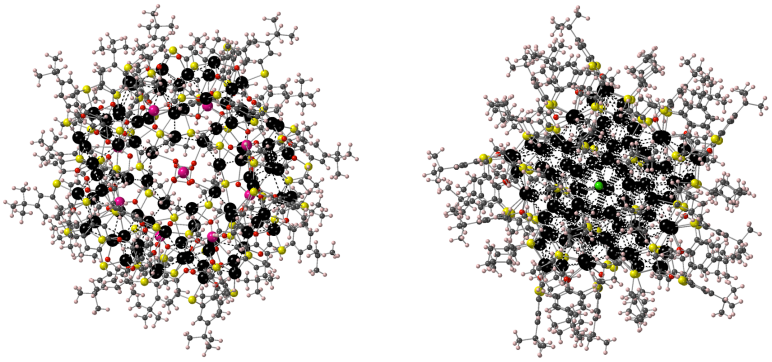

a b

Figure 6: A portion of the X-ray structure showing the large clusters capped by calix[4]arene ligands (a) CrO_4^{2-}⊂$Ag_{88}(TCA)_8(EtS)_{32}(OAc)_8$] and (b) $Ag_{155}(CyS)_{40}(TCA)_5Cl_2$. Ag-Ag interactions are represented as dashed lines. Adapted from Ref. [43] and [44].

All the reported clusters exhibit light absorption in the visible region (§ 6. 1. 2) in solution in organic solvents or in the solid state. For Ag_{21}, the catalytic activity for the reduction of 4-nitrophenol has been studied and the compound exhibits a good activity [38] (§ 6. 3. and table 3).

These data illustrate the capacity of TCA (or PTCA) to act as a protective organic shell for metallic clusters. In addition, in order to tune the nuclearity of the clusters, structuring Molybdenum oxide anions have been employed. A series of analogous silver NPs, protected with PTCA and $Mo^{VI}_2O_5^{2-}$ metalloligands were also leading to a large series of compounds presenting the following core: hexagonal $[Ag_{18}(Mo_2O_5PTCA)_6]$ or rectangular $[Ag_{18}S(Mo_2O_5(PTCA)_2)_2]$, displaying either an hexagonal or a rectangular shape (Figure 7 a and b) [45]. The compounds were obtained by the fusion of the anions with the capped macrocyclic entities.

Using the same approach and TCA, higher nuclearity were obtained: Ag_{42} species, presenting all the $[Ag_{11}(MoO_2\text{-}TCA)(EtS)_3]$ unit (Figure 7 c) [46]. The anticancer activity of these species was evaluated by the measurement of IC_{50} values. Finally an Ag_{49} unsymmetrical cage incorporating a $[Mo_6O_{22}]^{8-}$ anion, of formula $[(Mo_6O_{22})@H_3Ag_{49}(MO_3)_9(MoO_4)\text{-}(TCA)_6(iPrS)_{18}(CH_3CN)_2(H_2O)]$ unit (Figure 7 d) has been also reported, this was the basis of a polyoxometalate-templated Ag cluster protected by calix[4]arene macrocyclic ligands [47]. The compound presents a good catalytic activity towards CO_2 reduction (§ 6. 3. and table 3). Recently a $[Ag_{72}]$ molybdate protected compound has been reported [48].

For some of the compounds the light absorption properties has been studied (§ 6. 1. 2.).

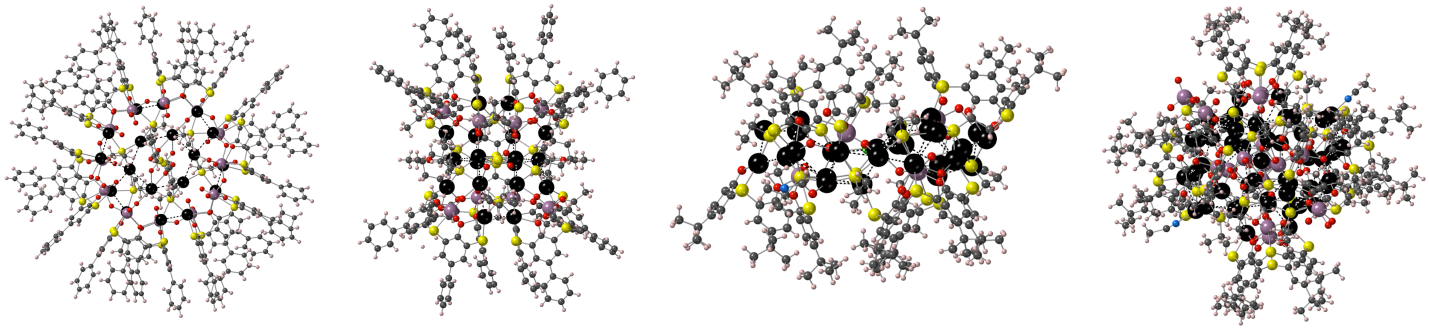

a b c d

Figure 7: A portion of the X-ray structure showing the cationic high nuclearity metallic clusters capped by calix[4]arene ligands (a) hexagonal $[Ag_{18}(Mo_2O_5PTCA)_6]$, (b) rectangular $[Ag_{18}S(Mo_2O_5(PTCA)_2)_2]$ (c) Ag_{42} build from $[Ag_{11}(MoO_2{-}TCA)(EtS)_3]$ species and (d) $[(Mo_6O_{22})@H_3Ag_{49}(MO_3)_9(MoO_4)$-$(TCA)_6(iPrS)_{18}(CH_3CN)_2(H_2O)]$. Solvent molecules are not presented for the sake of clarity. Ag-Ag interactions are represented as dashed lines. Adapted from Ref. [45], [46] and [47].

The protection of the Ag NPs involving thiacalix[4]arene derivatives has shown limitations and other metallic atoms, mostly in their divalent or trivalent oxidation state have been used for the formation of new supramolecular coordination species. The concept of protecting organic shell has been transferred to other metallic cores, like the polyoxometallates, and this will be presented in the next chapter.

2.2. Oxo (thio)-cluster decorated with Thiacalix[4]arene

This part is dedicated to the formation of high nuclearity clusters ($n \geq 10$) obtained from coordinating thiacalix[4]arene derivatives. First, we will examine the formation of homometallic clusters (*3d-4d* and *4f*) and also heterometallic species built without any linkers, only μ-oxo (O^{2-}), μ-hydroxo (OH^-) or μ-water (H_2O) bridging the metallic centres. Then the use of inorganic linkers and other small organic linkers will be investigated.

2.2.1. Homometallic nd clusters

Using the restrictions mentioned above, two types of high nuclearity clusters have been reported: Cu^I_{24} and M^{II}_{32}.

Cu^I_{24} has been obtained using the highly coordinating TMTCA derivative (figure 3) and a thiolate cluster with a unique hollow inorganic ball structure has been formed. The spherical compound of formula $[(MeCN)@TMTCACu^I_4]_6$ $\{Cu_{24}\}$ was identified as the first S-bridged TCA derivative high nuclearity cluster, built from neutral unusual $[Cu^I_4TMTCA]^{4+}$ shuttlecock-like species assembled through sulphur bridges (Figure 8 a) [49]. This is the only one available example of high nuclearity cluster using TMTCA. It exhibits interesting electrochemical properties.

Parallel to the use of TMTCA (figure 3), the use of TCA and divalent metals reproducibly leads to the formation of $\{M_{32}\}$ spherical clusters: three examples are provided in the literature: the formation of $[Co^{II}_{24}Co^{III}_8(\mu_3\text{-}O)_{24}(H_2O)_{24}(TCA)_4]$ [50], $[Ni^{II}_{32}(OH)_{40}TCA_6]$ [51] or $[M^{II}_{32}O_{16}(OH)_8(CH_3OH)_6TCA_6]$ (M = Ni, Co) [52] were reported and revealed the formation of a unique giant core-shell nanoclusters with 24 metals forming a sphere, surrounding an inner-cube formed by 8 metals (Figure 8 b, c and d).

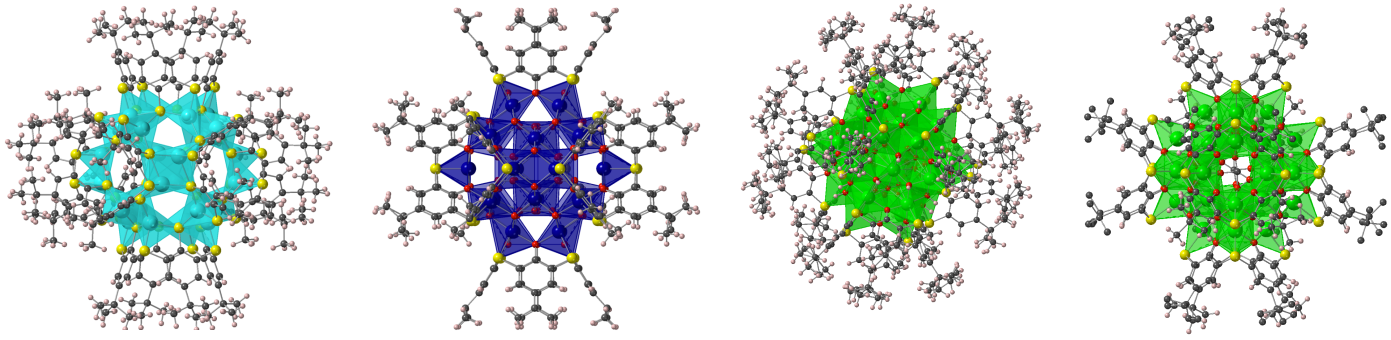

a b c d

Figure 8: A portion of the X-ray structure of high nuclearity {Cu_{24}} and {M_{32}} spherical clusters (≥ 24) involving the TCA derivatives and μ-oxo (O^{2-}), μ-hydroxo (OH^-) or μ-water (H_2O) bridging between the metallic centres (a) [(MeCN)@TMTCACu^I_4]$_6$ ({Cu_{24}}, the only TMTCA high nuclearity cluster) (b) [$Co^{II}_{24}Co^{III}_8$ (μ_3-O)$_{24}$(H_2O)$_{24}$(TCA)$_4$] ({Co_{32}}) (c) [Ni^{II}_{32}(OH)$_{40}$TCA$_6$] ({Ni_{32}}) and (d) [$M^{II}_{32}O_{16}$(OH)$_8$(CH_3OH)$_6$TCA$_6$] (M = Ni, Co) ({M_{32}}). Solvent molecules are not presented for the sake of clarity and H atoms in (d) are not all presented. Adapted from Ref. [49], [50], [51] and [52].

These reports illustrate the possibility of obtaining giant core (Oxo(-thio)-metallate)-shell (organic TCA derivatives) {M_{32}} or {M_{24}} nanoparticles. To the best of our knowledge, no analogous compounds involving *4f* metals have been reported in the literature.

Concerning the use of TCA derivatives and metal, different heterometallic clusters have been reported and that will be presented in the next chapter.

2.2.2. Heterometallic clusters

Such species are formed using TCA derivatives and small linkers.

2.2.2.a. Heterometallic 3d-4d clusters

As already seen for the decorated silver Nanoparticles, the use of structuring molybdenum oxide anions results in the formation of new structures, through the fusion of the anions with metalloligands, based on the use of thiacalix[4]arene derivatives. This will be illustrated here below. All the following reported are obtained using solvothermal synthetic conditions.

A new Co_4Mo_8 cluster of formula (NH_4)M^{II}_4(TCA)Cl[($Mo^V O_2$)$_2$S(CH_3O)]$_4$ (M = Co, Ni or Zn) has been obtained by the reaction of (NH_4)$_2MoS_2O_2$ (polythiooxomolybdate) with TCA and a metallic salt [53] (see Figure 9a). The dodecanuclear complexes exhibit high electrocatalytic activity and long-term catalytic stability for the Oxygen Evolution Reaction (OER) evolution (§ 6. 3. and table 3). By fusing other sides of the anion, sandwich-like complexes could be obtained. Two mixed valence complexes of formula [Ni^{II}_4(TCA)]$_2$[($Mo^V_5Mo^{VI}_3O_{24}$)(PO_4)] and [Ni^{II}_4(TCA)]$_2$[($Mo^V_5Mo^{VI}_3O_{24}$)(OH)(CO_3)] were reported, starting from $H_3PMo_{12}O_{40}$ (or H_2MoO_4) (Figure 9 b) [54]. The electrochemical properties as well as electrochemical sensing of the compounds were provided (§ 6. 4. and table 4) together with their electrocatalytic oxidation for glucose (§ 6. 3. and table 3). The same strategy was reported using $Na_2M^{VI}O_4$, and/or [$H_3PM_{12}O_{40}$] and two additional high nuclearity symmetrical compounds of formula [Co^{II}_{24}(TCA)$_6$($M^{VI}O_4$)$_8Cl_6$][$HPM_{12}O_{40}$] (M = Mo and W) were obtained. Their shape is close to the one reported for {M_{32}} compounds (§ 2. 3. 1.), where the role played by inner-cubes is played here by the Keggin-type anions [55], as shown in Figure 9 c. The electrochemical properties for both compounds were reported.

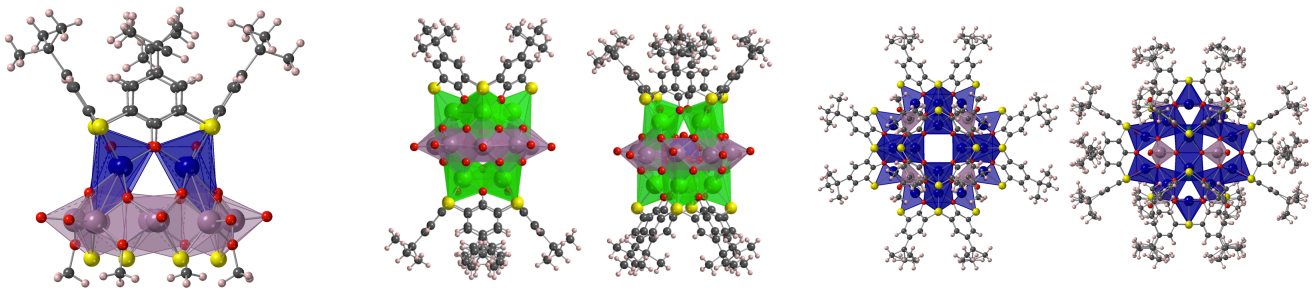

a b c

Figure 9: A portion of the X-ray structure of heterometallic 3d-4d clusters involving only TCA (a) $(NH_4)\{M_4^{II}(TCA)Cl[(Mo^{V}O_2)_2S(CH_3O)]_4\}$ (M = Co, Ni or Zn) (b) $[Ni^{II}_4(TCA)]_2[(Mo^{V}_5Mo^{VI}_3O_{24})(PO_4)]$ and $[Ni^{II}_4(TCA)]_2[(Mo^{V}_5Mo^{VI}_3O_{24})(OH)(CO_3)]$ (c) the highly symmetrical $[Co^{II}_{24}(TCA)_6(M^{VI}O_4)_8Cl_6][HPM_{12}O_{40}]$ (M = Mo and W). Solvent molecules are not presented for the sake of clarity. Mo and W atoms are represented in pale purple. Adapted from Ref. [53], [54] and [55].

2.2.2.b. Heterometallic ns-nd clusters

Complexes involving coordinated alkali cations are reported here below.

The mixture of H_4TCA in solvothermal conditions leads to the formation of different complexes, among them two $\{Mo_8Na_8\}$ complexes of formula $[Mo^{VI}_8Na_8(\mu_3\text{-}O)_{12}(\mu\text{-}O)_4\text{-}(TCA)_2(H_2TCA)_4(CH_3OH)_4]$ and $[Mo^{VI}_8Na_8(\mu_4\text{-}O)_4(\mu_3\text{-}O)_8(\mu O)_4(TCA)_2(H_2TCA)_4(CH_3OH)_5(H_2O)]$ exhibiting both an oval metallic shape with μ_3-O ligands and 6 calix[4]arene units [56] (Figure 10 a and b). The light absorption properties of these compounds were studied (§ 6. 1. 2.).

A higher nuclearity complex involving Ni(II) cations has also been described. The difference with the previous one, is that it contains a small organic linker: 1H-1,2,4-triazole-3-thiol (3-S-trz). A flying saucer-shaped compound of formula $[Ni^{II}_{18}Na_6(TCA)_6(3\text{-}S\text{-}trz)_6Cl_6(H_2O)_6]$ has been obtained in solvothermal conditions using $Ni^{II}(CH_3COO)_2$ and Na_2SO_2 as Ni and Na sources, respectively (Figure 10 c) [57]. This compound looks like a metallocycle ring, but it is not "flat", it is similar to a "truncated" Ni_{24} sphere.

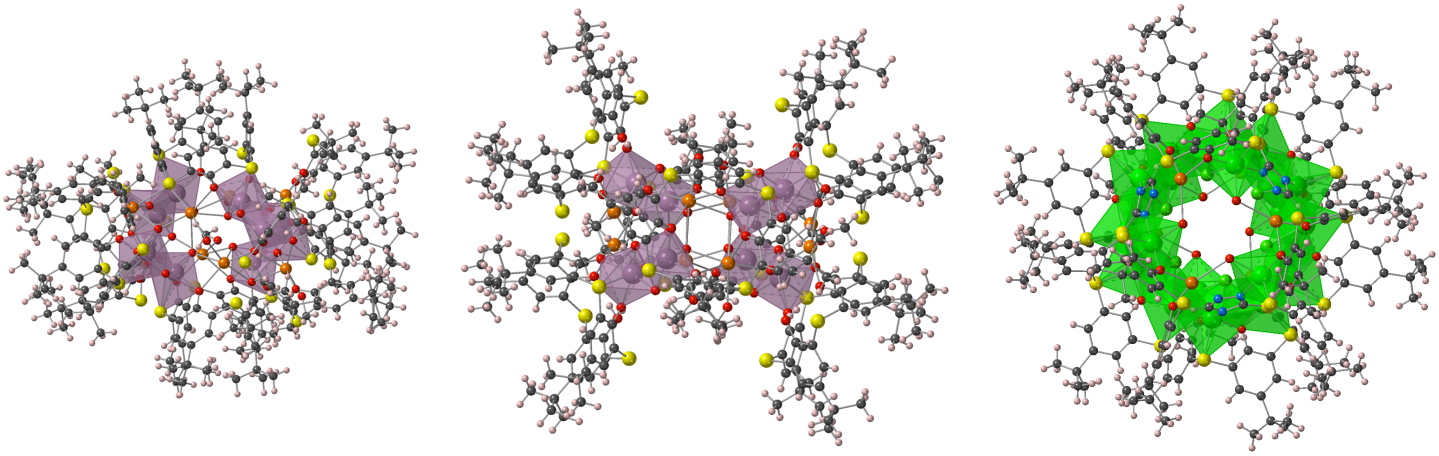

a b c

Figure 10: A portion of the X-ray structure of the heterometallic ns-nd clusters involving only TCA (a) and (b) $\{Mo_8Na_8\}$ complexes: $[Mo^{VI}_8Na_8(\mu_3\text{-}O)_{12}(\mu\text{-}O)_4\text{-}(TCA)_2(H_2TCA)_4(CH_3OH)_4]$ and $[Mo^{VI}_8Na_8(\mu_4\text{-}O)_4(\mu_3\text{-}O)_8(\mu O)_4(TCA)_2(H_2TCA)_4(CH_3OH)_5(H_2O)]$ (c) $[Ni^{II}_{18}Na_6(TCA)_6(3\text{-}S\text{-}trz)_6Cl_6(H_2O)_6]$. Solvent molecules are not presented for the sake of clarity. Mo atoms are represented in pale purple. Adapted from Ref. [56] and [57].

2.2.2.c. Heterometallic np-nd clusters

There is only one example of complex involving np metal. A complex of formula $Pb^{II}_8Ti^{IV}_7(\mu_2\text{-}O)_6(OH)6\text{-}(TCA)_6](OH)_2$ was observed using reflux heating of H_4TCA, $Pb^{II}(NO_3)_2$ and $Ti^{IV}(OiPr)_4$ [58] (Figure 11). This is a highly symmetrical cluster miming the $PbTiO_3$ extended perovskite system. It can be applied as electron-transport materials in perovskite solar cells (§ 6. 4. 1).

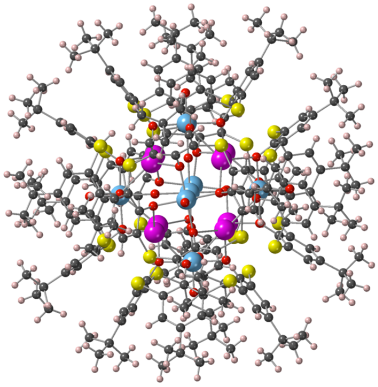

Figure 11: A portion of the X-ray structure of the heterometallic cluster of formula $Pb^{II}_8Ti^{IV}_7(\mu_2\text{-}O)_6(OH)_6\text{-}(TCA)_6](OH)_2$. Solvent molecules are not presented for the sake of clarity. Pb atoms are represented in pale blue and Ti atoms in pink. Adapted from Ref. [58].

2.2.2.d. Heterometallic ns-nd-4f clusters

Finally, to close this series of heterometallic compounds, a *3s*/*3d*/*4f* trimetallic cluster was reported, [59] mixing H_4TCA, $Ni^{II}Cl_2$, Dy^{III} $(OAc)_3$ and Na_2CO_3 in solvothermal conditions; a complex of formula $[Na_2Ni^{II}_{12}Ln^{III}_2(TCA)_3(\mu_7\text{-}CO_3)_3(\mu_3\text{-}OH)_4(\mu_3\text{-}Cl)_2\text{-}(OAc)_6(dma)_4]$ (Ln = Dy or Tb) was reported. It was based on trinary-cubane core composed of one $\{Ni_2Ln_2\}$ cubane units and two $[NaNi_2Ln]$ cubane units sharing one Ln^{III} ion, as shown in Figure 12.

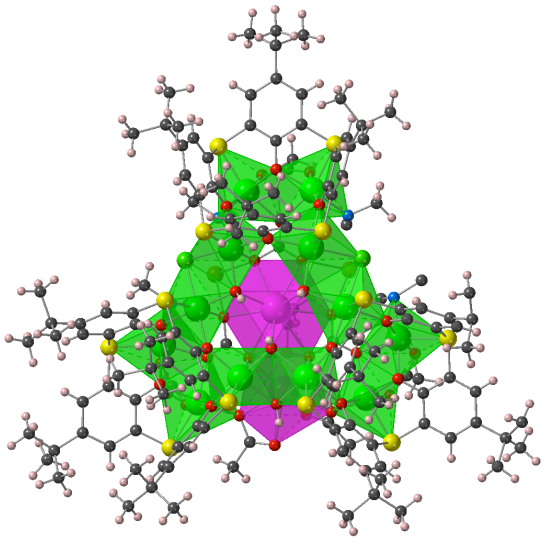

Figure 12: A portion of the X-ray structure of the $\{Ni_2Ln_2\}$ heterometallic cluster of formula $[Na_2Ni^{II}_{12}Ln^{III}_2(TCA)_3(\mu_7\text{-}CO_3)_3(\mu_3\text{-}OH)_4(\mu_3\text{-}Cl)_2\text{-}(OAc)_6(dma)_4]$ (Ln = Dy or Tb). Solvent molecules are not presented for the sake of clarity. Adapted from Ref. [59].

Another example of *ns-nd-4f* cages, involving large organic anionic linkers will be provided in the "other nuclearities" section (§ 5. 4.).

2.3. The use of H_4TCA and small inorganic linkers for the formation of homometallic clusters

The description of high nuclearity clusters will continue with the formation of clusters involving metallic linkers or small inorganic anions like CO_3^{2-} or phosphates.

2.3.1. Metallic linkers

Concerning the metallic linkers, one can mention the linking of two well-known sandwich-like tetranuclear compounds based on TCA, by two $Fe^{II}Cl_2$ units, leading to a neutral centrosymmetric decanuclear compound of formula $[Fe^{II}_{10}TCA_4Cl_4]$ (Figure 13 a) [28e]. An analogous Co_{10} compound has been observed, whereas the linker is a Cobalt azido derivative $Co^{II}(N_3)_2$, leading to a high nuclear compound of formula $[Co^{II}_{10}(TCA)_4(N_3)_4]$ [29a] (Figure 13 b). For both compounds, the routine magnetic properties were reported (§ 6. 1. 1. and table 1).

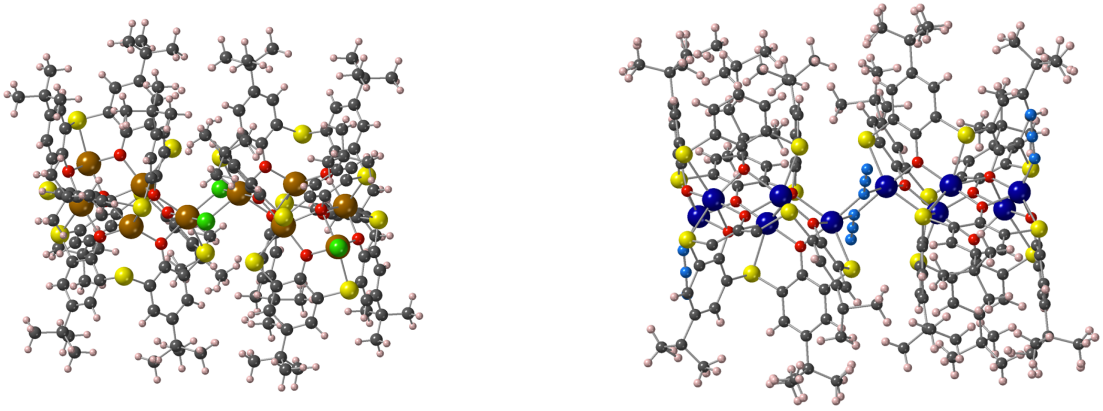

a b

Figure 13: A portion of the X-ray structure of the clusters based on TCA and metallic inorganic linkers where sandwich-like M_4 complexes are interconnected by bridging metalloligands (a) decanuclear $[Fe^{II}_{10}TCA_4Cl_4]$ and (b) $[Co^{II}_{10}(TCA)_4(N_3)_4]$. Solvent molecules are not presented for the sake of clarity. Adapted from Ref. [28e] and [29a].

2.3.2. Small carbonate or phosphate inorganic linkers

The use of small anionic carbonate or phosphate linkers for the formation of high nuclearity clusters was illustrated by the formation of high nuclearity $\{M_{24}\}$ species, that are not spherical.

The reaction of TCA with $Mn(OAc)_2$ and Na_2CO_3 in solvothermal conditions leads to the formation of a compound presenting the following core: $[Mn^{II}_{24}(TCA)_6(\mu_3\text{-}OH)_8(\mu\text{-}Cl)_3(\mu_5\text{-}CO_3)_6\text{-}(CH_3CH_2OH)_6]$ (Mn_{24}) where bridging carbonato, hydroxo and chloro are present in the cluster. In addition, coordinated ethanol was also present in the "organic shell" of the complex (Figure 14 a) [60]. The magnetic properties of this compound were analysed (§ 6. 1. 1. and table 1). Parallelly to this result, the reaction of $Cd^{II}Cl_2$ and TCA with concentrated H_3PO_4 in solvothermal conditions lead to the formation of a compound presenting the following core: $[H_2Cd^{II}_{24}(TCA)_6(PO_5)_6Cl_8(DMF)_6]$ [61]. The clusters display the shape of a flattened sphere, with 6 TCA surrounding the metal part, where the $[Cd^{II}_4Cl_3TCA]^+$ shuttlecock-like units were connected by peroxyphosphate PO_5^{3-} anions (Figure 14 b). This compound exhibits photocatalytic water splitting activities (§ 6. 3. and table 3) and also luminescent properties (§ 6. 1. 2.)

Using inorganic phosphate, other compounds were reported. For example, the combination in solvothermal conditions, of $Co^{II}(ClO_4)_2$, TCA and Hypophosphorous acid H_3PO_2 leads to the formation of a compound of formula $[Co^{II}_{20}(TCA)_5(\mu\text{-}H_2O)(\mu_3\text{-}OH)_4(HPO_4)_8]$ ($\{Co_{20}\}$) (Figure 14 c) [62], [63]. Whereas using disodium hydrogen phosphate Na_2HPO_4, a compound of formula $[Co^{II}_{24}\text{-}(TCA)_6(PO_4)_8(\mu_4\text{-}Cl)_6]$ ($\{Co_{24}\}$) was observed [63] (Figure 14 d). The $\{Co_{24}\}$ molecule present the same regular spherical shape as already

observed for other {M_{24}} species (§ 2. 3. 1.), where chlorine and phosphate anions are bridging the metal centres belonging to [$Co^{II}_4(\mu_4\text{-}Cl)TCA]^{3+}$ shuttlecock-like species. {Co_{20}} appears as a truncated octahedral {Co_{24}} compound, while cutting one face. The magnetic properties of both compounds were measured (§ 6. 1. 1. and table 1).

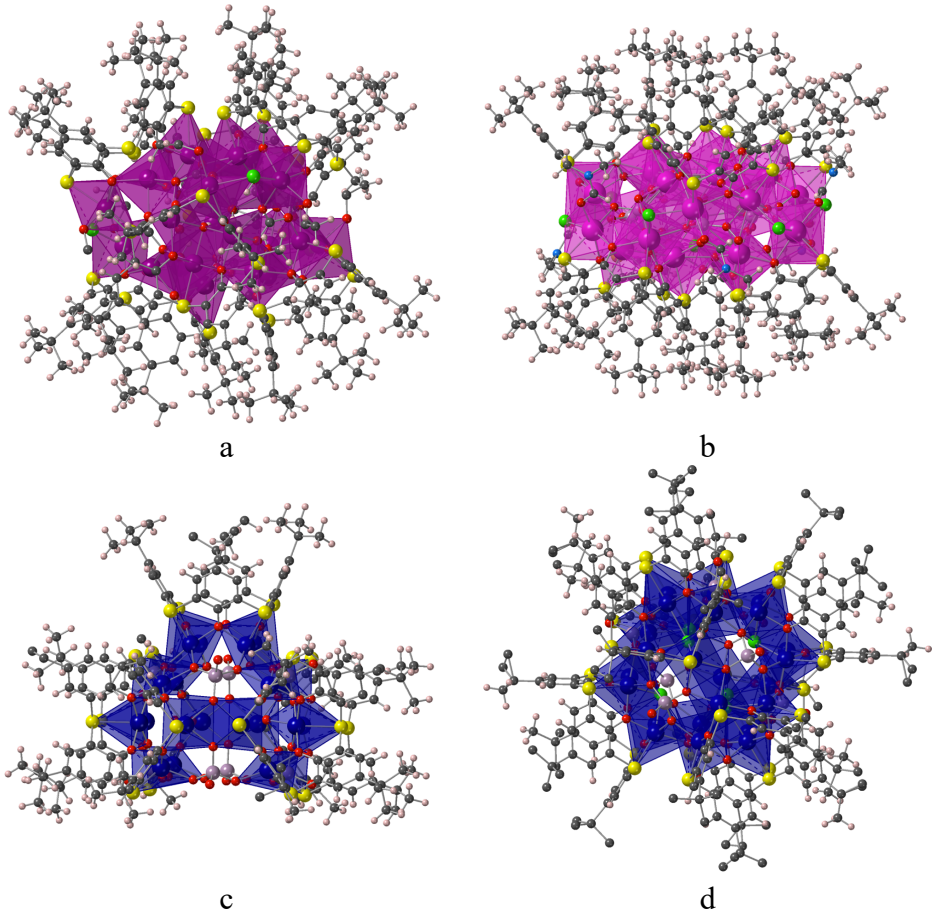

Figure 14: A portion of the X-ray structure of the {Mn_{24}}, {Cd_{24}}, {Co_{20}} and {Co_{24}} clusters based on TCA and the use of small inorganic linkers (a) [$Mn^{II}_{24}(TCA)_6(\mu_3\text{-}OH)_8(\mu\text{-}Cl)_3(\mu_5\text{-}CO_3)_6\text{-}(CH_3CH_2OH)_6$] obtained from carbonate moieties (b) [$H_2Cd^{II}_{24}(TCA)_6(PO_5)_6Cl_8(DMF)_6$], {$Cd_{24}$}, obtained using H_3PO_4 (c) [$Co^{II}_{20}(TCA)_5(\mu\text{-}H_2O)(\mu_3\text{-}OH)_4(HPO_4)_8$], obtained using H_3PO_2 and (d) spherical [$Co^{II}_{24}\text{-}(TCA)_6(PO_4)_8(\mu_4\text{-}Cl)_6$] obtained using Na_2HPO_4. H atoms in (d) and solvent molecules are not presented for the sake of clarity. Cd atoms are represented in pink. Adapted from Ref. [60], [61], [62] and [63].

2.4. More target specific and sophisticated species using a secondary small organic linker for the formation of homometallic clusters

Several secondary organic linkers have been used for the formation of high nuclearity clusters involving thiacalix[4]arene derivatives. They will be presented here below.

2.4.1. The use of H_4TCA derivatives and O donor linkers

Such linkers have been reported, especially for *3d* and *4f* metal clusters. For the reported compounds, only solvothermal conditions involving different solvents (MeOH, DMA, etc..) have been used.

2.4.1.a. The use of O donor linkers, TCA derivatives and 3d metals

Using phenylphosphonic acid, NaOH, H_4PTCA and a metal salt, two isostructural compounds of formula $[Na_2M^{II}_{12}(PTCA)_3(O_3PPh)_6(\mu\text{-}H_2O)(\mu_4\text{-}Cl)_2]$ (M = Ni, Co) were observed [63] (Figure 15 a). They result from the interconnection of 3 $[M^{II}_4(\mu_4\text{-}Cl)PTCA]^{4+}$ shuttlecock-like units with bridging chloro and phenylphosphonate anions, leading to a system displaying a "triangular" shape. Using H_4SO_2TCA and the same conditions, two isostructural compounds of formula $[Na_4M^{II}_{16}(SO_2TCA)_4(O_3PPh)_8(\mu_4\text{-}OH)_4(CH_3OH)_4]$ (M = Ni, Co) were also observed [63] (Figure 15 b), where 4 $[M^{II}_4(\mu_4\text{-}OH)SO_2TCA]^{3+}$ shuttlecock like units were bridged by hydroxo and phenylphosphonate anions, leading to a system presenting a "tetrahedral" shape. Using the same conditions, but a Mn(II) salt, a parent compound of formula $[Mn^{II}_{16}(SO_2TCA)_3(PhPO_3)_7(HPO_4)(\mu_4\text{-}OH)_3Cl(H_2O)(CH_3OH)_4]$ presenting 3 $[Mn^{II}_4(\mu_4\text{-}OH)SO_2TCA]^{3+}$ shuttlecock moieties, bridged by chloro, hydroxo and phenylphosphonate anions, and incorporating also 4 additional Mn^{2+} cations coordinated to phenyl phosphate anions [64] (Figure 15 c), were reported. Using *tert*-butylphosphonic acid instead of phenylphosphonic acid, and the same conditions, a compound of formula $[Mn^{II}_{14}(SO_2TCA)_3(tBuPO_3)_6(\mu_4\text{-}OH)_3Cl(H_2O)(CH_3OH)]$ (Figure 15 d), was obtained, presenting the same triangular shape and connection, and 4 additional Mn^{2+} cations coordinated to phenylphosphonate anions [64].

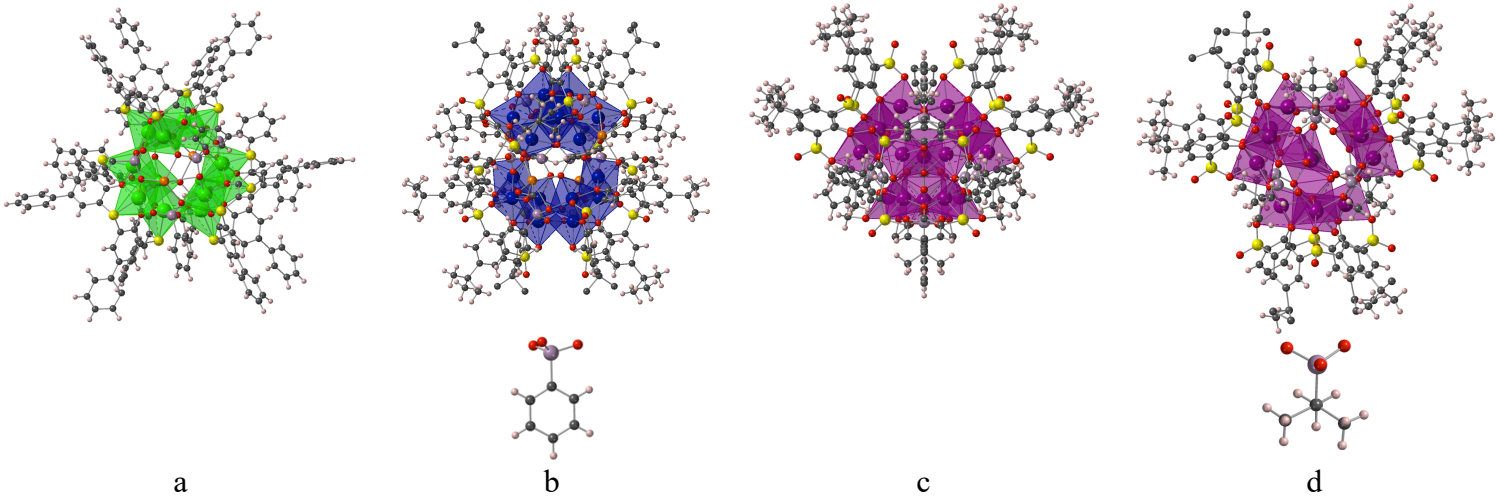

Figure 15: A portion of the X-ray structure of the clusters based on PTCA and SO_2TCA (a) dodecanuclear $[Na_2M^{II}_{12}(PTCA)_3(O_3PPh)_6(\mu\text{-}H_2O)(\mu\text{-}Cl)_2]$ (M = Ni, Co) (b) hexadecanuclear $Na_4Co^{II}_{16}(SO_2TCA)_4(O_3PPh)_8(\mu_4\text{-}OH)_4(CH_3OH)_4]$ (M = Ni, Co) (c) hexadecanuclear $[Mn^{II}_{16}(SO_2TCA)_3(PhPO_3)_7(HPO_4)(\mu_4\text{-}OH)_3Cl(H_2O)(CH_3OH)_4]$ and (d) tetradecanuclear $[Mn^{II}_{14}(SO_2TCA)_3(tBuPO_3)_6(\mu_4\text{-}OH)_3Cl(H_2O)(CH_3OH)]$. Solvent molecules are not presented for the sake of clarity. Adapted from Ref. [63] and [64].

2.4.1.b. The use of O donor linkers, H_4SO_2TCA and 4f metals

Using similar reaction conditions as previously reported (H_4SO_2TCA and organic phosphoric acids for *3d* metals) and $NdCl_3$, three new high nuclearity Nd-based clusters were obtained. When the methylphosphonic acid is involved in coordination, a cluster presenting an oval shape, of formula $[Nd^{III}_{10}(SO_2TCA)_4(MePO_3)_4(Cl)_2(OH)_4(H_2O)_2(DMF)_8(MeOH)_2]$ ($\{Nd_{10}\}$) has been obtained, whereas the increase of the length of the organic substituent (phenylphosphonic acid as coligand) led to formation of two different clusters, depending on the cooling rate during the synthesis: $[Nd^{III}_{11}(SO_2TCA)_3(PhPO_3)_6(Cl)_2(OH)_6(DMF)_{12}]$ ($\{Nd_{11}\}$, rugby-like ball shape) and highly deformed $[Nd^{III}_{19}(SO_2TCA)_5(PhPO_3)_5(CO_3)_6$

$(HCOO)_7(OH)_8(H_2O)_7(DMF)_{12}]$ ({Nd_{19}}) [65] (Figure 16 a-c). The compounds were found to be luminescent (§ 6. 1. 2.), as expected by the presence of Nd(III) cations, and exhibit magnetic interactions (§ 6. 1. 1. and table 1).

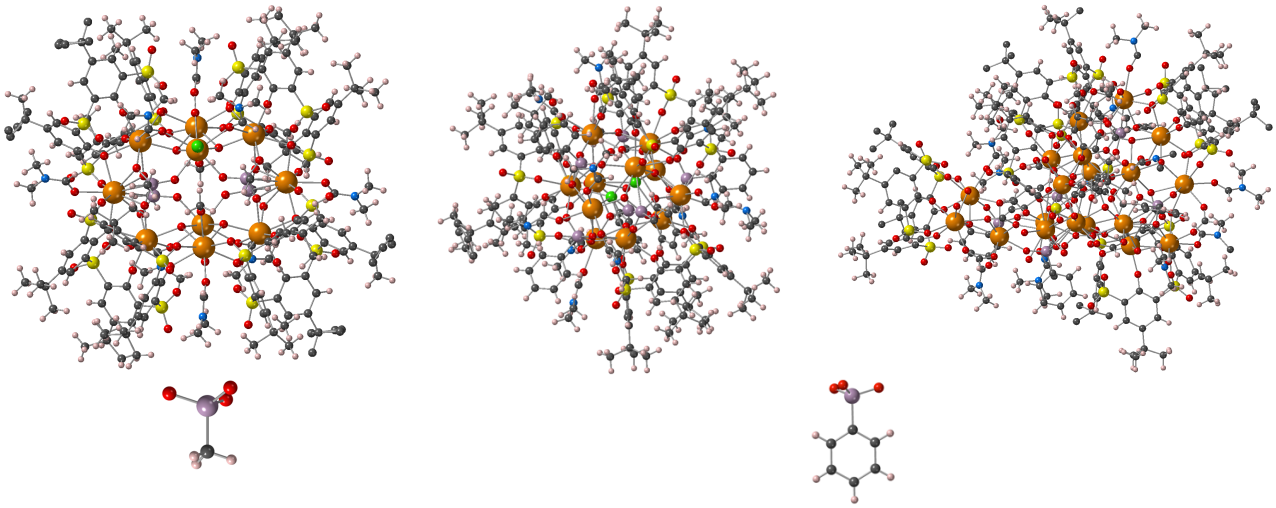

a b c

Figure 16: A portion of the X-ray structure of the clusters based on SO_2TCA and Nd^{3+} cations (a) oval-shaped {Nd_{10}} cluster of formula $[Nd^{III}_{10}(SO_2TCA)_4(MePO_3)_4(Cl)_2(OH)_4(H_2O)_2(DMF)_8(MeOH)_2]$ (b) {Nd_{11}}, rugby-like ball cluster of formula $[Nd^{III}_{11}(SO_2TCA)3(PhPO_3)_6(Cl)_2(OH)_6(DMF)_{12}]$ and (c) highly deformed {Nd_{19}} cluster of formula $[Nd^{III}_{19}(SO_2TCA)_5(PhPO_3)_5(CO_3)_6\,(HCOO)_7(OH)_8(H_2O)_7(DMF)_{12}]$. Nd atoms are represented in light brown. Solvent molecules and H atoms in (a) are not presented for the sake of clarity. Adapted from Ref. [65].

2.4.2. The use of H_4TCA derivatives and N donor linkers

For the building of high nuclearity clusters, N donor organic ligands have been also used. Two different examples have been provided in the literature to date.

The first example results from the use of H_4TCA, combined with $Co^{II}(NO_3)_2$, pyrazine and NaN_3. It leads to the *in situ* formation of the 5-methyl-1*H*-tetrazolate organic linker (Mtta, figure 17 a) and to a dodecanuclear cluster of formula $[Co^{II}_{12}(TCA)_3(HCOO)_2(\mu_6\text{-}CO_3)_2(\mu\text{-}Mtta)_4(\mu_4\text{-}Mtta)_2(dma)_2(Pz)_2]$ [66] (Figure 17 a) (Mtta = 5-methyl-1*H*-tetrazolate). The compound reveals to present a "triangular" shape, with the interconnection of 3 $[Co^{II}_4(\mu_4\text{-}HCOO)PTCA]^{3+}$ shuttlecock-like moieties bridged by acetato, carbonato and Mtta anions. In addition, dimethylamine and pyrazine were also present in the coordination sphere of the metals. By replacing H_4TCA with H_4PTCA and using the same synthetic conditions, two almost isostructural compounds of formula $[M^{II}_{12}(PTCA)_3(HCOO)_3(\mu_6\text{-}CO_3)_2(\mu\text{-}Mtta)(\mu\text{-}Mtta)_2(\mu_4\text{-}Mtta)_2(Py)_4]$ (M = Ni or Co) (Figure 17 b) were obtained, presenting the same geometry, while pyrazine or pyridine were present in the coordination sphere of the metals [66].

Using the same strategy, the combination of H_4SO_2TCA with $Co^{II}(acac)_2$ and 5-ph-tzH (5-phenyl-1H-tetrazole), a tetradecanuclear cluster of formula $[Co^{II}_{14}(OH)_2\text{-}(SO_2TCA)_4(5\text{-}ph\text{-}tz)_{10}(5\text{-}ph\text{-}tzH)_2(CH_3OH)_2]$ has been observed [67]. It is a centrosymmetric compound, based on the bridging of 2 $[Co^{II}_4(\mu_4\text{-}H_2O)SO_2TCA]^{4+}$ and 2 $[Co^{II}_3SO_2TCA]^{2+}$ shuttlecock-like moieties by hydroxo and 5-ph-tzH species (Figure 17 c).

The routine magnetic properties measurements of these compounds were performed (§ 6. 1. 1. and table 1).

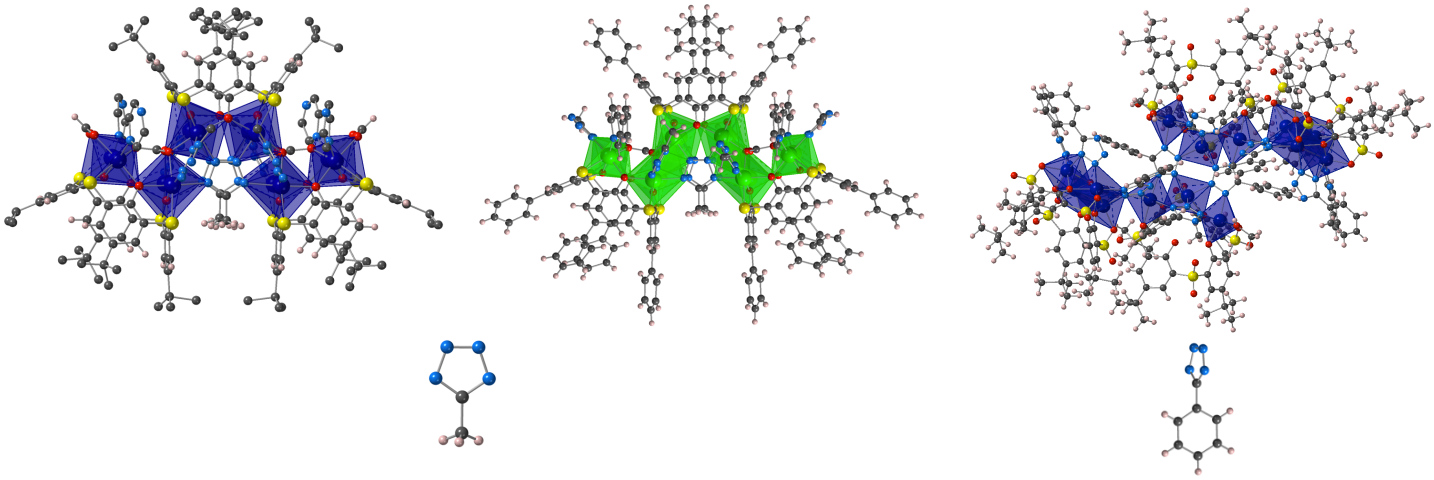

a b c

Figure 17: A portion of the X-ray structure of the clusters based on TCA derivatives and the use of N donor bridging ligands (a) a triangular-shaped dodecanuclear cluster of formula $[Co^{II}_{12}(TCA)_3(HCOO)_2(\mu_6\text{-}CO_3)_2(\mu\text{-}Mtta)_4(\mu_4\text{-}Mtta)_2(dma)_2(Pz)_2]$ (b) a triangular-shaped dodecanuclear cluster of formula $Ni^{II}_{12}(PTCA)_3(HCOO)_3(\mu_6\text{-}CO_3)_2(\mu\text{-}Mtta)(\mu\text{-}Mtta)_2(\mu_4\text{-}Mtta)_2(Py)_4]$ and (c) a centrosymmetric tetradecanuclear cluster of formula $[Co^{II}_{14}(OH)_2\text{-}(SO_2TCA)_4(5\text{-}ph\text{-}tz)_{10}(5\text{-}ph\text{-}tzH)_2(CH_3OH)_2]$. Solvent molecules and H atoms in (a) are not presented for the sake of clarity. Adapted from Ref. [66] and [67].

2.4.3. The use of H_4TCA and N/O donor linkers

In this part, only H_4TCA has been used for the formation of the complexes. Two examples involve the use of N/O donor ligands for the formation of high nuclearity clusters.

The first example appears by the combination of H_4TCA with $CoSO_4$, 1H-1,2,3-triazole-4,5-dicarboxylic acid and triethylamine, where a compound of formula $[Co_4(TCA)(SO_4)]_6[(L)_6(HCOO)_6]A$ (A are $(C_2H_5)_3NH^+$ counter anions and L is deprotonated 1*H*-1,2,3-triazole-4,5-dicarboxylic acid) [29b] (Figure 18 a) was formed. As for already reported M_{24} species (§ 2. 3. 1.), the compound results from the bridging of 6 $[Co^{II}_4(\mu_4\text{-}SO_4)TCA]^{2+}$ shuttlecock-like units by L and acetate anions. The gas sorption properties of this compound were reported (§ 6. 2. and table 2) together with its ability to adsorb Hg(II) cations (§ 6. 4. and table 4).

The second example is based on the combination of H_4TCA with $Co^{II}Cl_2$ and 1-hydroxy-2-(3-pyridyl)-ethylidene-1,1-diphosphonic acid, leading to a $\{Co_{26}\}$ compound of formula $[Co^{II}_{26}(TCA)_6\text{-}(HL)_4Cl_4(HCOO)_4(CH_3O)_2(OH)_2(DMF)_{10}(H_2O)_5]$ [68] (Figure 18 b), where its formation was based on the assembly of 6 $[Co^{II}_4TCA]^{4+}$ shuttlecock-like units, bridged by L and hydroxo anions, but also two $Co^{II}Cl_2$ metallaligands. The final compound adopts a flattened rodlike shape. Its electrochemical properties were investigated.

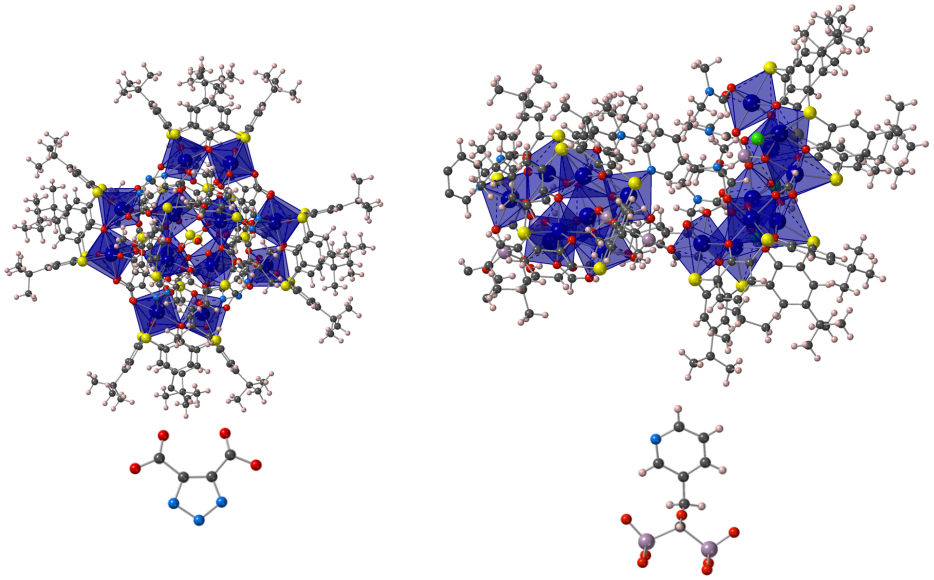

a b

Figure 18: A portion of the X-ray structure of the clusters based on TCA derivatives and the use of N/O donor bridging ligands (a) a spherical {Co_{24}} cluster of formula [Co^{II}_4(TCA)(SO_4)]$_6$[(L)$_6$(HCOO)$_6$]A (A are $(C_2H_5)_3NH^+$ counter anions and L is deprotonated 1H-1,2,3-triazole-4,5-dicarboxylic) and (b) a rod-shaped {Co_{26}} cluster of formula [Co^{II}_{26}(TCA)$_6$-(HL)$_4$Cl$_4$(HCOO)$_4$(CH$_3$O)$_2$(OH)$_2$(DMF)$_{10}$(H$_2$O)$_5$]. Solvent molecules are not presented for the sake of clarity. Adapted from Ref. [29b] and [68].

2.4.4. The use of H_4TCA and N/S donor linkers

Before closing this part dedicated to high nuclearity clusters, other types of organic linkers have been used: N/S donor ligands, which is illustrated by several examples.

The first example was obtained in two steps, by initially obtaining the Cu^I_6(2-PyS)$_6$ (2-PySH = 2-pyridinethiol) intermediate, that was then combined with H_4TCA in the presence of triethylamine. The reaction yielded a {Cu_{12}} complex of formula [Cu^I_3(HTCA)]$_2$[Cu^I_6(2-PyS)$_6$], build from a Cu^I_6(2-PyS)$_6$ building blocks bridging two [Cu^I_3HTCA] units (Figure 19 a) [69]. The compound presents interesting photothermal conversion properties both in the solid-state and in solution (§ 6. 5. 2.).

A {Ni_{24}} bowl-shaped compound of formula [Ni^{II}_{24}-(TCA)$_6$L$_5$(CO$_3$)$_5$(SO$_4$)(HCOO)Cl$_5$]A$_4$ (A = $(CH_3)_4N^+$) Ni_{24} was obtained by reaction between $Ni^{II}Cl_2$, $Ni^{II}SO_4$, H_4TCA and H_2L (H_2L = 2,5-dihydro-1,3,4-thiadiazole-2,5-dithiol) [29c] (Figure 19 b). The complex results from the assembly of 6 [Ni^{II}_4(μ_4-Cl)TCA]$^{3+}$ shuttlecock-like units by bulky bridging L^{2-}, carbonato, sulfato, chloro and acetate anions and displays a half sphere or bowl like shape. Its electrochemical properties were investigated.

The last example of these series is the formation of high nuclearity flattened bowl-shaped {Co_{27}} and two {Co_{28}} clusters. {Co_{27}} was obtained by combining H_4TCA, $Co^{II}(CH_3COO)_2$ and 1H-3-SH-trz (1H-1,2,4-triazole-3-thiol) leading to a compound of formula [Co^{II}_{27}(TCA)$_6$(3-SH-trz)$_8$(di-S-trz)$_4$(CO$_3$)$_{0.25}$(SO$_3$)$_{0.75}$Cl$_{10}$(OH)$_2$(CH$_3$OH)$_2$(H$_2$O)$_4$] (Figure 19 c) [57], where 3-SH-trz has been generated *in situ* during the reaction. The compound was formed by the bridging of 6 [Co^{II}_4TCA]$^{4+}$ shuttlecock-like moieties with the *in situ* formed triazolylthiolate unit, carbonato and hydroxo anions and an additional Co^{2+} cations. The same construction was observed for the further obtained flying saucer-like {Co_{28}} cluster: a compound of formula [Co^{II}_{28}(TCA)$_6$(3-SH-trz)$_8$(di-S-trz)$_4$(SO$_4$)Cl$_{10}$(OH)$_4$(CH$_3$OH)$_4$(H$_2$O)$_6$]

(Figure 19 d) which synthesis differs from the {Co_{27}} one, by the use of Na_2SO_4 and a second {Co_{28}} cluster of formula [$Co^{II}_{28}(TCA)_6(trz)_{16}(CO_3)Cl_{11}(OH)_3(CH_3OH)_2(H_2O)_6$] (Figure 19 e) which synthesis differs from the one reported for {Co_{27}}, by the use of a $Dy^{III}(NO_3)_3$ salt [57]. For the later one an additional bridging Co^{2+} cation has been found. For the 3 reported compounds, the magnetic properties were reported (§ 6. 1. 1. and table 1).

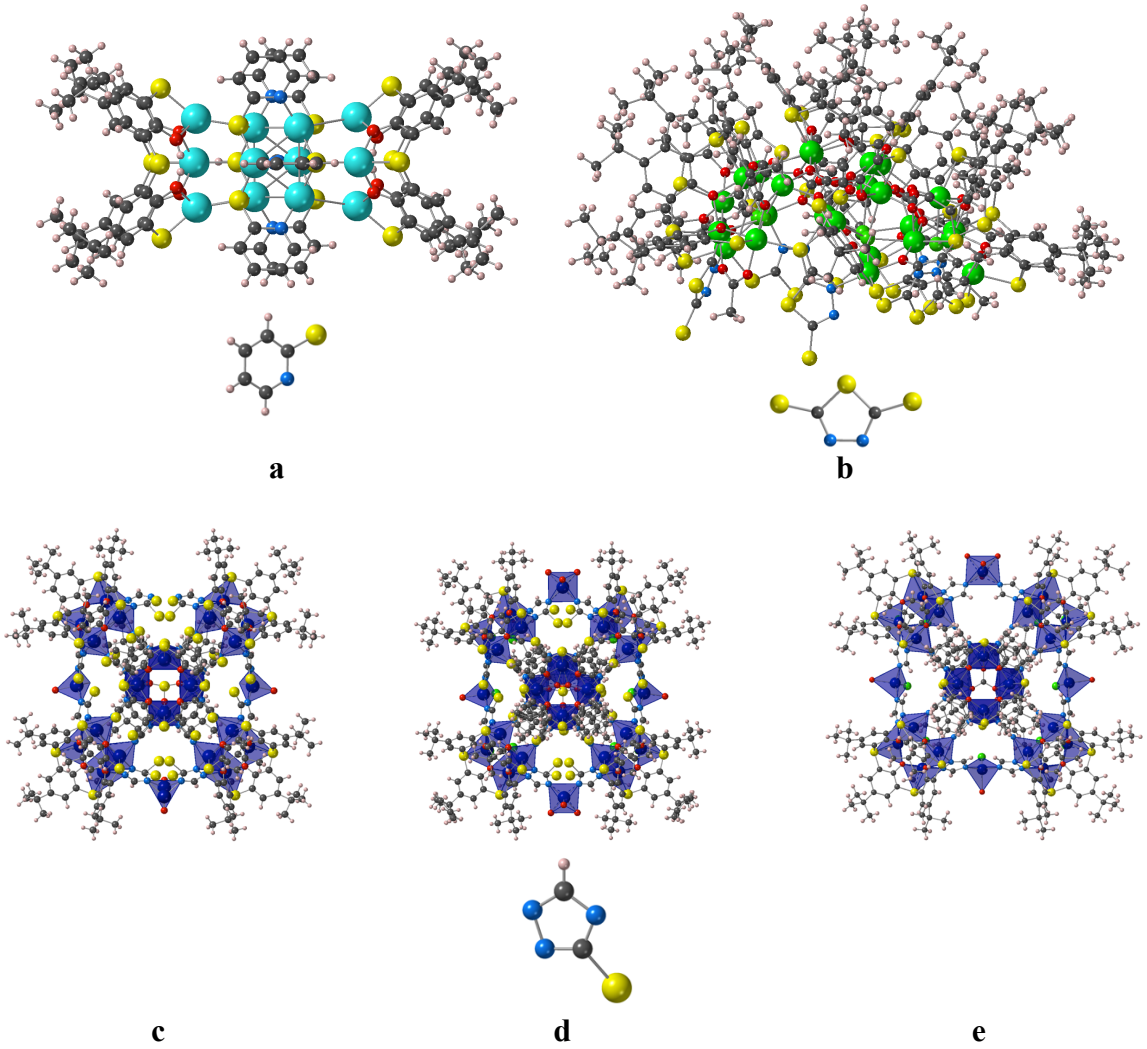

Figure 19: A portion of the X-ray structure of the clusters based on TCA derivatives and the use of N/S donor bridging ligands (a) {Cu_{12}} compound of formula [Cu^{I}_3(HTCA)]$_2$[Cu^{I}_6(2-PyS)6], and bowl-shaped clusters (b) {Ni_{24}} of formula [Ni^{II}_{24}-$(TCA)_6L_5(CO_3)_5(SO_4)(HCOO)Cl_5]A_4$ (A = $(CH_3)_4N^+$) (c) {Co_{27}} of formula [$Co^{II}_{27}(TCA)_6$(3-SH-trz)$_8$(di-S-trz)$_4(CO_3)_{0.25}(SO_3)_{0.75}Cl_{10}(OH)_2(CH_3OH)_2(H_2O)_4$] (d) {$Co_{28}$} of formula [$Co^{II}_{28}(TCA)_6$(3-SH-trz)$_8$(di-S-trz)$_4(SO_4)Cl_{10}(OH)_4(CH_3OH)_4(H_2O)_6$] and (e) {$Co_{28}$} of formula [$Co_2{}^{II}_8(TCA)_6(trz)_{16}(CO_3)Cl_{11}(OH)_3(CH_3OH)_2(H_2O)_6$]. Solvent molecules are not presented for the sake of clarity. Adapted from Ref. [29c], [69] and [57].

Beside the description of these high nuclearity clusters based on TCA derivatives, the formation of more symmetrical species will be possible while using small organic multitopic linkers, for example metallamacrocycles (see definition here below).

3. Formation of metallamacrocycles involving thiacalix[4]arenes

The field of **M**etalla**M**acro**C**ycles (MMCs) emerged during the development of supramolecular chemistry, and several examples of wheels and giant wheels, involving metal ions, have been provided in the literature [70]. The TCA derivatives also revealed to be able to form such spherical species (figure 20), when combined with ligands, and they will be presented here below.

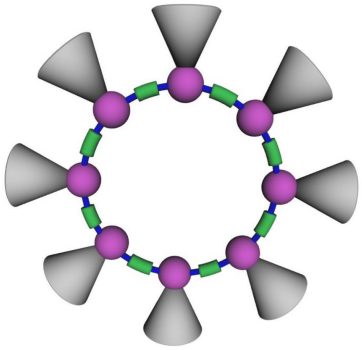

Figure 20: Schematic representation for metallamacrocycles.

3.1. Generalities

Starting from $[M^{II}_4(\mu_4\text{-}X)TCA]^{3+}$ (X = Cl, OH), $[M^{II}_4(\mu_4\text{-}H_2O)TCA]^{4+}$ or $[M^{II}_3(\mu_4\text{-}X)TCA]^{+}$ (X = Cl, OH), $[M^{II}_3(\mu_4\text{-}H_2O)YTCA]^{3+}$ shuttlecock-like subunits (Y = -, D, P, SO_2, see figure 3) connected *via* linkers, it appears possible to form spherical species, Metallamacrocycles, while the TCA derivatives appear as a shell around the metallic ring. As a consequence, the outer edge is usually more hydrophobic than the inner space (centre) of the formed wheel, that are more or less deformed. The size of the formed wheels depends on the number of thiacalix[4]arene subunits involved and of the "length" of the organic linkers. This will be discussed through the several examples shown below. The nature of the bridging ligands appears determinant for the formation of spherical MMC, as shown in the previous chapter.

3.2. Formation of Metallamacrocyles based on TCA and SO_2TCA

3.2.1. O organic linkers

The first metallamacrocycles based on TCA derivatives, was reported in 2004, by Iki *et al.*: it was an octalanthanide wheels based and SO_2TCA and Ln^{3+} (Ln= Pr, Gd, Sm, Nd) [32]. The procedure failed for Ho(III), due steric hindrance, because of the small ionic radius of Holmium(III). However, a few years later, the use of malonic acid leads to the formation of a larger dodecaholmium (III) wheel supported by SO_2TCA [71] with the formula $[Ho^{III}_{12}(SO_2TCA)_6(malonate)_4(AcO)_4(H_2O)_{14}]$ (Figure 21 a). This $\{Ho_{12}\}$ SO_2TCA based MMC was formed by 6 $[Ho^{III}SO_2TCA]^-$ moieties, bridged by six $[Ho^{III}(H_2O)_2]^{3+}$ entities and additional malonate and acetate ligands. The longest diameter of the wheel based on Ho---Ho distances was about 17.7 Å. The whole macrocycle presents a saddle-like shape pocket cavity that includes 4 EtOH molecules.

Two {Cu_{12}} and {Cu_{16}} MMCs based on TCA, Cu(II) and phenylphosphate were described recently by Liu *et al.* Three or 4 $[Cu^{II}_4(\mu_4\text{-}Cl)TCA]^{3+}$ shuttlecock-like units were connected with ancillary phenylphosphonate ligands to form anionic wheel-like nanostructures with skeletal formula $[Cu^{II}_{12}(TCA)_3Cl_3(PhPO_3)_{12}(H_2O)_2]^{3-}$ (Figure 21 b) and $[Cu_{16}(TCA)_4Cl_4(PhPO_3)_8]^{4-}$ (Figure 21 c) respectively [72]. Interestingly both μ_4-anions (Cl^- and $PhPO_3^{2-}$) can be substituted by salicylate ligands keeping the core intact. These MMC were used as catalysts in sulfide oxidation reactions (§ 6. 3. and table 3).

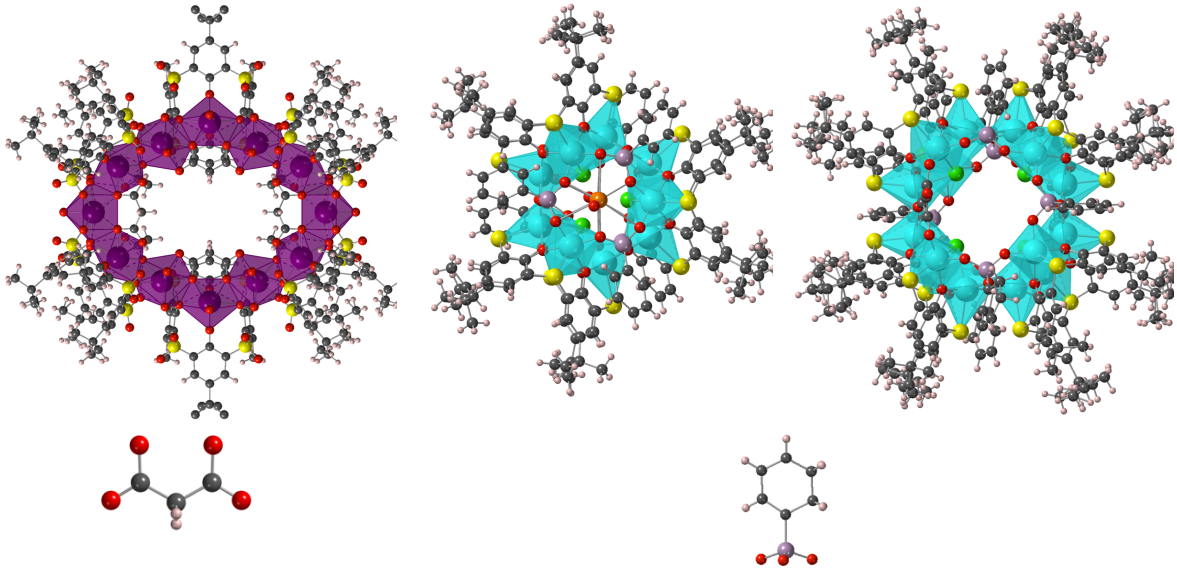

a **b** **c**

Figure 21: A portion of the X-ray structure of {Ho_{12}}, {Cu_{12}} and {Cu_{16}} MMCs a) $[Ho^{III}_{12}(SO_2TCA)_6(malonate)_4\ (AcO)_4\ (H_2O)_{14}]$ b) $[Cu^{II}_{12}(TCA)_3Cl_3(PhPO_3)_{12}(H_2O)_2]^{3-}$ and c) $[Cu^{II}_{16}(TCA)_4Cl_4(PhPO_3)_8]$. For clarity, solvent molecules are not presented. Ho atoms are represented in dark purple. Adapted from Ref. [71] and [72].

3.2.2. N organic linkers

The simplest TCA based-MMC was reported in 2012 by Hong *et al.*: it was a {Co_{16}} macrocycle based on TCA and 5-methyl tetrazolate (MTTa) of formula $[Co^{II}_{16}(TCA)_4(\mu_4\text{-}Cl)_4(HCOO)_2(\mu\text{-}Mtta)_6(\mu\text{-}Mtta)_8]$ (Figure 22 a) [66]. It consists of 4 $[Co^{II}_4(\mu_4\text{-}Cl)(\mu\text{-}Mtta)TCA]^{2+}$ shuttlecock-like building units linked by eight bidentate pyrazines moieties. 5-methyl tetrazole (HMtta) has been formed *in situ* from pyrazine and NaN_3 under solvothermal conditions. The positions of the 4 Co(II) within a shuttlecock-like unit are at the vertices of a square that is capped by TCA, so that the shape of the formed entity is a deformed square. The diameter of this wheel-like compound is about 25.7 Å. Magnetic studies indicate antiferromagnetic coupling between the Co(II) ions (§ 6. 1. 1. and table 1). This shape is close to what has been observe in related square-like species (§ 4. 2. 3 and 4. 2. 4)

But, the first reported TCA based-MMC was a {Co_{24}} species, that has been described in 2010 by Gao *et al.* [73]. Neutral $[Co^{II}_4(TCA)(trz)_2Cl_2(CH_3OH)(H_2O)]_6$ was formed under solvothermal conditions and contains 6 $[Co^{II}_4TCA]^{4+}$ shuttlecock-like units, linked by twelve 1,2,4-triazolate anions (Figure 22 b). Two Co(II) from $[Co^{II}_4TCA]^{4+}$ are bonded to two phenoxy oxygens of the lower rim of TCA^{4-}, to one bridging sulphur atom, one nitrogen atom of a triazolate anion and to one Cl^- anion. The two other Co(II) are six-coordinated being bonded to two phenoxy oxygens, and one sulphur of the TCA, one solvent molecule (H_2O or MeOH) and

two triazolates. The thickness of the {Co_{24}} MMC is *ca*. 21.5 Å, and its diameter about 29.9 Å. Solvent molecules ($CHCl_3$ and MeOH) were trapped in the interstices of the lattice and can be easily removed. The magnetic properties were measured (§ 6. 1. 1. and table 1). This thiacalix[4]arene-supported {Co_{24}} MMC has been annealed into metallic Co_9S_8 NPs and involved as electrode material in ion Li-batteries [74] (§ 6. 5.1.).

The combination of H_4SO_2TCA, under solvothermal conditions in the presence of $Co^{II}(OAc)_2$ and 1,2,4-triazole, leads to another neutral {Co_{24}} MMC species of formula $[Co^{II}_{24}(SO_2TCA)_8(trz)_{16}(CH_3OH)_8]$ [75]. This nest-like MMC with two parallel [16-MCo-4] door rings was based on 8 $[Co^{II}_3(\mu_3\text{-MeOH})SO_2TCA]^{2+}$ shuttlecock-like units bridged by 16 triazolate anions (Figure 22 c). In the $[Co^{II}_3(\mu_3\text{-MeOH})SO_2TCA]^{2+}$ subunits, the three Co^{2+} cations form a quasi-isosceles triangle, bridged by a μ_3-O of a central methanol and bonded to four phenoxy O atoms and three sulfonyl oxygen of SO_2TCA^{4-} ligand. The diameter of this {Co_{24}} MMC is about 28.2 Å, somewhat smaller than the one obtained for the TCA analogue [73]. The magnetic properties of this MMC were studied (§ 6. 1. 1. and table 1).

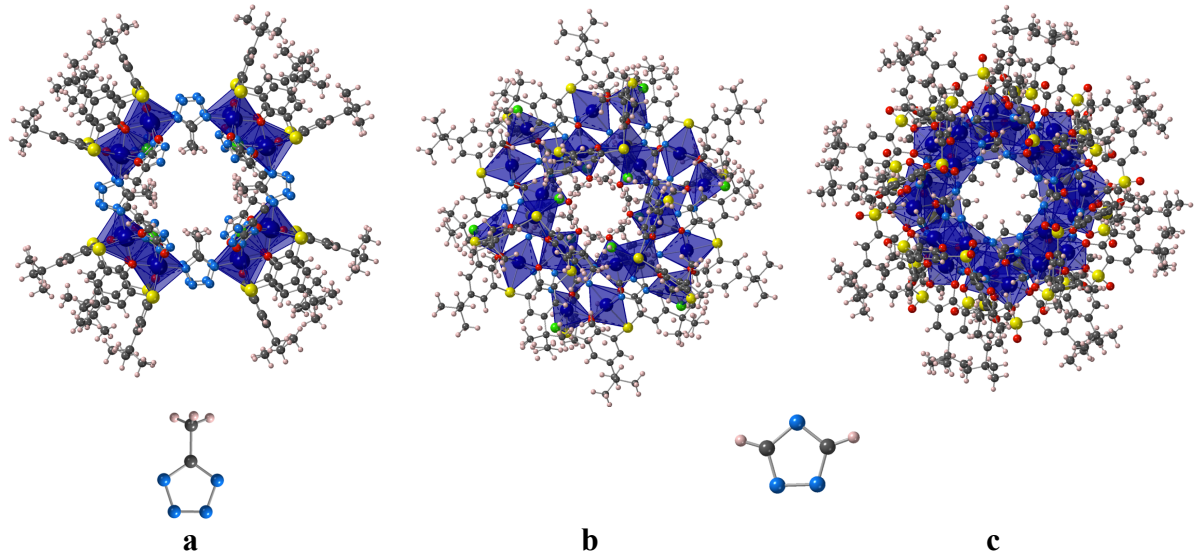

a **b** **c**

Figure 22: A portion of the X-ray structure of the {Co_{16}} and {Co_{24}} metallamacrocycles (a) $[Co^{II}_{16}(TCA)_4(\mu_4\text{-}Cl)_4(HCOO)_2(\mu\text{-Mtta})_6(\mu\text{-Mtta})_8]$ (b) $[Co^{II}_{24}(TCA)_6(trz)_{12}Cl_{12}(CH_3OH)_6(H_2O)_6]$ and (c) $[Co^{II}_{24}(SO_2TCA)_8(trz)_{16}(CH_3OH)_8]$. For clarity, solvent molecules are not presented Adapted from Ref. [66], [73] and [75].

3.2.3. N,O organic linkers

An original flowerlike anionic MMC containing 6 $[Ni^{II}_4TCA]^{4+}$ shuttlecock-like units, 6 deprotonated risedronic acid (HL^{4-}), four additional Ni^{2+} ions, together with two phosphates, two chlorides, one μ_3-oxo and additional solvents molecules has been obtained and presents the formula $[Ni^{II}_{28}(TCA)_6(HL)_6(PO_4)_2(\mu_3\text{-O})_2Cl_2(CH_3OH)_{14}(H_2O)_2(DMF)_8]^{4-}$ (Figure 23) [68]. It contains 14 crystallographically independent six-coordinated Ni(II) cations, involved in 3 $[Ni^{II}_4TCA]^{4+}$ shuttlecock-like units, and pyridine, hydroxyl and HL^{4-} ligands. The outer dimension of the resulting MMC is *ca* 41 x 23 x19 $Å^3$ (based on opposite C_{butyl}-C_{butyl} atoms). The compound has been studied for catalytic OER (§ 6. 3. and table 3).

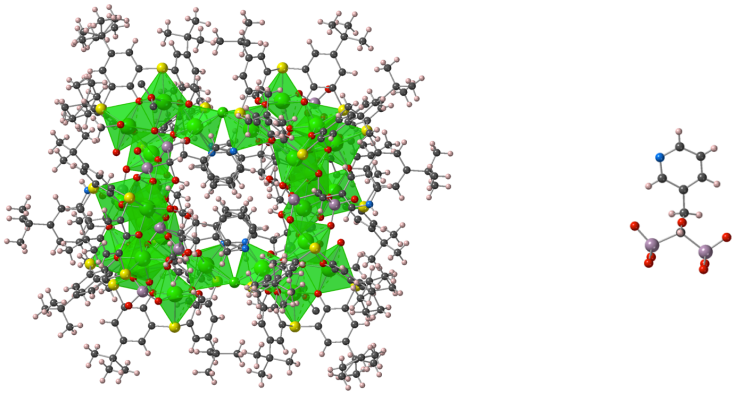

Figure 23: A portion of the X-ray structure of the MMC $[Ni^{II}_{28}(TCA)_6(HL)_6(PO_4)_2(\mu_3\text{-}O)_2Cl_2(CH_3OH)_{14}(H_2O)_2(DMF)_8][(CH_3NH_2CH_3)_4]$. For clarity, solvent molecules are not presented. Adapted from Ref. [68].

Self-assembly of H_4TCA and 3,5-pyrazoledicarboxylicacid (H_3pdc) with Co^{2+} under solvothermal conditions leads to a series of four different giant cobalt calix[4]arene MMCs [76], that are described here below. A 30-membered wheel-shaped hexanionic ring, $\{Co_{30}\}$-**A** of formula $[Co^{II}_{30}(TCA)_6(pdc)_{12}(MeO)_6(MeOH)_8(H_2O)_6]$ (Figure 24 a) was formed, containing 6 $[Co^{II}_4TCA]^{4+}$ shuttlecock-like units (with similar connectivity with the $\{Co_{24}\}$-wheel described in 2010 by Gao *et al.* [73] based on triazole) and 6 additional Co^{2+} linked by twelve 3,5-dicarboxylatopyrazolate (pdc^{3-}). The pdc^{3-} anions were coordinated to the Co_4-TCA subunits and to the additional Co^{2+} ions forming thus a $\{Co_5\}$ unit. A slight modification of the experimental procedure leads to a similar 30-membered MMC, $\{Co_{30}\}$-**B** of formula $[Co^{II}_{30}(TCA)_6(pdc)_{12}(MeO)_6(H_2O)_{12}]$, in which the six MeOH molecules terminally coordinated to the Co ions of the rim in $\{Co_{30}\}$-**A** were replaced by six water molecules. The $\{Co_{30}\}$-**B** has a perfect hexagonal shape compared to the slight distortion observed for $\{Co_{30}\}$-**A** (Figure 24 b). The outer diameter (distance between opposite methyl groups) is 36.2 Å and 35.8 Å for $\{Co_{30}\}$-**A** and $\{Co_{30}\}$-**B**, respectively. Six uncoordinated carboxylate oxygen atoms confined the inner cavity leading to an inner diameter of only 11.4 Å for $\{Co_{30}\}$-**A** and 11.8 Å for $\{Co_{30}\}$-**B**.

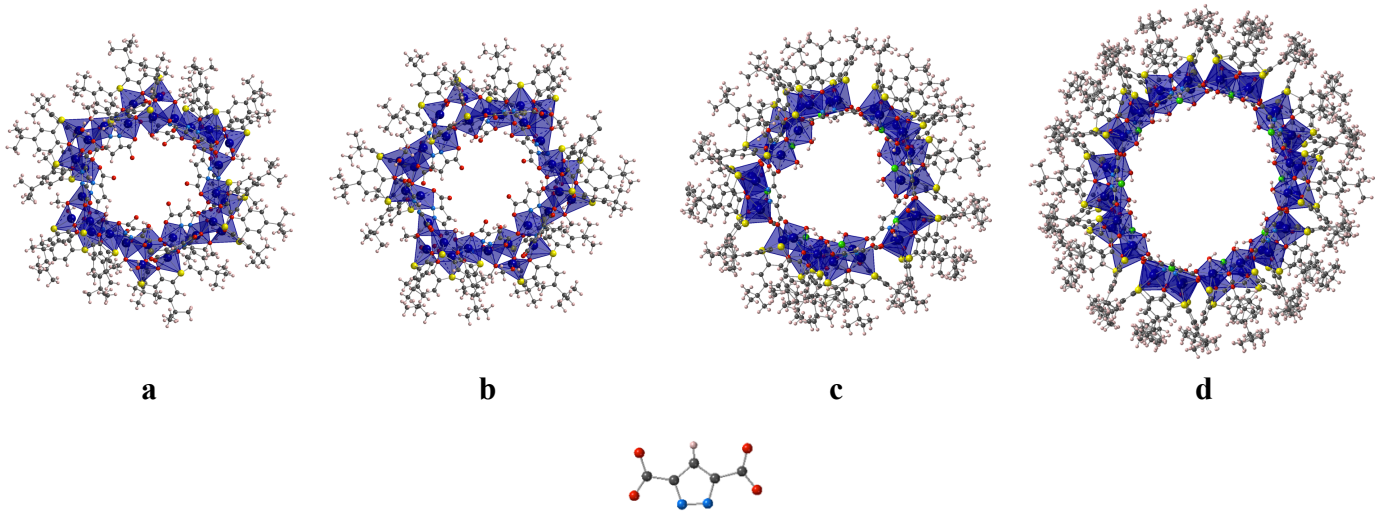

Figure 24: A portion of the X-ray structure of the series of TCA/3,5-pyrazoledicarboxylate based metallamacrocycles a) $\{Co_{30}\}$-**A**, b) $\{Co_{30}\}$-**B**, c) **{**$Co_{32}\}$-**A** and d) $\{Co_{40}\}$. For clarity, the solvent molecules and uncoordinated carboxylate anions within the cavity are not presented. Adapted from ref [76].

A {Co_{32}}-**A**, a 32 membered ring including 8 $[Co^{II}_4\mu\text{-}Cl(\mu_4\text{-}H_2O_2)TCA]^{3+}$ shuttlecock-like units linked by 8 pdc^{3-}, leading to an eight-point star-shaped MMC of formula $[Co^{II}_{32}Cl_8(TCA)_8(pdc)_8(H_2O)_{16}]$ (Figure 24 c). The outer diameter of {Co_{32}}-**A** is *ca* 34.2 Å, slightly smaller than the one of {Co_{30}}-**A** or **B** while its aperture is *ca* 14.9 Å. Recrystallization of {Co_{32}}-**A** in DMF leads to {Co_{32}}-**B** and {Co_{32}}-**C** that have a similar ring structure than the one adopted by {Co_{32}}-**A**, but a different packing. The performance of {Co_{32}}-**A** as an adsorbent has been measured with three common dyes (methyl blue, rhodamine B disodium fluorescein) (§ 6. 4. and table 4). Interestingly, the recrystallization Co_{32}-**A** leads after 2 weeks to the formation of a small amount (*ca*. 5%) of a novel {Co_{40}} MMC, of formula $[Co^{II}_{40}Cl_{10}(TCA)_{10}(pdc)_{10}(H_2O)_{20}]$ (Figure 24 d). The whole structure can be described as an overlap of two $[Co^{II}_4Cl(TCA)]_5(pdc)_5(H_2O)_{10}]$ pentagonal rings, staggered and bridged by pdc^{3-} ligands thus forming a ten-point star-shaped molecular wheel. The dimension of this {C_{40}} MMC is *ca* 40.1 x 36.7 x 24.2 $Å^3$ and its inner diameter is *ca* 20.3 Å.

3.2.4. N,S organic linkers

A {Ni_{18}} coordination wheel of formula $[Ni^{II}_{18}Cl_6(TCA)_6(MNA)_6]$ involving 6 $[Ni^{II}_3(\mu_3\text{-}Cl)TCA]^{2+}$ shuttlecock-like units and six 2-mercaptonicotinate moieties (MNA^{2-}) has been reported [77] The dimension of the MMC is *ca* 25.7 x 27.5 x 15.1 $Å^3$. Each of the six $[Ni^{II}_3(\mu_3\text{-}Cl)TCA]^{2+}$ subunits is connected to four others by three MNA^{2-} tridentate ligands leading to a wheel like structure with a hexagonal prismatic central pore (Figure 25 a) of *ca* 9.0 x 9.0 x 13.3 $Å^3$. This {Ni_{18}} MMC has been proven to be an efficient catalyst for electrochemical reduction of glucose in N_2, O_2 or air (§ 6. 3. and table 3). Moreover, this {Ni_{18}} wheel is able to accommodate metal clusters of Au, Pd, Pt, Ir, Ru, Rh and also Au/Pd that shows excellent electrocatalytic activity for Hydrogen Evolution Reaction (§ 6. 3. and table 3).

Later, the same group described the formation of anionic {Ni_{20}} and {Ni_{32}} coordination wheels displaying a twist double-bowl shape and of formula $[Ni^{II}_{20}(TCA)_5(L)_5(SO_4)_5Cl_5]^{5-}$ (Figure 25 b) and $[Ni^{II}_{32}(TCA)_8(L)_8(CO_3)_4(HCOO)_2Cl_8]^{2-}$ (Figure 25 c) [29c], where L is 1,3,4-thiadiazole-2,5-dithiolate anion. The {Ni_{20}} compound can be described as an entity having two open ends with diameter of 14.0 and 10.1 Å. 5 $[Ni^{II}_4TCA]^{4+}$ shuttlecock-like units are bridged by five tetradentate L^{2-} along the upper rim and five sulfate anions along the lower rim, whereas {Ni_{32}} contains 8 $[Ni^{II}_4TCA]^{4+}$ subunits connected by 8 L^{2-} acting as pentadentate ligands and four carbonate anions (generated from decomposition of DMF). The overall shape can be described as the connection of two bowl-shaped units through a centrosymmetric operation thus leading to a double-bowl-shaped. The catalytic performance for electrochemical oxidation of glucose of these 2 MMCs has been evaluated, evidencing that {Ni_{20}} exhibits the best activity (§ 6. 3. and table 3).

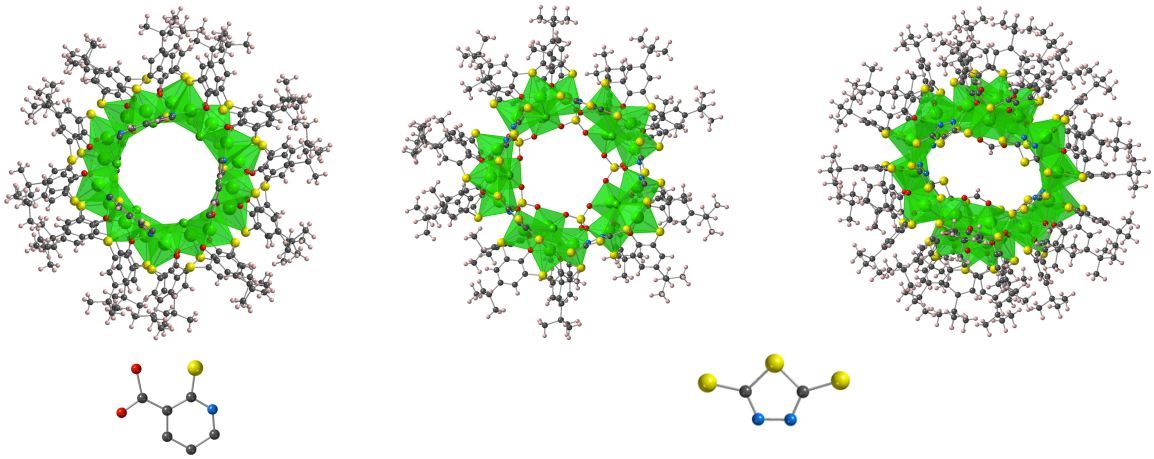

a **b** **c**

Figure 25: A portion of the X-ray structure of the series of the TCA based metallamacrocycles a) $[Ni^{II}_{18}Cl_6(TCA)_6(MNA)_6]$ b) $[Ni^{II}_{20}(TCA)_5(L)_5(SO_4)_5Cl_5]^{5-}$ and c) $[Ni^{II}_{32}(TCA)_8(L)_8(CO_3)_4(HCOO)_2Cl_8]^{2-}$. For clarity, the solvent molecules are not presented. Adapted from ref [77] and [29c]

Thus, one may conclude that the formation of metallamacrocycles based on TCA derivatives is evidenced using small O, N,O or N,S organic linkers. Using larger ligands, nanocapsules and cages, which are described below, are obtained.

4. MOCs based on thiacalix[4]arenes: nanocapsules and cages

4.1. Context

The use calix[4]arene derivatives for the formation of capsules and cages has been already documented. In 2014, Dalgarno *et al*. reported the formation of assembled molecular capsules, also called molecular containers or molecular cages, based on calix[4]arene, resorcin[4]arene, pyrogallol[4]arene and cyclotricatechylene [78], whereas in 2015 Papparaldo *et al*. reported capsules based on Resorcin[4]arene and Calix[n]arene [79]. In 2022, Zhou and Fang *et al.* reported the use thiacalix[4]arene (among many other macrocycles) for the formation of cages, together with their applications in the field photochemistry, catalysis, energy storage and molecular recognition [80].

In 2014, through their huge pioneering work in that field, Bi and Liao reviewed the stunning work concerning the formation of cages based on thiacalix[4]arene [81], and the use of di or tricarboxylic ligands. This important work was the beginning of a huge number of examples, and here below, we attempt to provide its rationalization through the obtention of these fascinating coordination porous cages, together with the presentation of the new recently reported examples emerged since that time, starting from the lowest nuclearity (pocket-like cages) to highest (octahedral and more sophisticated species).

As already mentioned, in this part, the representation of this molecular cages (CPK model) is different from the one used for the metallic clusters (Polyhedral model).

4.2. Barrel-like thiacalix[4]arene based MOCs (Pocket-like and Square-like)

Barrel-like calix[4]arene-based Metal-Organic Cages (MOCs) is a family that includes cages with two calix[4]arene units (pocket-like) or four calix[4]arene units (square-like) (Figure 26). H_4TCA or H_4SO_2TCA are both used to build both species.

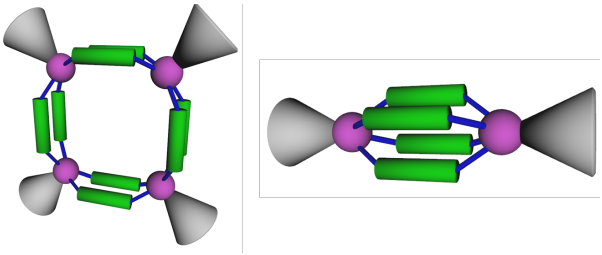

Figure 26: Two geometry types of barrel-like MOCs: square-shaped (left) and pocket-shaped (right)

The units are built either from shuttlecock-like units derived from $[M^{II}_4(\mu_4\text{-}H_2O)TCA]^{4+}$ ($[M^{II}_4(\mu_4\text{-}H_2O)SO_2TCA]^{4+}$) or $[M^{II}_3(\mu_4\text{-}H_2O)TCA]^{2+}$ (M^{II}_3 $(\mu_4\text{-}H_2O)SO_2TCA]^{4+}$) (or others), assembled with 2, 3, 4 or 8 bridging organic ligands, based on ditopic ligands (mainly dicarboxylate or tetrazolate).

All the compounds (neutral or anionic) present the same coordination pattern, and "barrel-like" ("pocket-like" or "square-like") compounds are formed, presenting an internal cavity for "pocket-like", external porosity and the size of the pores is depending on the size of the used ligands.

Pocket-like compounds (Figure 26 right) are formed while using dicarboxylate L ligands, and present the $\{M_8\}$ or $\{M_6\}$ nuclearity and the general formula $\mathbf{[M^{II}_n(TCA)_2L_m]^{p-}}$ (or $\mathbf{[M^{II}_n(SO_2TCA)_2L_m]^{p-}}$) (n = 6 or 8 and m = 2, 3 or 4).

Square-like compounds (Figure 26 left) are obtained while using V-shaped dicarboxylic (O donor) or tetrazolate (N donor) L derivative and present the $\{M_{16}\}$ or $\{M_{12}\}$ nuclearities and the general formula $\mathbf{[M^{II}_n(TCA)_4L_8]^{p-}}$ (or $\mathbf{[M^{II}_n(SO_2TCA)_4L_8]^{p-}}$) (n = 12 or 16).

For all compounds, the influence of the location of the carboxylate moieties on the ligand, the flexibility of the L ligand, the nature of the substituents will be illustrated by different examples provided here below.

4.2.1. Pocket-like MOCs based on H_4TCA: $[M^{II}_n(TCA)_2L_m]^p$ (n = 6 or 8 and m = 3 or 4)

Only two examples are provided in this part.

The first example of pocket-like compound was reported in 2013. By mixing under solvothermal conditions H_4TCA, $MCl_2{\bullet}6H_2O$ (M = Co or Fe) and isonicotinic acid (H_2INA) two anionic compounds of formula $[(TCA)_2M^{II}_8(\mu\text{-}Cl)_2][(M^{II}(INA)_2Cl_2)_4]^{2-}$ (M = Fe and Co) were obtained (Figure 27 a) [82]. The formation of anionic $\{M_{12}\}$-MOCs is based on the condensation of 2 $[M^{II}_4(\mu_4\text{-}Cl)TCA]^{3+}$ shuttlecock-like units by four $[(M^{II}(INA)_2Cl_2)]^{2-}$ complexes built from isonicotinic acid, these fragments playing the role of angular O-donor linkers. The nuclearity of the formed pocket-like species is equal to 12. The dinitrogen adsorption properties of these porous species were studied (§ 6. 2. and table 2).

A few years later, the solvothermal condensation of chiral (1R,3S)-(+)-camphoric acid (H_2CAM), H_4TCA and $Co^{II}Cl_2 \cdot 6H_2O$ yielded a neutral chiral $\{Co_8\}$-MOC cage-assembly of formula $[Co^{II}_8(TCA)_2(CAM)_3(\mu_4\text{-}Cl)_2(CH_3OH)_2(dma)_2]$ (dma-dimethylamine) (Figure 27 b) [83]. The reported structure consists of 2 $[Co^{II}_4(\mu_4\text{-}Cl)(MeOH)(dma)TCA]^+$ shuttlecock-like units that are connected through three fragments of anions derived from camphoric acid (CAM^{2-}), which play a role of angular O-donor linkers. Gas sorption properties of the species (§ 6. 2. and table 2) were studied together with magnetic measurements (§ 6. 1. 1. and table 1).

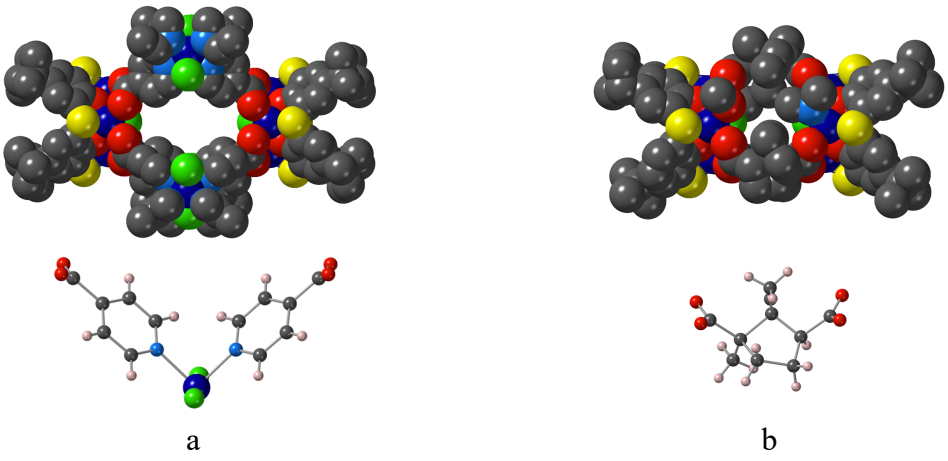

Figure 27: A portion of the X-ray structure of the pocket-like species: (a) anionic $[(TCA)_2M^{II}_8(\mu\text{-}Cl)_2][(M^{II}(INA)_2Cl_2)_4]^{2-}$ (M = Fe and Co) and $[(Fe(INA)_2Cl_2)]^{2-}$ linker (INA = isonicotinate dianion) and (b) neutral chiral $[(TCA)_2Co^{II}_8(\mu\text{-}Cl)_2(MeOH)_2(dma)_2][(CAM)_3]$ (CAM = dianion derived from 1R,3S)-(+)-camphoric acid). Solvent molecules are not presented for the sake of clarity. Adapted from Ref. [82] and [83].

4.2.2. Pocket-like MOCs based on H_4SO_2TCA: $[M^{II}_n(SO_2TCA)_2L_m]^{p-}$ (n = 6 or 8 and m = 2, 3 or 4)

The compounds will be presented by increasing the degree of sophistication of the building organic linkers.

Neutral $\{M_8\}$-MOCs were obtained under solvothermal or liquid-liquid diffusion conditions with the use of H_4SO_2TCA, succinic acid (H_2SUC) and corresponding nitrate hexahydrate; they display the formula $[(SO_2TCA)_2M^{II}_8(\mu\text{-}H_2O)_2][(SUC)_4]$ (M = Co, Ni) (Figure 28 a) [84]. In our team, we demonstrated the formation of four different MOCs: two achiral and two chiral with the same formula, some of other neutral metallic complexes being present in the surrounding of the MOC in crystal. The obtained MOCs are built from two $[M^{II}_4(\mu_4\text{-}H_2O)SO_2TCA]^{4+}$ (M = Co; Ni) shuttlecock-like units, connected by four succinate anions (SUC^{2-}).

Using H_4SO_2TCA 1,2-benzenedicarboxylic acid (H_2OBDC) or 2,3-naphthalenedicarboxylic acid (H_2NDC) and corresponding nitrate hexahydrate in solvothermal conditions, neutral $\{M_8\}$-MOCs of formula $[(SO_2TCA)_2M^{II}_8(\mu\text{-}H_2O)_2][(OBDC)_4]$ (Figure 28 b) and $[(SO_2TCA)_2M^{II}_8(\mu\text{-}OH)_2][(NDC)_4]$ (M = Co, Ni) (Figure 28 c) were obtained [85]. All four MOCs share the same coordination pattern with 2 $[M^{II}_4(\mu_4\text{-}H_2O)SO_2TCA]^{4+}$ shuttlecock-like units connected through four corresponding dicarboxylate fragments ($OBDC^{2-}$ or NDC^{2-}). Molecular recognition towards cations dyes (§ 6. 4. and table 4) as well as gas sorption properties (§ 6. 2. and table 2) were studied.

By analogy with what was obtained for H_2TCA [83], using chiral (1R,3S)-(+)-camphoric acid (H_2CAM), H_4TCA and $CoCl_2•6H_2O$ a neutral chiral {Co_8}-MOC of formula $[Co^{II}_8(SO_2TCA)_2(CAM)_2(\mu_4\text{-}H_2O)_2Cl_4]$ (Figure 28 d) was obtained, where only two ligands are bridging the $[Co^{II}_4(\mu_4\text{-}H_2O)SO_2TCA]^{4+}$ shuttlecock-like units. Magnetic measurements (§ 6. 1. 1. and table 1) were studied together with gas sorption properties (§ 6. 2. and table 2).

Two neutral {Co_8}-MOCs of formula $[(SO_2TCA)_2Co^{II}_8(\mu\text{-}H_2O)_2][(NDC\text{-}X)_4]$ (X = Br, H) (figure X, e and f), obtained under solvothermal conditions with the use of H_4SO_2TCA, $CoCl_2•6H_2O$ and 1,8-naphthalenedicarboxylic acid (H_2NDC-H) or 4-bromo-1,8-naphthalenedicarboxylic acid (H_2NDC-Br), were reported [86] (Figure 28 e-f). Their coordination pattern was based on 2 $[Co^{II}_4(\mu_4\text{-}H_2O)SO_2TCA]^{4+}$ shuttlecock-like units connected by four dicarboxylate fragments ({NDC-H}$^{2-}$ or {NDC-Br}$^{2-}$). For these compounds, gas sorption properties and iodine capture were studied (§ 6. 2. and table 2).

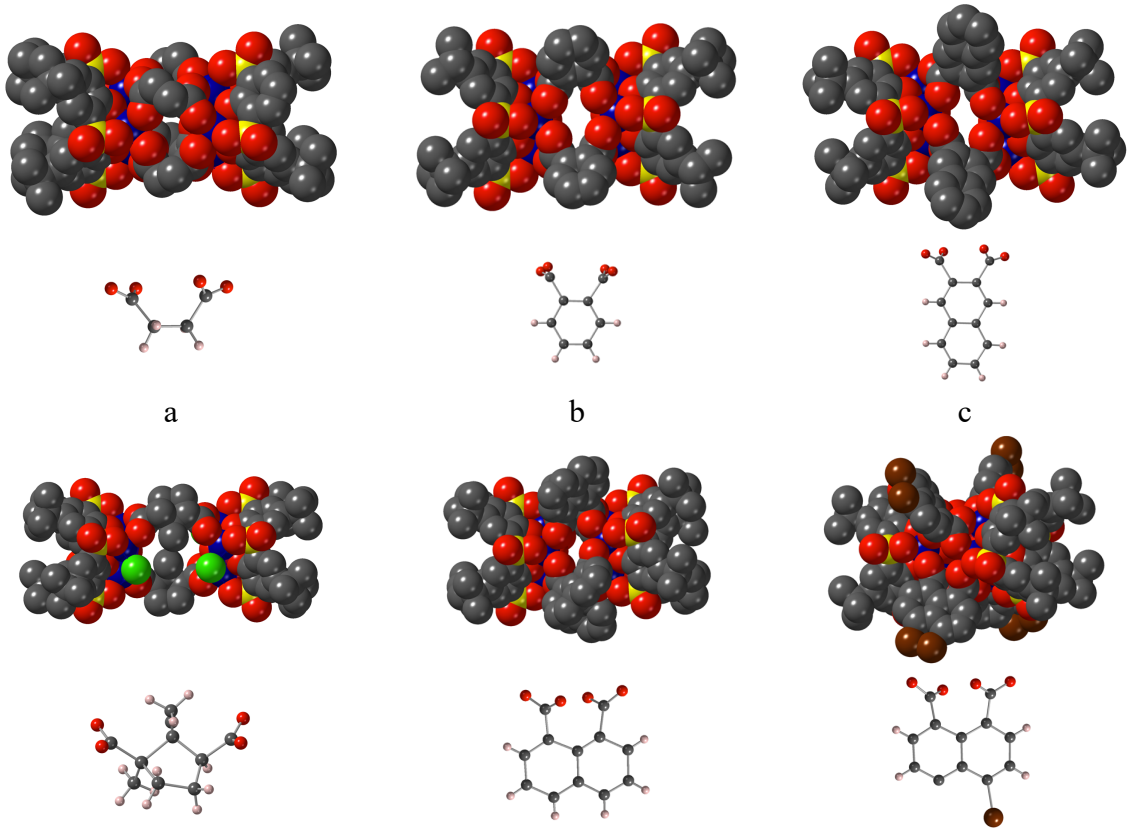

Figure 28: A portion of the X-ray structure of the neutral {M_8}-MOCs pocket-like compounds (a) $[(SO_2TCA)_2M^{II}_8(\mu\text{-}H_2O)_2][(SUC)_4]$ (M = Co, Ni) (SUC = succinate dianion), (b) $[(SO_2TCA)_2M^{II}_8(\mu\text{-}H_2O)_2][(OBDC)_4]$ (M = Co, Ni) (OBDC = 1,2-benzenedicarboxylate dianion), (c) $[(SO_2TCA)_2M^{II}_8(\mu\text{-}OH)_2][(NDC)_4]$ (M = Co, Ni) (NDC = naphthalenedicarboxylate dianion) (d) chiral $[Co^{II}_8(SO_2TCA)_2(CAM)_2(\mu_4\text{-}H_2O)_2Cl_4]$ (CAM = chiral (1R,3S)-(+)-camphorate dianion) (e) $[(SO_2TCA)_2Co^{II}_8(\mu\text{-}H_2O)_2][(NDC\text{-}H)_4]$ (NDC-H = 1,8-naphthalenedicarboxylate dianion) and (f) $[(SO_2TCA)_2Co_8{}^{II}(\mu\text{-}H_2O)_2][(NDC\text{-}Br)_4]$ (NDC-Br = 4-bromo-1,8-naphthalenedicarboxylate dianion); Solvent molecules are not presented for the sake of clarity, disordered Br atoms are presented for (f). Adapted from Ref. [83], [84], [85] and [86]

Longer coordinating ligands have been used, leading to species with larger cavities.

Under solvothermal conditions, H_4SO_2TCA, $M(NO_3)_2•6H_2O$ (M = Co or Ni) and 4,4'-methylenedibenzoic acid (H_2MDB), 4-((4-carboxybenzyl)amino)benzoic acid (H_2CBAB) or

4,4'-(azanediylbis(methylene))dibenzoic acid (H_2ADBD), isoreticular {M_8}-MOCs of formula $[(SO_2TCA)_2Co^{II}_8(\mu\text{-}H_2O)_2][(MDB)_4]$, $[(SO_2TCA)_2Co^{II}_8(\mu\text{-}H_2O)_2][(CBAB)_4]$ or $[(SO_2TCA)_2Ni^{II}_8(\mu\text{-}H_2O)_2][(ADBD)_4]$ were reported [87], together with their catalytic activities (§ 6. 3. and table 3) and molecular recognition properties (§ 6. 4. and table 4). They are based on the fusing of 2 the $[M^{II}_4(\mu_4\text{-}H_2O)SO_2TCA]^{4+}$ (M = Co or Ni) shuttlecock-like units by four dibenzoate fragments (Figure 29 a-c). An analogous compound presenting the same recognition pattern, and of formula $[(SO_2TCA)_2Zn^{II}_8(\mu\text{-}H_2O)_2][(MDB)_4]$ was reported [88]. The Ni(II) analogue [89] was also reported, and its gas and solvent adsorption properties were investigated (§ 6. 2. and table 2).

By mixing, under solvothermal conditions, H_4SO_2TCA, 4-carboxy-1-(4-carboxybenzyl)pyridinium bromide (H_2CBPyBr) and corresponding nitrate hexahydrate, neutral {M_8}-MOCs of formula $[(SO_2TCA)_2M^{II}_8(\mu\text{-}OH)_2][(CBPy)_4]$ (M = Co and Ni) [90] and $[(SO_2TCA)_2Zn^{II}_8(\mu\text{-}OH)_2][(CBPy)_4]$ [91] were reported (Figure 29 d). Their formation is based on the bridging of 2 $[M^{II}_4(\mu_4\text{-}OH)SO_2TCA]^{3+}$ (M = Co, Ni and Zn) shuttlecock-like units by four dicarboxylate $CBPy^-$ moieties (pyridine is a protonated species). The obtained MOCs were studied for their electrocatalytic activity in the oxygen evolution reaction (§ 6. 3. and table 3) and also host-guest interactions (§ 6. 4. and table 4).

Using more bulky dicarboxylic ligands, like 2,7,9-triphenyl-9H-carbazole-3,6-dicarboxylic acid (H_2TPCD) a series of isomorphous {M_8}-MOCs of formula $[(SO_2TCA)_2M^{II}_8(\mu\text{-}X)_2][(TPCD)_4]$ (M = Mg, Mn, Co, and Ni; X = OMe; H_2O) (Figure 29 e-f) were reported [92]. All four compounds share almost the same coordination pattern: 2 $[M^{II}_4(\mu_4\text{-}X)SO_2TCA]^{4+}$ (M = Mg, Mn, Co, and Ni; X = OMe; H_2O) shuttlecock-like units connected by four $TPCD^{2-}$ dianions), with minor differences in μ_4-X fragments positions of the shuttlecock-like units: for {Co_8}-MOC, X was coordinated methanol molecules; for {Ni_8} and {Mn_8}-MOCs water molecules were refined (X = H_2O); the nature of the μ_4-X shared between metal ions atom disposed in the centre of {Mg^{II}_4} clusters of MOC was not unambiguously defined. The gas sorption properties of the compounds (§ 6. 2. and table 2) were thoroughly investigated.

Finally, it is interesting to note that the use of a dicarboxylic macrocyclic linker based on a calix[4]arene (dccalix) in combination with H_4SO_2TCA leads to formation of two compounds of formula $(dccalix)_2(SO_2TCA)_2(M^{II}_3(\mu\text{-}OH_2)_2)_2(DMF)_2$ (M = Co and Ni), and presenting a hollow cyclic shape were obtained, and reported by our team [93] (Figure 29 g). Their formation results from the fusing of 2 $[M^{II}_3(\mu_4\text{-}H_2O)_2(DMF)SO_2TCA]^{2+}$ (M = Co and Ni) shuttlecock-like units by a calix[4]arene moiety presenting two available carboxylate groups. The compound present interesting solvent vapours properties (§ 6. 2. and table 2).

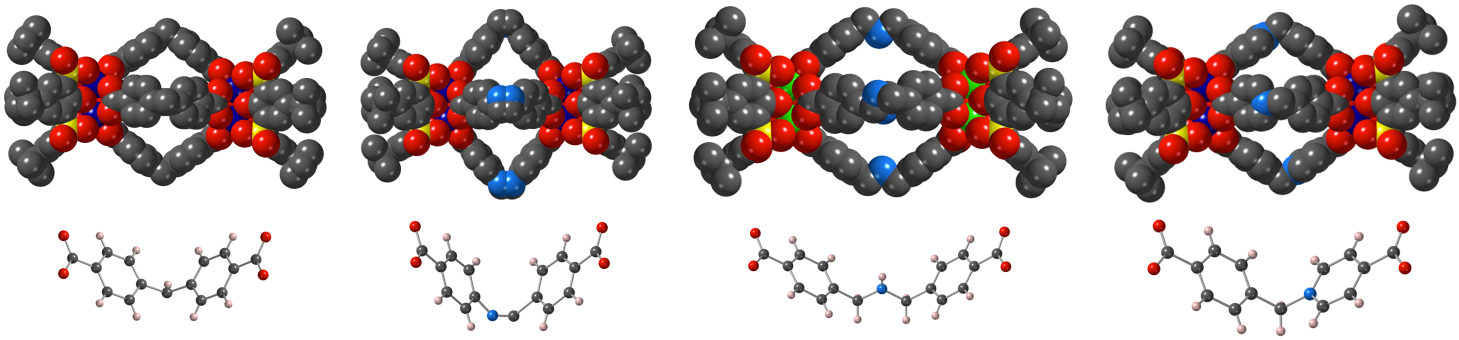

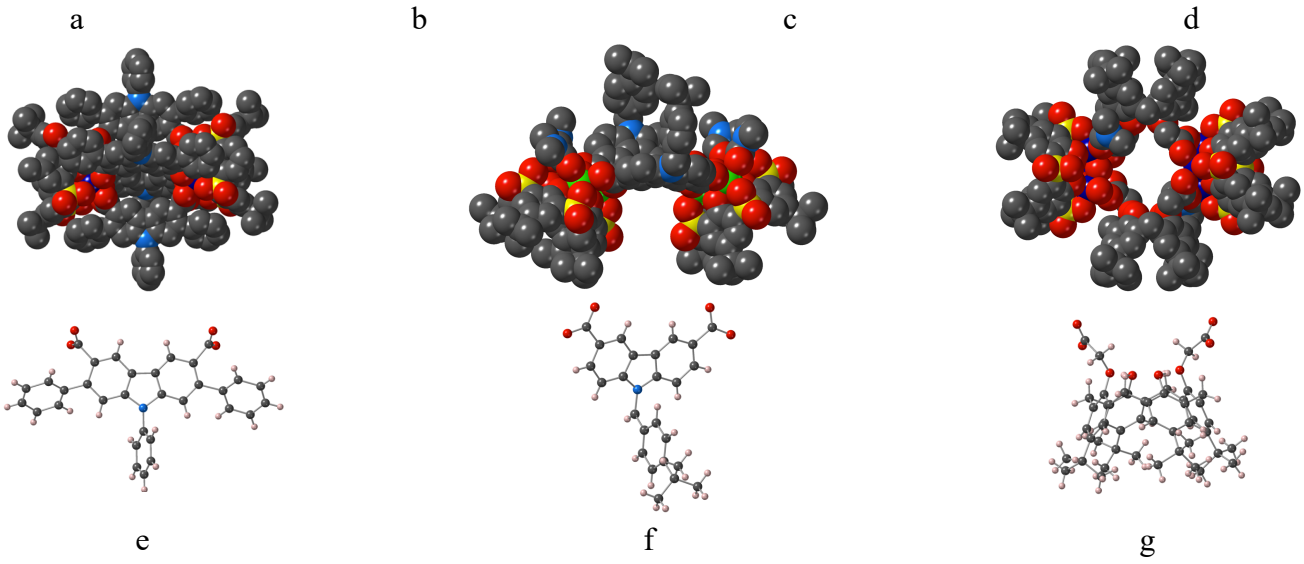

Figure 29: A portion of the X-ray structure of the neutral {Mn_8}-MOCs pocket-like compounds (a) $[(SO_2TCA)_2M^{II}_8(\mu\text{-}H_2O)_2][(MDB)_4]$ (M = Co, Ni and Zn) and MDB = 4,4'-methylenedibenzoate dianion (b) $[(SO_2TCA)_2Co^{II}_8(\mu\text{-}H_2O)_2][(CBAB)_4]$, CBAB = 4-((4-carboxybenzyl)amino)benzoate dianion (c) $[(SO_2TCA)_2Ni^{II}_8(\mu\text{-}H_2O)_2][(ADBD)_4]$ ADBD = 4,4'-(azanediylbis(methylene))dibenzoate dianion, (d) $[(SO_2TCA)_2M^{II}_8(\mu\text{-}OH)_2][(CBPy)_4]$ (M = Co, Ni and Zn) (CBPy = monoanion derived from 4-carboxy-1-(4-carboxybenzyl)pyridinium) (e) and (f) $[(SO_2TCA)_2M^{II}_8(\mu\text{-}X)_2][(TPCD)_4]$ (M = Mg, Mn, Co, and Ni; X = OMe; H_2O) TPCD = 2,7,9-triphenyl-9H-carbazole-3,6-dicarboxylate anion and (g) $(dccalix)_2(SO_2TCA)_2(M^{II}_3(\mu\text{-}OH_2)_2)_2(DMF)_2$ dccalix: dianion derived from dicarboxyliccalix[4]arene (dccalix) and M = Co and Ni). Solvent molecules are not presented for the sake of clarity, and disorder is present in some of the compounds. Adapted from Refs. [88]-[93].

While the pocket-like compounds are built from short and flexible dicarboxylic derivatives, the square-like Metal-Organic Cages are mainly built from V-shaped 1,3 benzenedicarboxylic and tetrazole derivatives. Examples will be provided here below.

4.2.3. Square-like MOCs based on H_4TCA and isophtalate derivatives: $[M^{II}_n(TCA)_4L_8]^{p-}$ (n = 12 or 16).

Under solvothermal conditions combination of H_4TCA, $CoCl_2 \cdot H_2O$ and isophthalic acid (H_2IP) or 2,6-pyridinedicarboxylic acid (H_2PD) leaded to the anionic {M_{16}}-MOCs of formula $\{[(TCA)_4Co^{II}_{16}(\mu\text{-}Cl_4)](IP)_8\}^{4-}[(CH_3)_4N^+]_4$ (Figure 30 a) and $[(TCA)_4Co^{II}_{16}(\mu\text{-}Cl_4)](PD)_8{}^{4-}[(CH_3)_4N^+]_4$ (Figure 30 b) [94]. Both isomorphous MOCs were formed by fusing 4 $[Co^{II}_4(\mu_4\text{-}Cl)TCA]^{3+}$ shuttlecock-like units linked with IPA and PDA dicarboxylate moieties and tetramethylammonium played the compounds, gas sorption properties were investigated (§ 6. 2. and table 2) together with photothermal properties (§ 6. 5. 2.).

a b

Figure 30: A portion of the X-ray structure of the neutral square-like M_{16} compounds based on H_4TCA: (a) $[(TCA)_4Co^{II}_{16}(\mu\text{-}Cl_4)](IP)_8^{4-}$ (IP = isophtalate anion) and (b) $[(TCA)_4Co^{II}_{16}(\mu\text{-}Cl_4)](PD)_8^{4-}$ (PD = 2,6-pyridinedicarboxylate anion) Solvent molecules are not presented for the sake of clarity. Adapted from Ref. [94]

Then, isophtalate derivatives have been intensively used for the formation of new square-like compounds based on H_4TCA, that were formed from the fusing 4 $[Ni^{II}_4(\mu_4\text{-}Cl)TCA]^{3+}$ shuttlecock-like units with eight dicarboxylate anionic ligands: A $\{Ni_{16}\}$-MOC of formula $[(TCA)_4Ni^{II}_{16}(\mu\text{-}Cl)_4][(5\text{-}NH_2\text{-}1,3\text{-}BDC)_8]$ (Figure 31 a) [95] with cavity size of 12.7 × 12.7 × 12.1 $Å^3$, has been obtained under solvothermal conditions by combining H_4TCA, $NiCl_2•6H_2O$ and 5-amino-1,3-benzenedicarboxylic acid ($5\text{-}NH_2\text{-}1,3\text{-}BDCH_2$). Two similar neutral $\{Co_{16}\}$-MOCs of formulas $H_4[(TCA)_4Co^{II}_{16}(\mu\text{-}Cl)_4][(L')_8]$ and $H_4[(TCA)_4Co^{II}_{16}(\mu\text{-}Cl)_4][(L'')_8]$ (Figure 31 b and c) were also reported (L' = anion derived from 5-(pyridine-3-yl)isophthalic acid and L'' = anion derived 5-(5-fluoropyridin-3-yl)isophthalic acid) in the presence of HCl [96]. The cavity size of the compounds is 12.6 × 12.6 × 12.0 $Å^3$. Oher types of clusters were obtained by increasing the pH to basic (§ 5. 3. 3.). Porosity (§ 6. 2. and table 2) and dye adsorption (§ 6. 4. and table 4) properties were investigated for these square cages.

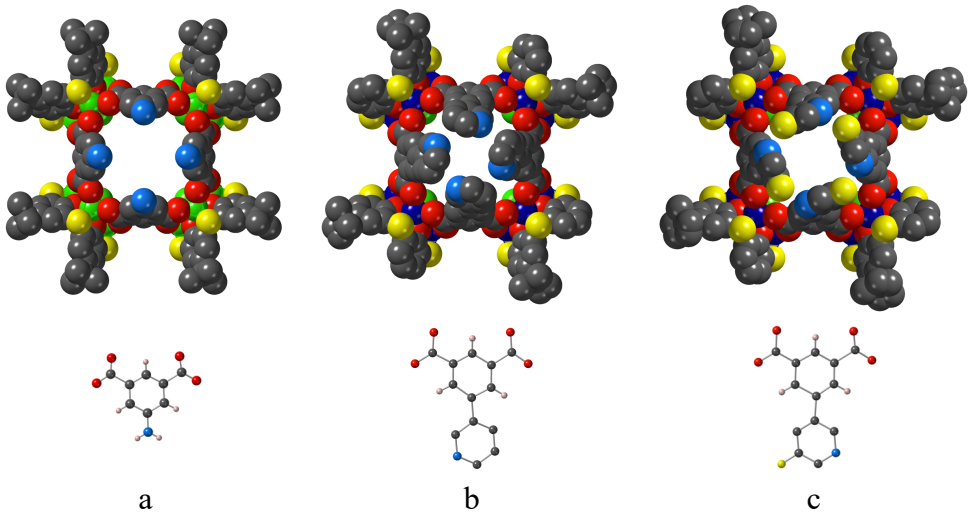

a b c

Figure 31: A portion of the X-ray structure of the neutral square-like $\{M_{16}\}$-MOCs based on H_4TCA and isophtalate derivatives: (a) $[(TCA)_4Ni^{II}_{16}(\mu\text{-}Cl)_4][(5\text{-}NH_2\text{-}1,3\text{-}BDC)_8]$ ($5\text{-}NH_2\text{-}1,3\text{-}BDC$ = anion derived from 5-amino-1,3-benzenedicarboxylic acid); (b) $H_4[(TCA)_4Co^{II}_{16}(\mu\text{-}Cl)_4][(L')_8]$ (L' = 5-(pyridine-3-yl)isophthalate anion); (c) $[(TCA)_4Co^{II}_{16}(\mu\text{-}Cl)_4][(L'')_8]$ (L'' = 5-(5-fluoropyridin-3-yl)isophthalate anion); All atoms and solvent molecules are not presented for the sake of clarity, and for (b) and (c), some *tert*-butyl groups are omitted. Adapted from Ref. [95]and [96]

4.2.4. Square-like MOCs based on H_4SO_2TCA: $[M^{II}_n(SO_2TCA)_4L_8]^{p-}$ (n = 12 or 16).

In this part, O donor linkers like isophtalate derivatives will be distinguished from N donor linkers.

4.2.4.a. The use of O donor linkers: isophtalate derivatives

Analogously to what has been obtained with H_4TCA combined with isophtalate [94], two similar $\{M_{16}\}$-MOCs of formulas $[(SO_2TCA)_4M^{II}_{16}(\mu\text{-}H_2O)_4][(1,3\text{-}BDC)_8]$ (M = Co or Ni) (Figure 32 a), which is neutral, and $[(SO_2TCA)_4M^{II}_{16}(\mu\text{-}H_2O)_4][(5\text{-}SO_3\text{-}1,3\text{-}BDC)_8]$ (M = Co or Ni) (Figure 32 b), which is anionic were reported [97], using H_4SO_2TCA, $Co(NO_3)_2{\bullet}6H_2O$ or $Ni(NO_3)_2{\bullet}6H_2O$ and 1,3-benzenedicarboxylic acid (1,3-$BDCH_2$) or 5-sulfo-1,3-benzenedicarboxylic acid (5-SO_3-1,3-$BDCH_2$) under solvothermal conditions. In general, they have been built from the bridging of 4 $[M^{II}_4(\mu_4\text{-}H_2O)SO_2TCA]^{4+}$ (M = Co or Ni) shuttlecock-like units by benzenedicarboxylate moieties. Porosity (§ 6. 2. and table 2) and dye adsorption properties (§ 6. 4 and table 4) were investigated for these cages (Cavity size 13.7 × 13.7 × 10.3 $Å^3$). These cages were also reported to be attached *via* click chemistry, on surfaces and their porous properties were then investigated (§ 6. 2. and table 2) [98].

A whole series of very similar neutral $\{M_{16}\}$ MOCs (M = Co or Ni) have been reported with other derivatives of isophtalic acid: 5-methyl-1,3-benzenedicarboxylic acid (5-Me-1,3-BDC), 5-hydroxy-1,3-benzenedicarboxylic acid (5-OH-1,3-BDC), 5- bromo-1,3-benzenedicarboxylic acid, 5-propoxy-1,3-benzenedicarboxylic acid and 5-heptoxyoxyisophthalic acid with general formula $[(SO_2TCA)_4M^{II}_{16}(\mu\text{-}H_2O)_4][L_8]$ [99] (Figure 32 c). However, they present the same connectivity pattern as presented for the aforementioned examples [97]. N_2 and CO_2 adsorption properties were investigated for these MOCs (§ 6. 2. and table 2) (Cavity size 13.8 × 13.8 × 11.7 $Å^3$).

Another $\{Co^{II}_{16}\}$ MOC, presenting the same connectivity pattern as discussed above, and based on 5-(prop-2-yn-1-yloxy)isophthalic acid (5-Pr-1,3-BDC) linker, of formula $[(SO_2TCA)_4Co^{II}_{16}(\mu\text{-}H_2O)_4][(5\text{-}Pr\text{-}1,3\text{-}BDC)_8]$, has been reported (Figure 32 d) [100]. In addition, authors reported the post-synthetic modification with the use of alkyne-azide cycloaddition reactions, starting from a compound of formula $[(SO_2TCA)_4Co^{II}_{16}(\mu\text{-}H_2O)_4][(5\text{-}N_3\text{,}1,3\text{-}BDC)_8]$ (Figure 32 e) (Cavity size 13.9 × 13.9 × 11.9 $Å^3$).

A structurally similar $\{Zn_{16}\}$-MOC based on ionic 5-[(3-methyl-imidazol-1-yl) chloride]-1,3-benzene-dicarboxylate linker ($(5\text{-}Me\text{-}im\text{-}1,3\text{-}BDC)^+(Cl^-)$) of formula $[Zn^{II}_4(SO_2TCA)(\mu_4\text{-}OH)]_4\text{-}(5\text{-}Me\text{-}im\text{-}1,3\text{-}BDC)_8Cl_8$ was reported [101] (Figure 32 f). It is important to note that, for this compound, the imidazole moiety doesn't belong to the coordination pattern; the cavity size of this compound is 14.4 × 13.9 × 11.8 $Å^3$. The obtained MOC was post-modified in order to obtain porous liquid metal-organic cage able to be involved in drug delivery (§ 6. 5. 3.).

Very recently, $\{Co_{16}\}$-MOCs and $\{Mg_{16}\}$-MOCs were obtained by postsynthetic modification from the 5-bromoisophthalic acid [102]. New square-like compounds were obtained $[(SO_2TCA)_4M^{II}_{16}(\mu\text{-}H_2O)_4][(5\text{-}N\text{-}1,3\text{-}BDC)_8]$(M = Co or Mg, 5-Ac-1,3-BDC = 5-amino isophthalate anion), $[(SO_2TCA)_4Co^{II}_{16}(\mu\text{-}H_2O)_4][(5\text{-}Ac\text{-}1,3\text{-}BDC)_8]$ (5-Ac-1,3-BDC = 5-Acetylamide isophthalate anion) and (i) $(SO_2TCA)_4Mg^{II}_{16}(\mu\text{-}H_2O)_4][(5\text{-}hex\text{-}1,3\text{-}BDC)_8]$ 5-Hexanoylamide isophthalate anion). They present similar cavity size, and their porous properties were investigated. (§ 6. 2. and table 2)

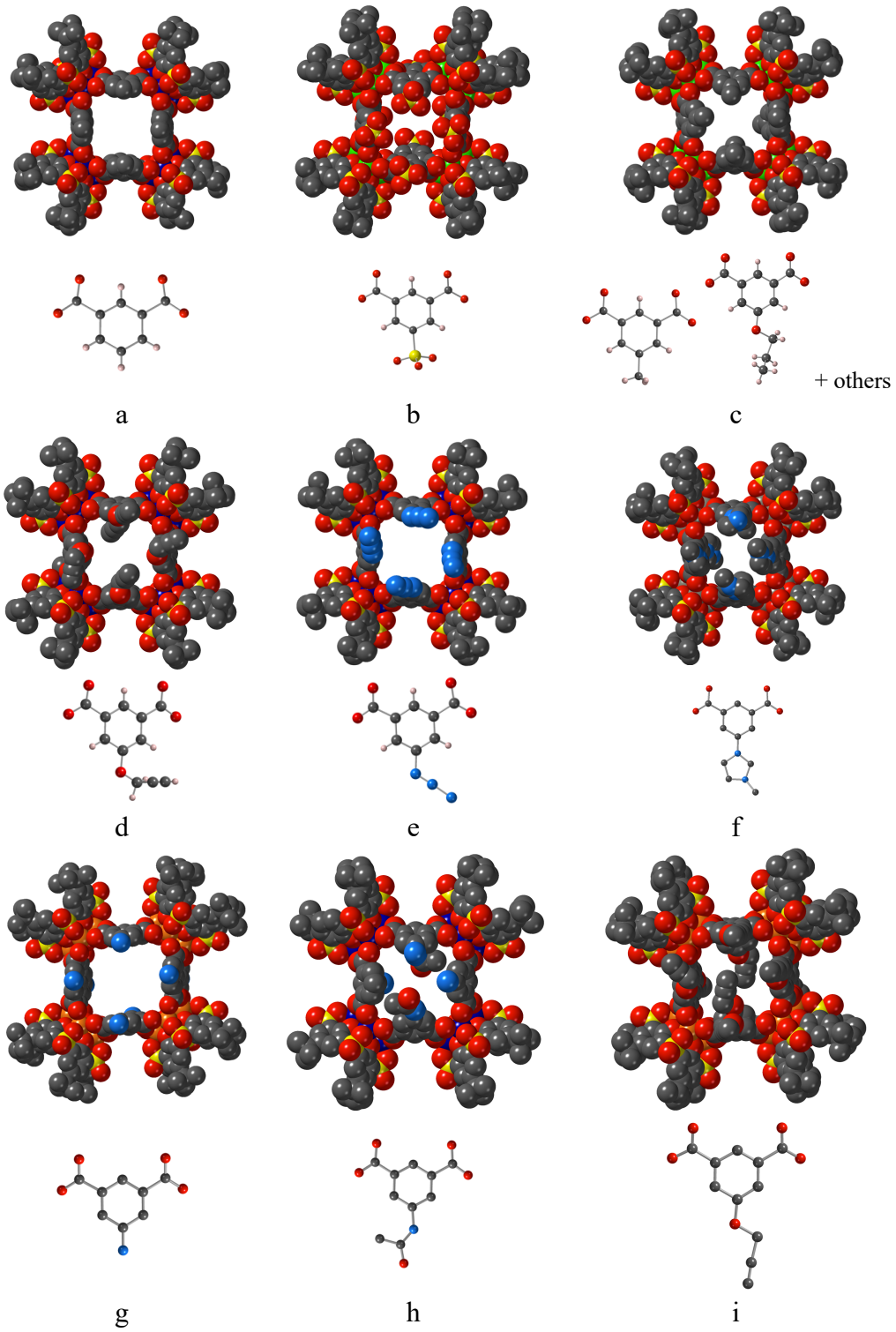

Figure 32: A portion of the X-ray structure of square-like {M_{16}}-MOCs based on H_4SO_2TCA and isophtalate derivatives: (a) $[(SO_2TCA)_4M^{II}_{16}(\mu\text{-}H_2O)_4][(1,3\text{-}BDC)_8]$ (M = Co or Ni) (1,3-BDC =1,3-benzenedicarboxylate anion), (b) $[(SO_2TCA)_4M^{II}_{16}(\mu\text{-}H_2O)_4][(5\text{-}SO_3\text{-}1,3\text{-}BDC)_8]$ (M = Co or Ni) (5-SO_3-1,3-BDC =5-sulfo-1,3-benzenedicarboxylate anion) (c) $[(SO_2TCA)_4M^{II}_{16}(\mu\text{-}H_2O)_4][L_8]$ (M = Co or Ni) with L = 5-methyl-1,3-benzenedicarboxylate anion, (5-Me-1,3-BDC), 5-hydroxy-1,3-benzenedicarboxylate anion (5-OH-1,3-BDC), 5-bromo-1,3-benzenedicarboxylate anion, 5-propoxy-1,3-benzenedicarboxylate anion and 5-heptoxyoxyisophthalate anion, (d) $[(SO_2TCA)_4Co^{II}_{16}(\mu\text{-}H_2O)_4][(5\text{-}Pr\text{-}1,3\text{-}BDC)_8]$ (5-Pr-1,3-BDC =5-(prop-2-yn-1-yloxy)isophthalate anion), (e) $[(SO_2TCA)_4Co^{II}_{16}(\mu\text{-}H_2O)_4][(5\text{-}A\text{-}BDC)_8]$ (5-A-BDC =5-azidoisophthalate anion); (f) $[Zn^{II}_4(SO_2TCA)(\mu_4\text{-}OH)]_4\text{-}(5\text{-}Me\text{-}im\text{-}1,3\text{-}BDC)_8Cl_8$, 5-Me-im-1,3-BDC = 5-[(3-methyl-imidazol-1-yl)

chloride]−1,3-benzene-dicarboxylate, (g) $[(SO_2TCA)_4M^{II}_{16}(\mu\text{-}H_2O)_4][(5\text{-}N\text{-}1,3\text{-}BDC)_8]$(M = Co or Mg) (5-Ac-1,3-BDC = 5-amino isophthalate anion)), (h) $(SO_2TCA)_4Co^{II}_{16}(\mu\text{-}H_2O)_4][(5\text{-}Ac\text{-}1,3\text{-}BDC)_8]$ (5-Ac-1,3-BDC = 5-Acetylamide isophthalate anion)) and (i) $(SO_2TCA)_4M^{II}_{16}(\mu\text{-}H_2O)_4][(5\text{-}hex\text{-}1,3\text{-}BDC)_8]$(M = Co or Mg) 5-Hexanoylamide isophthalate anion. H-atoms and solvent molecules are not presented for the sake of clarity. Adapted from Ref. [97], [99], [100] [101] and [102].

MOCs based on longer dicarboxylic isophtalate derivatives (except one) will be described here below.

By mixing, under solvothermal conditions, H_4SO_2TCA, $Zn(NO_3)_2$ and 5,5-(*p*-phenylene-*bis*-(methanamino)-di-isophthalic acid (H_4PMTC) a neutral MOC of formula $[(SO_2TCA)_4Zn^{II}_{16}(\mu\text{-}H_2O)_4][PMTC]_4$ (Figure 33 a) was obtained [103]. This $\{Zn_{16}\}$-MOC is based on the fusing of 4 $[Zn^{II}_4(\mu_4\text{-}H_2O)SO_2TCA]^{4+}$ shuttlecock-like units connected with four O-donor linkers of 5,5-(*p*-phenylene-*bis*-(methanamino)-di-isophthalate; This is a very unusual stoichiometry, obtained due to the steric hindrance imposed by the ligand. Remarkably, one fragment of linker is coordinating three shuttlecock-like units, leading to a cube-shaped compound, this is the only example found in the literature, related with its flexibility and long size, and thus the cavity size is *ca.* 13.7 × 14.4 × 14.0 $Å^3$. Targeted drug delivery properties were investigated for this compound (§ 6. 5. 3.)

Using H_4SO_2TCA, [5-(pyren-1-ylmethyl)amino]isophthalic acid (H_2PIP) and $Co(NO_3)_2•6H_2O$ or $M(NO_3)_2•6H_2O$, a series of $\{M_{16}\}$-MOCs of formula $[(SO_2TCA)_4M^{II}_{16}(\mu\text{-}H_2O)_4][PIP]_8$ (M = Co, Zn) (Figure 33 b) was obtained [104]. They all present the same coordination pattern as already observed for other square like compounds (4 $[M^{II}_4(\mu_4\text{-}H_2O)SO_2TCA]^{4+}$ shuttlecock-like units + 8 coordinating ligands) with cavity size of *ca.* 14.0 × 13.2 × 13.3 $Å^3$, but the cavity appears less accessible, due to steric hindrance. The proton recognition properties of the compounds were studied (§ 6. 4. and table 4).

Finally, an unexpected neutral isostructural $\{M_{16}\}$-MOC of formula $[(SO_2TCA)_4M^{II}_{16}(\mu\text{-}H_2O)_4][AQ]_8$ (M = Co, Ni and Zn) (Figure 33 c) were obtained under solvothermal conditions with the use of H_4SO_2TCA, 9,10-dihydro-9,10-dioxo-2,7-anthracenedicarboxylic acid (H_2AQ) and the corresponding metal nitrate [105]; They are presenting the same coordination pattern as already observed for other square like compounds (4 $[M^{II}_4(\mu_4\text{-}H_2O)SO_2TCA]^{4+}$ shuttlecock-like units + 8 coordinating ligands). The used ligand doesn't present the same characteristics as the other ligands used for the formation of square-like compounds, but still a compound with large open cavities (*ca.* 20.9 × 20.9 × 11.9 $Å^3$) is formed. The photocatalytic activity of some of the compounds was determined (§ 6. 3. and table 3).

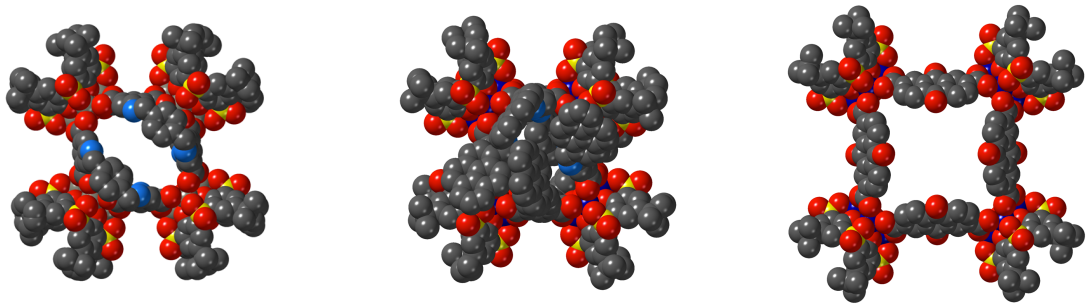

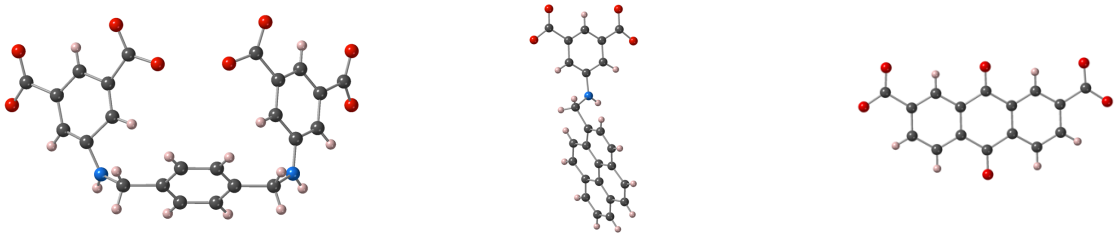

a b c

Figure 33: A portion of the X-ray structure of neutral square-like {M_{16}}-MOCs based on H_4SO_2TCA (a) $[(SO_2TCA)_4Zn^{II}_{16}(\mu\text{-}H_2O)_4][PMTC]_4$ (PTMC = 5,5-(*p*-phenylene-*bis*-(methanamino)-di-isophthalate anion) (b) $[(SO_2TCA)_4M^{II}_{16}(\mu\text{-}H_2O)_4][PIP]_8$ (M = Co and Zn and PIP = [5-(pyren-1-ylmethyl)amino]isophthalate anion) (c) $[(SO_2TCA)_4M^{II}_{16}(\mu\text{-}H_2O)_4][AQ]_8$ (M = Co, Ni and Zn and PIP = 9,10-dihydro-9,10-dioxo-2,7-anthracenedicarboxylate anion). Solvent molecules are not presented for the sake of clarity. Adapted from Ref. [103], [104] and [105]

4.2.4.b. The use of tri and tetrazolate N donor linkers

Only two examples have been provided using H_4SO_2TCA and N-donor ligands.

A cationic charged {Co_{16}}-MOC, obtained in solvothermal conditions from H_4SO_2TCA, $Co(acac)_2$ and 5-amino-1*H*-tetrazole (5-NH_2-tzH) of formula $[(SO_2TCA)_4Co^{II}_{12}(\mu\text{-}MeOH)_2(MeOH)_4][(5\text{-}NH_2\text{-}tz)_8]^{4+}$ has been reported [67] (Figure 34 a). It is built from two different shuttlecock-like units: a rarely observed $[Co^{II}_3(\mu_4\text{-}MeOH)SO_2TCA]^{3+}$ and $[Co^{II}_3(MeOH)_2SO_2TCA]^{3+}$ bridged by eight 5-amino-1*H*-tetrazole N-donor angular linkers. The routine magnetic properties of the compound have been presented (§ 6. 1. 1. and table 1).

Recently, three isostructural {M_{16}}-MOCs of formula $[(SO_2TCA)_4M^{II}_{16}(\mu\text{-}H_2O)_4][BTT]_8$ (M = Co, Fe and $Co_{0.5}Fe_{0.5}$) (Figure 34 b) (of them is heterometallic) were obtained under solvothermal conditions while combining H_4SO_2TCA, $CoCl_2{\bullet}6H_2O$ or $FeCl_3{\bullet}6H_2O$ and 1,3-*bis*-(2*H*-tetrazol-5-yl)benzene (H_2BTT) [106]. They are presenting the same coordination pattern as already observed for other square like compounds (4 shuttlecock-like units + 8 coordinating ligands). The activity for the oxygen evolution reaction was investigated (§ 6. 3. and table 3). Very recently a similar anionic square-like {Co_{16}}-MOC of formula $[(SO_2TCA)_4Co^{II}_{16}(\mu_4\text{-}OH)_4][BDT]_8]^{4-}$ has been obtained in the same conditions starting from 1,3-*bis*-(1*H*-1,2,3-triazol-5-yl)benzene (H_2BDT) [107]. N_2, H_2, CH_4 and CO_2 adsorption properties were investigated for this anionic square-like MOC (§ 6. 2. and table 2)

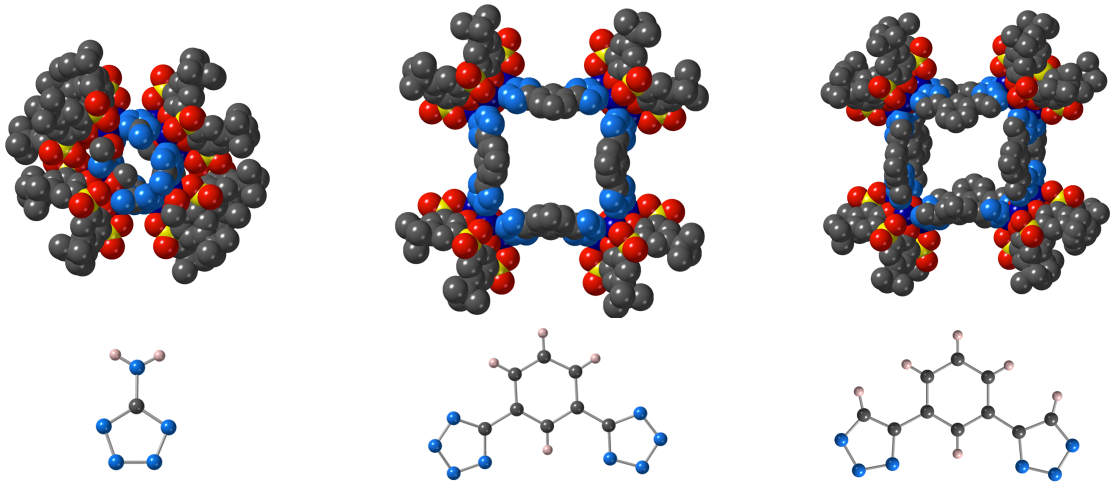

a b c

Figure 34: A portion of the X-ray structure of square-like compounds based on H_4SO_2TCA (a) Co_{12} cationic $\{[(SO_2TCA)_4Co^{II}_{12}(\mu\text{-}MeOH)_2(MeOH)_4][(5\text{-}NH_2\text{-}tz)_8]\}$ (5-NH_2-tz=5-amino-1*H*-tetrazolate anion) and (b) neutral M_{16} $[(SO_2TCA)_4M^{II}_{16}(\mu\text{-}H_2O)_4][BTT]_8$ (M = Co, Fe and $Co_{0.5}Fe_{0.5}$ BTT= *bis*(2*H*-tetrazol-5-yl)benzene) and (c) anionic $[(SO_2TCA)_4Co^{II}_{16}(\mu_4\text{-}OH)_4][BDT]_8]^{4-}$ BDT = 1H 1,2,3-triazol-5-yl)benzene. Solvent molecules are not presented for the sake of clarity. Adapted from Ref. [67], [106] and [107].

4.3. Octahedral and deformed Octahedral thiacalix[4]arene based MOCs

The calix[4]arene based $\{M_{24}\}$-MOCs (Molecular Coordination cages) displaying octahedral geometries are obtained when thiacalix[4]arene (H_4TCA) or sulfonylcalix[4]arene (H_4SO_2TCA) derivatives are used in combination with di- or tritopic carboxylate organic or metal-organic linkers, generally possessing a the rigid molecular scaffold, in presence of divalent M^{II} cations (M = Fe^{II}, Co, Ni, Zn, Mg). In all cases, the tetranuclear $[M^{II}_4YTCA]^{4+}$ (Y = -, D, P, SO_2, see also figure 3) shuttlecock-like units (Figure 35), acting as *tetrakis*-connecting node, are involved for the construction of porous supramolecular architecture with calix[4]arene: linker ratio, equal to 6:12 or 6:8 for edge or face-linked octahedra, respectively. The formed species present the following formula: $\mathbf{[M^{II}_{24}(\mu_4\text{-}X)_6(YTCA)_6L_{12}]^{6-}}$ (X = Cl or OH) $\mathbf{[M^{II}_{24}(\mu_4\text{-}H_2O)_6(YTCA)_6L_{12}]}$ for edge-linked species (Figure 36) or $\mathbf{[M^{II}_{24}(\mu_4\text{-}X)_6(YTCA)_6L_8]^{6-}}$ (X = Cl or OH) $\mathbf{[M^{II}_{24}(\mu_4\text{-}H_2O)_6(YTCA)_6L_8]^{+}}$ (Y = -, D, P, SO_2) for face-linked species (Figure 42), where L are a di- or tritopic ligands and Y represents the TCA derivatives shown in Figure 35.

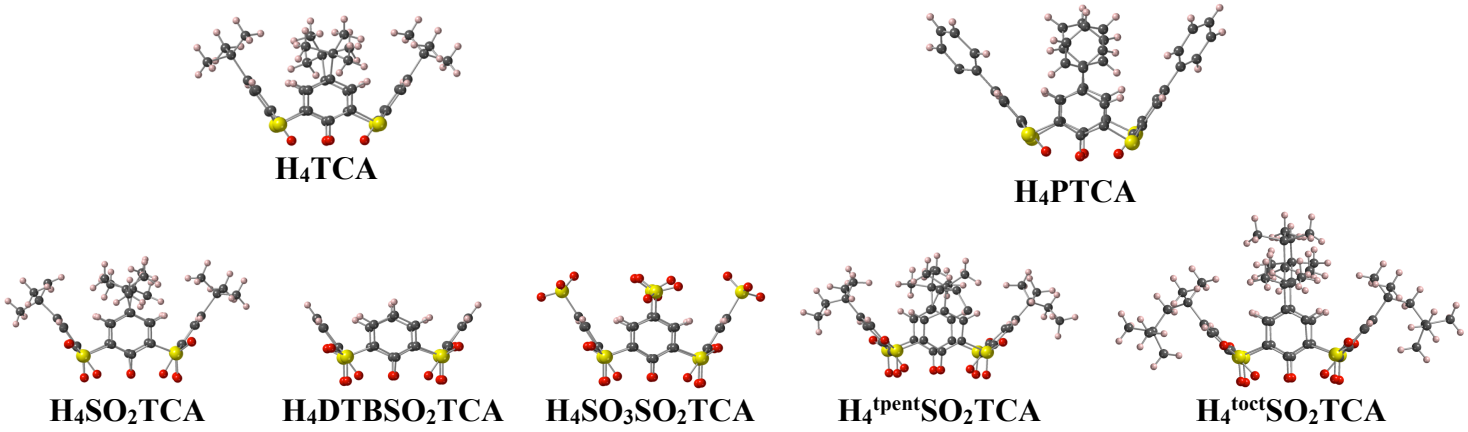

Figure 35: Schematic representation of the TCA derivatives used for the formation of octahedral cages

In this part, all the reported compounds present the same coordination pattern. The synthesis of such coordination species will not be discussed and is based on solvothermal reactions of metal salts, corresponding thiacalix[4]arene and the ligand in stochiometric conditions in DMF. For these compounds, there are several applications, and especially gas sorption properties due to their intriguing structure, displaying tuneable pore size. (see § 6. 2.)

4.3.1. The use of ditopic carboxylate linkers: $[M^{II}_{24}(\mu_4\text{-}X)_6(YTCA)_6L_{12}]^{6-}$ (X = Cl or OH) $[M^{II}_{24}(\mu_4\text{-}H_2O)_6(YTCA)_6L_{12}]$

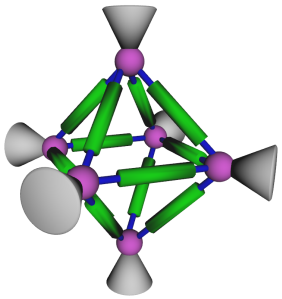

Figure 36: Schematic representation of octahedral cages $[M^{II}_{24}(\mu_4\text{-}X)_6(YTCA)_6L_{12}]^{6-}$ (X = Cl or OH) $[M^{II}_{24}(\mu_4\text{-}H_2O)_6(YTCA)_6L_{12}]$

4.3.1.a. H_4TCA and terephthalate based anionic MOCs

The only examples of anionic octahedral cage of anion type, involving thiacalix[4]arene-cobalt^{II} clusters and terephthalate anion (1,4-BDC^{2-}) as linear ditopic organic linker was reported by Hong *et al* in 2012 [108]. The compound presents the formula $[Co^{II}_{24}(\mu_4\text{-}Cl)_6(TCA)_6(1,4\text{-}BDC)_{12}]^{6-}$ (Figure 37 a), and displays a spheric cavity volume of *ca*. 700 A^3 and height triangular portals with side length of *ca*. 6.5 Å. Some gas sorption measurements were performed (§ 6. 2. and table 2).

Using a Fe(II) salt instead of a Co(II) salt, a similar compound of formula $[Fe^{II}_{24}(\mu_4\text{-}Cl)_6(SO_2TCA)_6(1,4\text{-}BDC)_{12}]^{6-}$ (Figure 37 b) was synthesized [109] that also present some interesting gas sorption properties (§ 6. 2. and table 2).

These are the only examples of compounds of formula $[M^{II}_{24}(\mu_4\text{-}Cl)_6(TCA)_6L_{12}]^{6-}$ based on TCA.

4.3.1.b. H_4SO_2TCA and terephthalate derivatives based MOCs

Switching to the more coordinating SO_2TCA, a large variety of octahedral compounds is obtained.

A neutral cage of formula $[Co^{II}_{24}(\mu_4\text{-}H_2O)_6(SO_2TCA)_6(1,4\text{-}BDC)_{12}$ was generated using sulfonylcalix[4]arene (H_4SO_2TCA) [110] (Figure 37 c), and an analogous compound based on Ni(II) was also reported [99]. Moreover, similar coordination compounds of general formula $[M^{II}_{24}(\mu_4\text{-}H_2O)_6(Y)_6(1,4\text{-}BDC)_{12}]$ (M= Co, Ni or Mg), involving upper rim derivatives of sulfonylcalix[4]arene (Y), decorated with p-*tert*-butyl (SO_2TCA), p-*tert*-pentyl ($^{tpen}SO_2TCA$) and p-*tert*-octyl ($^{toct}SO_2TCA$) groups (see TCA derivatives Figure 35), were also prepared (Figure 37 d) [110]. For these compounds, the size of the cavity is *ca.* 16.9 × 16.9 × 16.9 Å^3 and they have demonstrated a high adsorption capacity towards methylene blue and aspirin molecules in solution as well as in the solid state (§ 6. 4. and table 4). Their gas sorption properties were reported (§ 6. 2. and table 2).

A novel approach to access tuneable assemblies of MOCs in two-dimensional thin films was implemented using a chloroform solution of $[Co^{II}_{24}(\mu_4\text{-}H_2O)_6(SO_2TCA)_6(1,4\text{-}BDC)_{12}]$ deposited onto air-water interface [111]. The orientation of MOCs molecules within the Langmuir films was revealed to be strongly dependent from the acidity of the aqueous subphase.

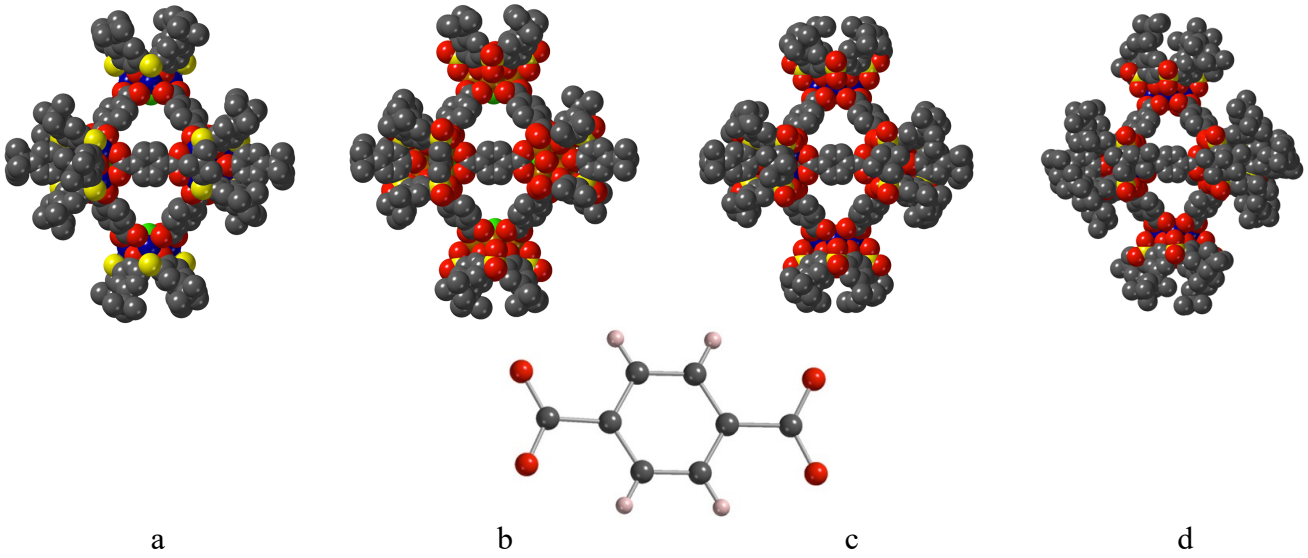

Figure 37: A portion of the X-ray structure of {M_{24}}-MOCs octahedral cages of general formula [Co^{II}_{24}(μ_4-X)$_6$(YTCA)$_6$(1,4-BDC)$_{12}$] based on terephthalate anions (1,4-BDC) and TCA derivatives (Y = -, D, P, SO_2, see figure 3) (a) H_4TCA, leading to the anionic cage [Co^{II}_{24}(μ_4-Cl)$_6$(TCA)$_6$(1,4-BDC)$_{12}$]$^{6-}$, (b) H_4SO_2TCA leading to the anionic cage [Fe^{II}_{24}(μ_4-Cl)$_6$(SO_2TCA)$_6$(1,4-BDC)$_{12}$]$^{6-}$; (c) H_4SO_2TCA leading to the neutral cage [Co^{II}_{24}(μ_4-H_2O)$_6$(SO_2TCA)$_6$(1,4-BDC)$_{12}$] and (d) $H_4{}^{toct}SO_2$TCA leading to the neutral cage [Co^{II}_{24}(μ_4-H_2O)$_6$($^{toct}SO_2$TCA)$_6$(1,4-BDC)$_{12}$. Solvent molecules are not presented for the sake of clarity. Adapted from Ref. [108], [109] and [110].

Then series of isoreticular sulfonylcalix[4]arene-capped porous octahedral coordination cages were obtained using the functionalized derivatives of terephthalate anion: 2-bromo- [99], 2,5- dihydroxy - [99], 2,3-dihydroxy- [112], 2-amino- [113], 2-imidazolyl- [114] substituents on 1,4 dibenzoate anions, giving rise to neutral compounds displaying the following formula [M^{II}_{24}(μ_4-H_2O)$_6$(SO_2TCA)$_6$(L_n)$_{12}$] (M = Co, Ni, Zn; n =1-5). For all these compounds, the size of the cavities is *ca.* 17.1 × 17.1 × 17.1 Å^3. All presented examples demonstrate a high reproducibility of the supramolecular connectivity pattern: independently on the nature and size of the side-appended group, the formation of octahedral coordination cages was observed.

However, the appearance of the grafted functional groups significantly affects their properties. In particular, it is found out that the solubility of [Ni^{II}_{24}(μ_4-H_2O)(SO_2TCA)$_6$(L_n)$_{12}$] (n = 1-3) cages in DMF, chloroform, methylene chloride, acetone, THF, benzene, toluene, ethyl acetate can be significantly increased compared with the solubility of the parent [Co^{II}_{24}(μ_4-H_2O)$_6$(SO_2TCA)$_6$(1,4-BDC)$_{12}$] compound [99] [110].

The anchoring of two hydroxy groups at 2 and 3 positions of the terephthalate anion yielded to an octahedral cage [Co^{II}_{24}(μ_4-H_2O)$_6$(SO_2TCA)$_6$(2,3-dihydroxy-1,4-BDC)$_{12}$] [112] containing large channels of *ca.* 8.0 Å that enables the guest encapsulation (eosin Y and methylene blue) (§ 6. 4. and table 4) (Figure 38 a). While the anchoring of 2,5- dihydroxy on the terephthalate anion yielded a compound [Ni^{II}_{24}(μ_4-H_2O)$_6$(SO_2TCA)$_6$(2,5-dihydroxy-1,4-BDC)$_{12}$] that presents a high surface area [99] (§ 6. 2. and table 2) (Figure 38 b). The analogous compound based on 2-bromo1,4-BDC (or 2-methyl 1,4-BDC) was also reported, together with the study of its gas sorption properties [99] (§ 6. 2. and table 2) (Figure 38 c).

The insertion of amino group at the benzene ring of terephthalate resulted in the formation of a compound presenting the following formula [Zn^{II}_{24}(μ_4-H_2O)$_6$(SO_2TCA)$_6$(2-NH_2-1,4-BDC)$_{12}$], [113] which demonstrated exciting adsorption ability, achieving high Xe/Kr

separation performance (§ 6. 2. and table 2). Other related MOCs based on L = 3,3′-diamino-1,1′-biphenyl-4,4′-dicarboxylate or 3,3″-diamino-1,1′:4′,1″-terphenyl-4,4″-dicarboxylate) were reported [113] which were also investigated for their gas sorption properties (§ 6. 2. and table 2).

Positively charged octahedral cages $[M^{II}_{24}(\mu_4\text{-}H_2O)_6(SO_2TCA)_6(2\text{-}Im\text{-}1,4\text{-}BDC)_{12}]^{12+}$ [114] (M=Co, Ni) were designed (Figure 38 d), using an imidazolium substituent anchored into the side position of terephtalic acid (2-Im-1,4-BDC); I^-, Cl^- or sulphate anions were found to be present in the unit cell. The $[Co_{24}(\mu_4\text{-}H_2O)_6(SO_2TCA)_6(2\text{-}Im\text{-}1,4\text{-}BDC)_{12}]^{12+}$ cage presents high solubility in epoxides, and provided enhanced performance for CO_2 cycloaddition catalysis (§ 6. 3. and table 3).

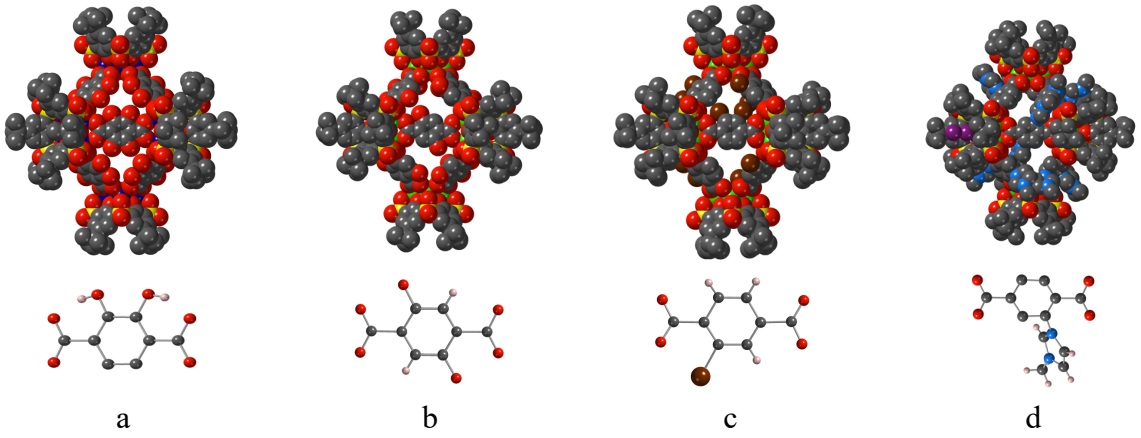

Figure 38: A portion of the X-ray structure of octahedral cages of general formula $[M^{II}_{24}(\mu_4\text{-}H_2O)_6(SO_2TCA)_6(L)_{12}]$ based (a) L = 2-bromoterephthalate anion and M = Ni; (b) 2,5-dihidroxyterephthalate anion and M = Ni (c) 2,3-dihidroxyterephthalate anion and M = Co (d) positively charged cage L = 2-imidazolylterephthalate anion and M = Ni. H atoms and solvent molecules are not presented for the sake of clarity and disorder was found for compound presented in (c) and (e) where atoms have been omitted. I-atoms are represented in violet. Adapted from Ref. [99], [114] and [112].

The use of modified ditopic organic linkers was investigated. For example, anthraquinone-1,4-dicarboxylate anionic linker (1,4-AQDC) was used, leading to the formation of a neutral compound of formula $[Co^{II}_{24}(\mu_4\text{-}H_2O)_6(SO_2TCA)_6(1,4\text{-}AQDC)_{12}]$, (Figure 39) [105]. It is interesting to note that, for this compound, the anthraquinone moiety is nonbonding and the compound presents a cavity size of 17.0 × 17.0 × 17.0 $Å^3$. This MOC exhibits a lower activity and stereoselectivity in photocatalysed cycloaddition reactions (§ 6. 3. and table 3).

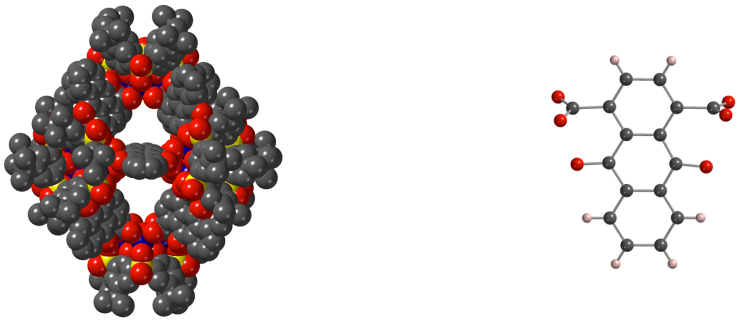

Figure 39: A portion of the X-ray structure of neutral octahedral cage of general formula $[Co^{II}_{24}(\mu_4\text{-}H_2O)_6(SO_2TCA)_6(1,4\text{-}AQDC)_{12}]$ (AQDC = anthraquinone-1,4-dicarboxylate dianion. Solvent molecules are not presented for the sake of clarity. Adapted from Ref. [105].

4.3.1.c. An example involving H_4TCA and N,O donor multitopic ligand

In 2014, an example involving the multitopic ligand 2,2′-Bipyridine-4,4′-dicarboxylic Acid (H_2bpdc) and H_4TCA was provided by Bi and Liao, which demonstrated the formation of anionic octahedral cages of formula $[[M^{II}_4(TCA)(\mu\text{-}Cl)]_2[M^{II}_4(TCA)(\mu\text{-}SO_4)]_4(bpdc)_8]^{2-}$ (M = Fe or Co) [115]. In these isostructural compounds (figure 40), 8 $bpdc^{2-}$ anions are paving the octahedral faces and two types of shuttlecock-like units are present in the cage: $[M^{II}_4(\mu_4\text{-}Cl)TCA]^{3+}$ and $[M^{II}_4(\mu_4\text{-}SO_4)TCA]^{2+}$ (M = Fe or Co), so that the cages adopt the unconventional 2^- charges. The gas sorption and magnetic properties (Co compound) of both compounds were studied.

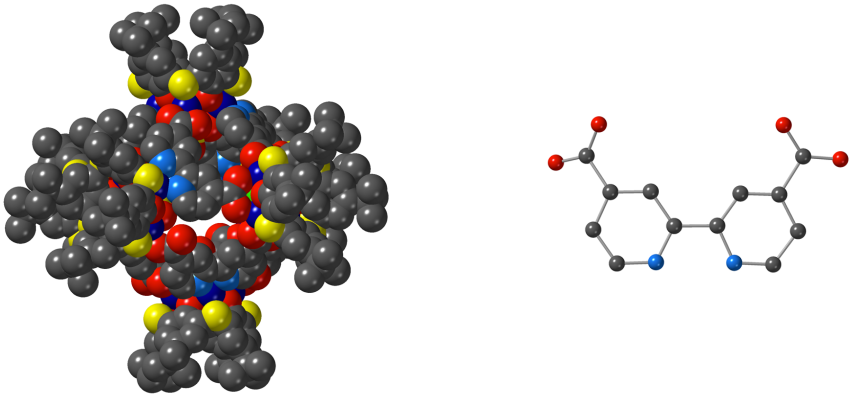

Figure 40: A portion of the X-ray structure of anionic octahedral cage of general formula $[[M^{II}_4(TCA)(\mu\text{-}Cl)]_2[M^{II}_4(TCA)(\mu\text{-}SO_4)]_4(bpdc)_8]^{2-}$ (M = Fe or Co) (bpdc = 2,2′-Bipyridine-4,4′-dicarboxylate dianion. Solvent molecules are not presented for the sake of clarity. Adapted from Ref. [115].

4.3.1.d. H_4SO_2TCA and metal-organic linker based MOC

This is the only example of metallic based ditopic ligand used for the formation of $\{Zn_{24}Mn_{12}\}$-MOC octahedral TCA-cage provided in the literature.

Using chiral metallosalen Mn(III)-based complex (MnL), bearing outward orientated carboxylate groups self-assembled with the Zn^{II}_4-sulfonylcalix[4]arene clusters afforded the formation of a neutral chiral octahedral cage of formula $[Zn^{II}_{24}(\mu_4\text{-}H_2O)_6(SO_2TCA)_6(MnL)_{12}]$ [116] (Figure 41), displaying an inner cavity size of *ca.* 28.4 × 28.4 × 28.4 Å^3 with trigonal window dimension of 18.6×18.7×19.2 Å^3 (including the van der Waals radii), which is high for octahedral cages. The permanent porosity the cage was studied through CO_2 adsorption (§ 6. 2. and table 2) and the compound reveals to present interesting enantioselective catalysis (§ 6. 3. and table 3), due to the large accessibility of the Mn centres.

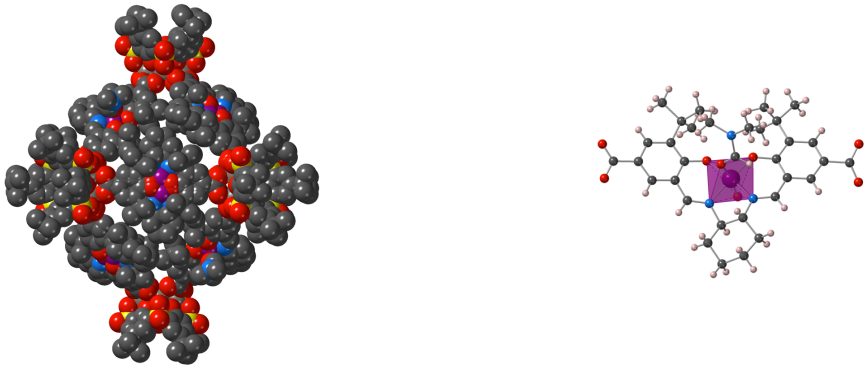

Figure 41: A portion of the X-ray structure of neutral octahedral {$Zn_{24}Mn_{12}$}-MOC of general formula [$Zn^{II}_{24}(\mu_4$-$H_2O)_6(SO_2TCA)_6(MnL)_{12}$] (L = chiral metallosalen dicarboxylate ligand). Solvent molecules are not presented for the sake of clarity. Adapted from Ref. [116].

4.3.2. The use of tritopic symmetrical organic carboxylate linkers: $[M^{II}_{24}(\mu_4$-$X)_6(YTCA)_6L_8]^{6-}$ (X = Cl or OH) $[M^{II}_{24}(\mu_4$-$H_2O)_6(YTCA)_6L_8]$

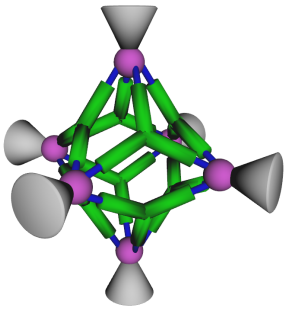

Figure 42: Schematic representation of octahedral cages $[M^{II}_{24}(\mu_4$-$X)_6(YTCA)_6L_8]^{6-}$ (X = Cl or OH) $[M^{II}_{24}(\mu_4$-$H_2O)_6(YTCA)_6L_8]$

Besides the examples involving ditopic ligands, a huge number of resulting octahedral TCA-based cages have been reported using rigid tritopic ligands.

4.3.2.a. H_4TCA/H_4PTCA based MOCs

The first example of anionic octahedral coordination cage was provided by Zhang *et al.* in 2012, while using 1,3,5-tricarboxylate (1,3,5-BTC^{2-}) (trimesate) and [Co_4-TCA]-clusters leading to an anionic compound of formula $[Co^{II}_{24}(\mu_4$-$Cl)_6(TCA)_6(1,3,5$-$BTC)_8]^{6-}$ (Figure 43 a) [117]. The diameters of the internal spherical cavity are found to be equal to approximately 17 Å.

Two isoreticular compounds were reported: an anionic $[Fe^{II}_{24}(\mu_4$-$Cl)_6(TCA)_6(1,3,5$-$BTC)_8]^{6-}$ was observed together with its adsorption properties, including of C_2/C_3-hydrocarbons separation [109] (§ 6. 2. and table 2) and a neutral $[Mg^{II}_{24}(\mu_4$-$H_2O)_6(TCA)_6(BTC)_8]$ [118], that presents good sensing towards species like Fe(III), MnO_4^- anion, nitrobenzene and 2,4-dinitrophenol in aqueous medium (§ 6. 4. and table 4).

Using H_4PTCA (Figure 35), an isoreticular compound of formula $[Co^{II}_{24}(\mu_4$-$Cl)_6(PTCA)_6(1,3,5$-$BTC)_8]^{6-}$ was also obtained, presenting a slightly larger cavity [117] (Figure 43 b).

It is possible to increase the length of the linker by using 1,3,5-*tris*(4-carboxyphenyl)benzene (H_3BTB) acting as *tris*-connecting triangle linker. Using H_4TCA, a $[Co^{II}_{24}(\mu_4\text{-}Cl)_6(TCA)_6(BTB)_8]^{6-}$ cage displaying the inner cavity size of *ca*. 17 Å, and the same inner size was also observed while using H_4PTCA (Figure 35) leading to a compound of formula ($[Co^{II}_{24}(\mu_4\text{-}Cl)_6(PTCA)_6(BTB)_8]^{6-}$) (Figure 43 c-d) [117]. The N_2 sorption studies of activated cages were reported together with iodine uptake (§ 6. 2. and table 2).

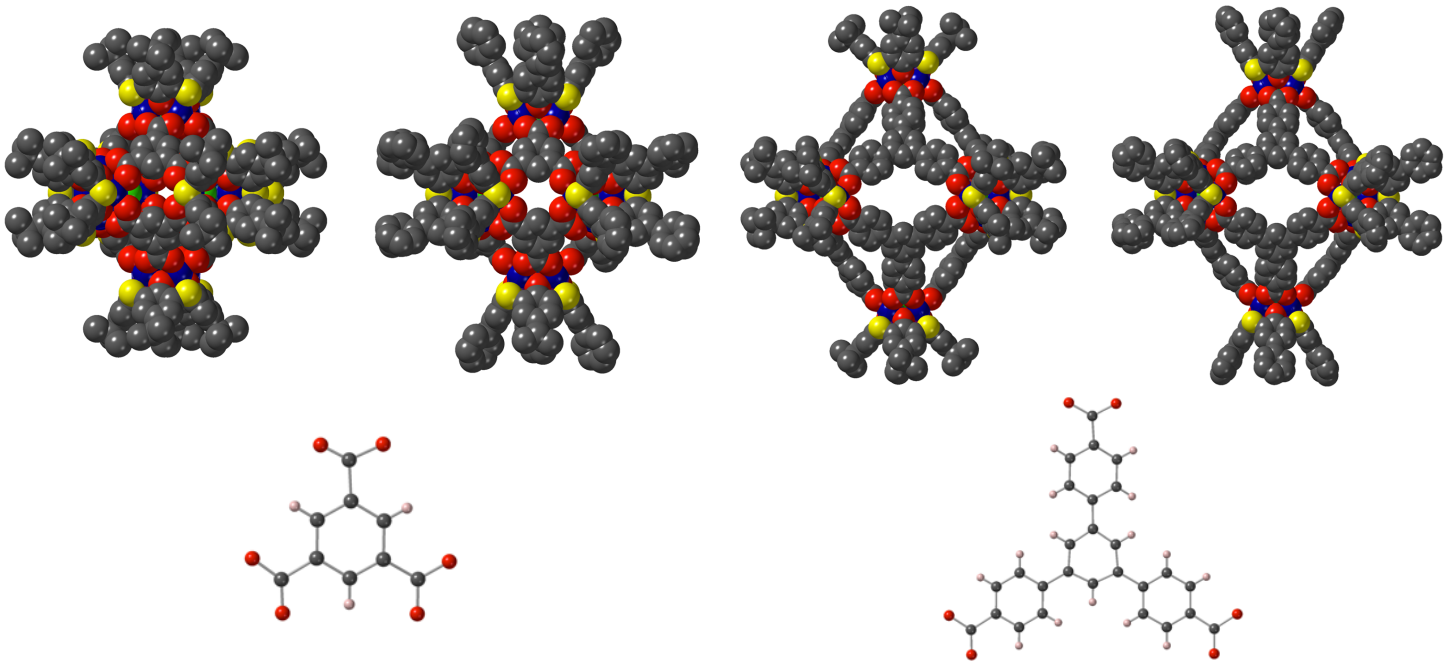

a b c d

Figure 43: A portion of the X-ray structure of anionic $\{M_{24}\}$-MOCs of general formula $[Co^{II}_{24}(\mu_4\text{-}Cl)_6(L1)_6(L2)_8]^{6-}$, (a) L1 = TCA, L2= benzene-1,3,5-tricarboxylate (1,3,5-BTC); (b) L1 = PTCA, L2= benzene-1,3,5-tricarboxylate (1,3,5-BTC); (c) L1 = TCA, L2= 1,3,5-*tris*(4-carboxyphenyl)benzene (BTB); (d) L1 = PTCA, L2= 1,3,5-*tris*(4-carboxyphenyl)benzene (BTB). Solvent molecules are not presented for the sake of clarity. Adapted from Ref. [117].

Using the parent tritopic ligand pyridine-2,4,6-tricarboxylate ($2,4,6\text{-}PTC^{2-}$) presenting the same metrics than $1,3,5\text{-}BTC^{2-}$, an isoreticular species was obtained, and in the reported conditions, alkali cations were found to be present in the anionic cage of formula $[Co^{II}_{24}Na_4(\mu_4\text{-}Cl)_6(TCA)_6(2,4,6\text{-}PTC)_8]^{2-}$ (Figure 44) [119], with a cavity size of *ca.* 12.8 × 12.8 × 12.8 $Å^3$. The post-synthetic modification by ion exchange of Na^+ with Cu^{2+} afforded the $Cu@Co_{24}$ cluster, exhibiting interesting photocatalytic properties (§ 6. 3. and table 3).

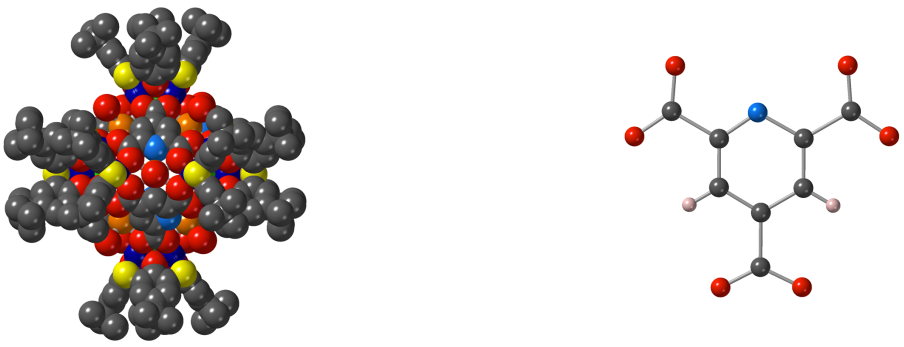

Figure 44: A portion of the X-ray structure of anionic $[Co^{II}_{24}Na_4(\mu_4\text{-}Cl)_6(TCA)_6(2,4,6\text{-}PTC)_8]^{2-}$; PTC = pyridine-2,4,6-tricarboxylate. Solvent molecules are not presented for the sake of clarity. Sodium atoms are represented in orange. Adapted from Ref. [119].

4.3.2.b. H_4SO_2TCA derivatives based MOCs

As expected, a switch from H_4TCA to H_4SO_2TCA, reacting with Co(II) ions in presence of $H_3$1,3,5-BTC, resulted in formation of an anionic octahedral cages of general formula $[M^{II}_{24}(\mu_4\text{-}L)_6(SO_2TCA)_6(1,3,5\text{-}BTC)_8]^{6-}$ (L=OH^- or Cl^-) (cavity size of approximately 15 Å,) or neutral $[M^{II}_{24}(\mu_4\text{-}H_2O)_6(SO_2TCA)_6(1,3,5\text{-}BTC)_8]$ cages (M=Fe, Ni, Co, Mg,) [120], [121], [109]. (Figure 45 a). When BTC is replaced by the more flexible cyclohexane analogue CTC^{2-} (cyclohexane-1,3,5-tricarboxylate), a compound of formula $[Co^{II}_{24}(\mu_4\text{-}H_2O)_6(SO_2TCA)_6(CTC)_8]$ was obtained [122] (Figure 45 c), evidencing the adaptability of such systems.

The neutral analogues $[M^{II}_{24}(\mu_4\text{-}H_2O)_6(DTBSO_2TCA)_6(1,3,5\text{-}BTC)_8]$ (M = Ni or Co) (Figure 45 b) and $[Co^{II}_{24}(\mu_4\text{-}H_2O)_6(DTBSO_2TCA)_6(CTC)_8]$ (Figure 45 d) compounds were also obtained, while H_4DTBSO_2TCA was H_4SO_2TCA with eliminated *tert*-Bu groups (H_4DTBSO_2TCA) (Figure 35). The size of the cavity of these compounds is *ca.* 14.1 × 14.0 × 14.0 $Å^3$.

The adsorption properties of these species were investigated showing a high CO_2/N_2 or C_3- over C_2- sorption selectivity [121] [109] (§ 6. 2. and table 2).

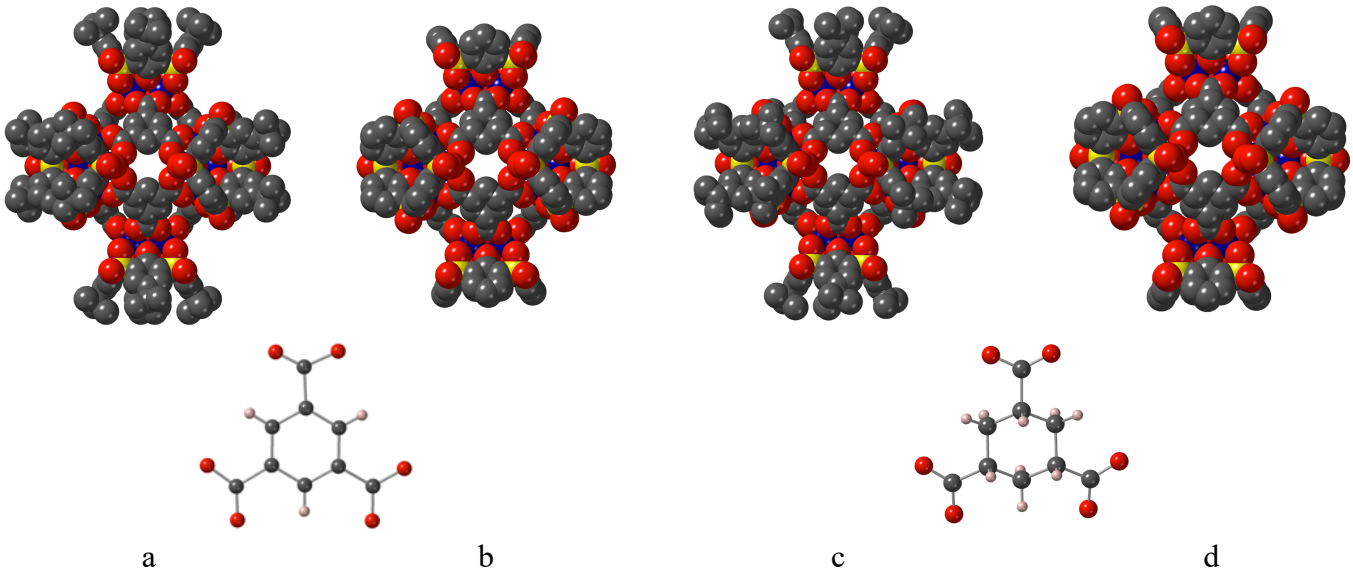

a b c d

Figure 45: A portion of the X-ray structure of octahedral $\{M_{24}\}$-MOCs (a) $[Co^{II}_{24}(\mu_4\text{-}H_2O)_6(SO_2TCA)_6(1,3,5\text{-}BTC)_8]$ (b) $[M^{II}_{24}(\mu_4\text{-}H_2O)_6(DTBSO_2TCA)_6(1,3,5\text{-}BTC)_8]$ (M = Ni or Co) (c) $[Co^{II}_{24}(\mu_4\text{-}H_2O)_6(SO_2TCA)_6(1,3,5\text{-}CTC)_8]$ and (d) $[Co^{II}_{24}(\mu_4\text{-}H_2O)_6(DTBSO_2TCA)_6(1,3,5\text{-}CTC)_8]$. Solvent molecules are not presented for the sake of clarity. Adapted from Ref. [121] and [122].

The same way as it was reported for TCA based octahedral cages, with SO_2TCA, the incorporation of larger triangular linkers such as H_3BTB (1,3,5-*tris*(4-carboxyphenyl)benzene) afforded octahedral cages of general formula $[M^{II}_{24}(\mu_4\text{-}OH)_6(SO_2TCA)_6(BTB)_8]^{6-}$ [120],[123],[124], [125] (Figure 46 a) (M = Co, Ni and Mn). These cages were studied for their gas sorption abilities (§ 6. 2. and table 2), their drug delivery abilities [123] (§ 6. 5. 3.) and their catalytic activity in the Knoevenagel condensation [125] (§ 6. 3. and table 3).

It was demonstrated that the enhancing of the encapsulation abilities of the octahedral cage towards cationic guest molecules can be achieved by replacement of the anionic macrocycle from SO_2TCA^{4-} to highly charged $(SO_3)SO_2TCA^{8-}$ ligands (Figure 35), affording the formation of the super-negatively charged $[Co^{II}_{24}(\mu_4\text{-}OH)_6((SO_3)SO_2TCA)_6(BTB)_8]^{30-}$ cage (Figure 46 b) [124], [125], [126], [127], with cavity size of *ca.* 24.5 × 24.5 × 24.5 Å^3. The anionic character of that cavity showed strong electrostatic interactions towards positive guests (§ 5.4. table 4), as well as carbonium ions, generated during the Knoevenagel condensation reaction, with an enhanced catalytic activity [125] (§ 6. 3. and table 3). In addition, a $Ru(bipy)Cl_2$ catalyst (bipy = 2,2'-bipyridine) catalyst was encapsulated in it for high catalytic activities performances [126] (§ 6. 3. and table 3). The highly negatively charged cages were also used for the stabilization of *in situ* formed *3d* (Co/Ni/Cu) and *4d* (Ru/Rh/Pd) metallic NPs and their catalytic activity was studied [127], [128] (§ 6. 3. and table 3).

A derivative of BTB^{2-} ligand, $2\text{-}NH_2\text{-}BTB^{2-}$ was used for the formation of $[M^{II}_{24}(\mu_4\text{-}OH_2)_6(SO_2TCA)_6(2\text{-}NH_2BTB)_8]$ neutral porous coordination cages (M = Co, Mn and Mg) and their capacity in energy storage devices evaluated [129] (§ 6. 5. 1.) (Figure 46 c).

The use of more electron deficient linker, displaying a similar size and geometry, 4,4′,4″-[1,3,5]triazine-2,4,6-triyl-tribenzote anion ($TATB^{2-}$) in combination with H_4SO_2TCA and Fe(II) ions led to formation of an anionic cage $[Fe^{II}_{24}(\mu_4\text{-}Cl)_6(SO_2TCA)_6(TATB)_8]^{6-}$ (Figure 46 d) [109] or neutral cages $[M^{II}_{24}(\mu_4\text{-}OH_2)_6(SO_2TCA)_6(TATB)_8]$ (M = Co, Mn and Mg) [129] with cavity size of *ca.* 24.3 × 24.3 × 24.5 Å^3. The gas sorption (CO_2/N_2 or C_3- over C_2- sorption selectivity) properties of $[Fe^{II}_{24}(\mu_4\text{-}Cl)_6(SO_2TCA)_6(TATB)_8]^{6-}$ were carefully analysed [109] (§ 6. 2. and table 2) as well as their activities in energy storage devices [129] (§ 6. 5. 1.).

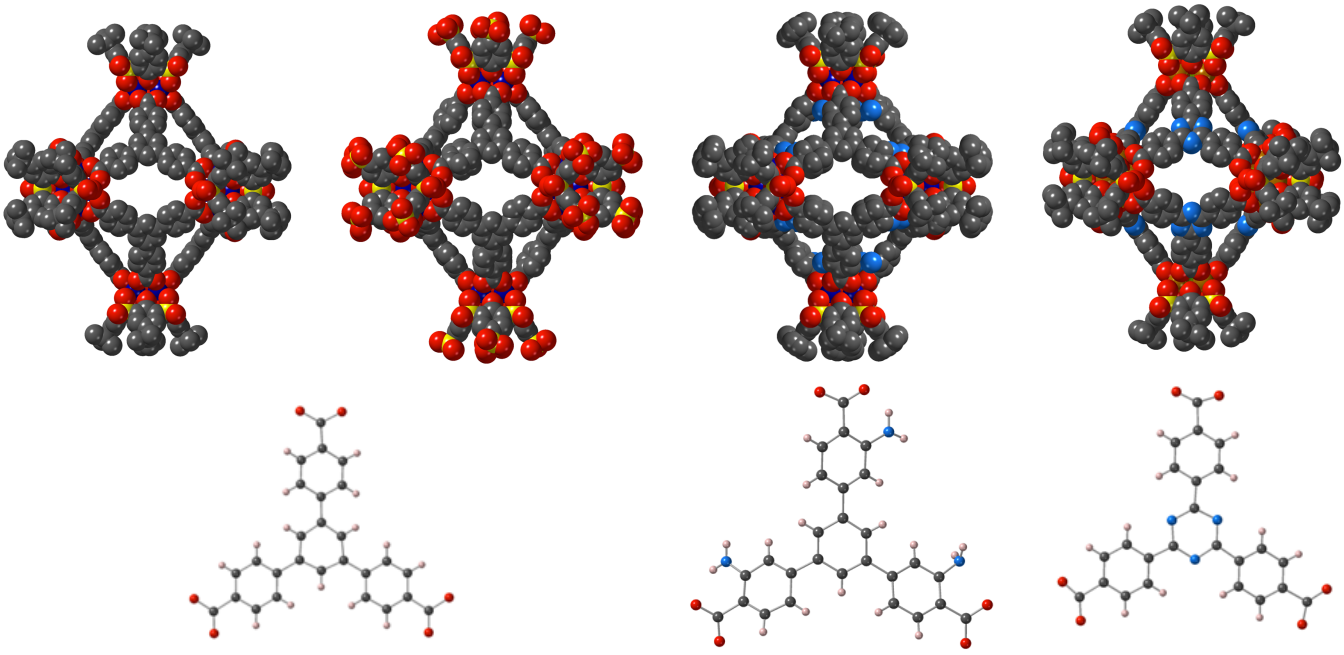

Figure 46: A portion of the X-ray structure of anionic {M_{24}}-MOCs of formula (a) $[Co^{II}_{24}(\mu_4\text{-}OH)_6(SO_2TCA)_6(BTB)_8]^{6-}$; (BTB =1,3,5-*tris*(4-carboxyphenyl)benzene); (b) $[Co^{II}_{24}(\mu_4\text{-}OH)_6((SO_3)SO_2TCA)_6(BTB)_8]^{30-}$; (c) $[M^{II}_{24}(\mu_4\text{-}OH_2)_6(SO_2TCA)_6(2\text{-}NH_2BTB)_8]$ and (d) $[Fe^{II}_{24}(\mu_4\text{-}Cl)_6(SO_2TCA)_6(TATB)_8]^{6-}$ TATB = 4,4′,4″-[1,3,5]triazine-2,4,6-triyl-tribenzoate. Solvent molecules are not presented for the sake of clarity. Adapted from Ref. [120], [124], [129] and [109].

The increase of the inner cavity size of the face-directed SO_2TCA based cages till 23 Å was achieved using 4,4',4''-(benzene-1,3,5-triyl-tris(ethyne-2,1-diyl))tribenzoate (BTE^{2-}), leading to octahedral cages of $[Co^{II}_{24}(\mu_4\text{-}H_2O)_6(SO_2TCA)_6(BTE)_8]$ (Figure 47 a) [120]. Twelve shuttle-like apertures were located on the edges of the coordination octahedron with the portals surface of *ca*. 16.8 × 9.6 Å. The gas sorption properties of these species were studied (§ 6. 2. and table 2)

The further elongation of the panel linker by the use of 4,4′,4″-(benzene-1,3,5-triyl-tris(benzene-4,1-diyl))tribenzoate (BBC^{2-}) resulted in the formation of the giant octahedral cage $[Co^{II}_{24}(\mu_4\text{-}OH)_6(SO_2TCA)_6(BBC)_8]^{6-}$ with inner cavity diameter of 27 Å (Figure 47 b) [123], [129]. Twelve apertures, located on the octahedron edges, exhibit the portals having a surface of *ca*. 20 Å × 11 Å. Further the $[Co^{II}_{24}(\mu_4\text{-}OH)_6(SO_2TCA)_6(BBC)_8]^{6-}$ cage was used for the drug Ibuprophen uptake/release from the solution (§ 6. 5. 3.). The same cage was also involved in energy storage devices [129] (§ 6. 5. 1.).

Using a larger and highly rigid tricationic species (tribenzoate derivative of N-phenylene-phenothiazine (PPT)), neutral octahedral cages of formula $[M^{II}_{24}(\mu_4\text{-}H_2O)_6(SO_2TCA)_6(PPT)_8]$ (M = Zn, Ni, Co), with inner cavity diameter of *ca.* 31 Å (Figure 47 c), are obtained [130],[131],[132], that were used as cargo for drug transports towards multiple cancer cells (§ 6. 5. 3.).

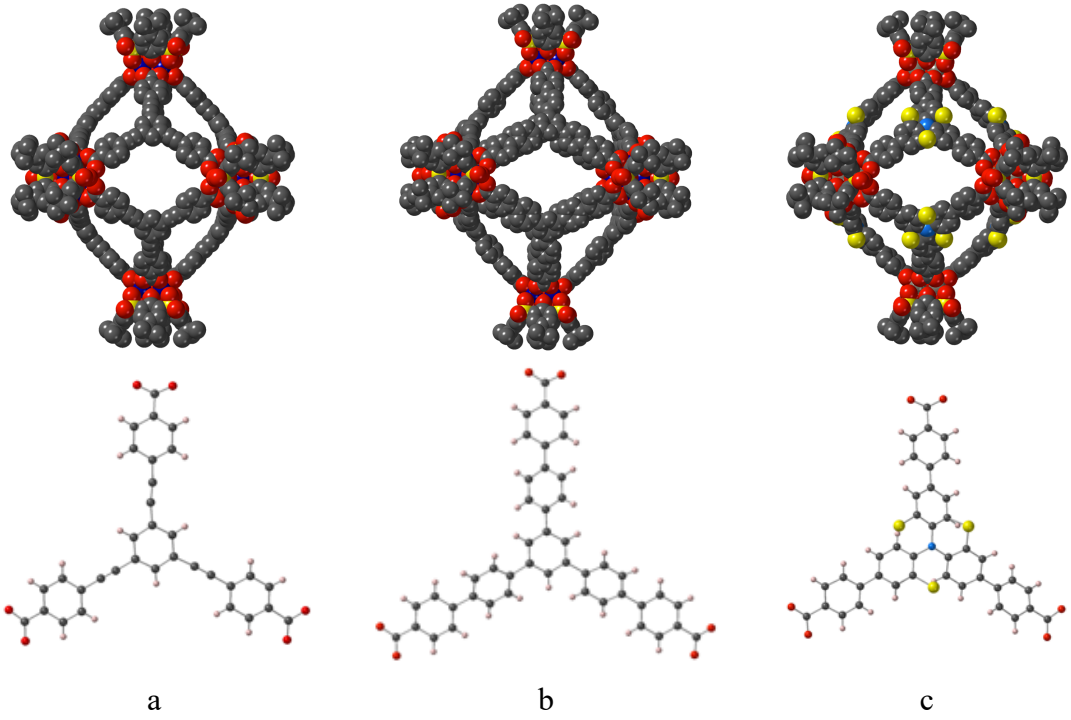

Figure 47: A portion of the X-ray structure of {M_{24}}-MOCs of formula (a) $[Co^{II}_{24}(\mu_4\text{-}H_2O)_6(SO_2TCA)_6(BTE)_8]$ BTE =4,4',4''-(benzene-1,3,5-triyl-*tris*-(ethyne-2,1-diyl))tribenzoate; (b) $[Co^{II}_{24}(\mu_4\text{-}OH)_6(SO_2TCA)_6(BBC)_8]^{6-}$ BBC = 4,4′,4″-(benzene-1,3,5-triyl-tris(benzene-4,1-diyl))tribenzoate and (c) $[Zn^{II}_{24}(\mu_4\text{-}H_2O)_6(SO_2TCA)_6(PPT)_8]$ PPT = N-phenylene-phenothiazine derivative. Solvent molecules are not presented for the sake of clarity. Adapted from Ref. [120], [123] and [130].

4.3.3. The use of tritopic N,O-donor organic linkers.

A few N,O-donor organic linkers were also reported for the formation of octahedral cages. Their lower symmetry is not in favour of the formation of such symmetrical species. The compounds present a small cavity size.

Two examples based on the use of H_4TCA thiacalix[4]arene and one based on H_4SO_2TCA are reported here below.

The first one was obtained while using 1H-1,2,3-triazole-4,5-dicarboxylate anion behaving as a deformed tritopic ligand, and leading to an anionic compound of formula $[Co_4(TCA)(SO_4)]_6(L)_6(HCOO)_6^{12-}$ (L =1*H*-1,2,3-triazole-4,5- dicarboxylate) [29b] (Figure 48 a) with cavity size of *ca.* 5.3 × 5.3 × 5.3 $Å^3$. The gas sorption properties of such compound were measured (§ 6. 2. and table 2) and also their affinities towards polluting Hg^{2+} cations (§ 6. 4. and table 4).

The second one was obtained using imidazole-4,5-dicarboxylate anion (IDC^{2-}), and the anionic Co_{26} compound presents the following formula $[Co^{II}_{18}(\mu_3\text{-}Cl)_6(H_2O)_{12}(TCA)_6(Co^{II}_8\text{-}(IDC)_{12}]^{6-}$ (Figure 48 b) [133] with cavity size of *ca.* 4.8 × 6.2 × 13.1 $Å^3$. It was formed from the less encountered $[Co^{II}_3SO_2TCA]^{2+}$ shuttlecock-like units bridged by the *in situ* formed cuboid $[Co^{II}_8\text{-}(IDC)_{12}]^{8-}$ complex located at the centre of the octahedron, leading to a deformed octahedral species. The oxygen reduction catalytic activities of this species were explored (§ 6. 3. and table 3).

The last recent example based on the use of H_4SO_2TCA and 1,3-*bis*-(1*H*-1,2,3-triazol-5-yl)benzene (H_2BDT) leading to isostructural anionic octahedral compounds of formula $[M^{II}_{24}(\mu_4\text{-}OH)_4(SO_2TCA)_6BDT]_8]^{6-}$ (M = Co, Fe) which gas sorption properties were studied (§ 6. 2. and table 2) [107].

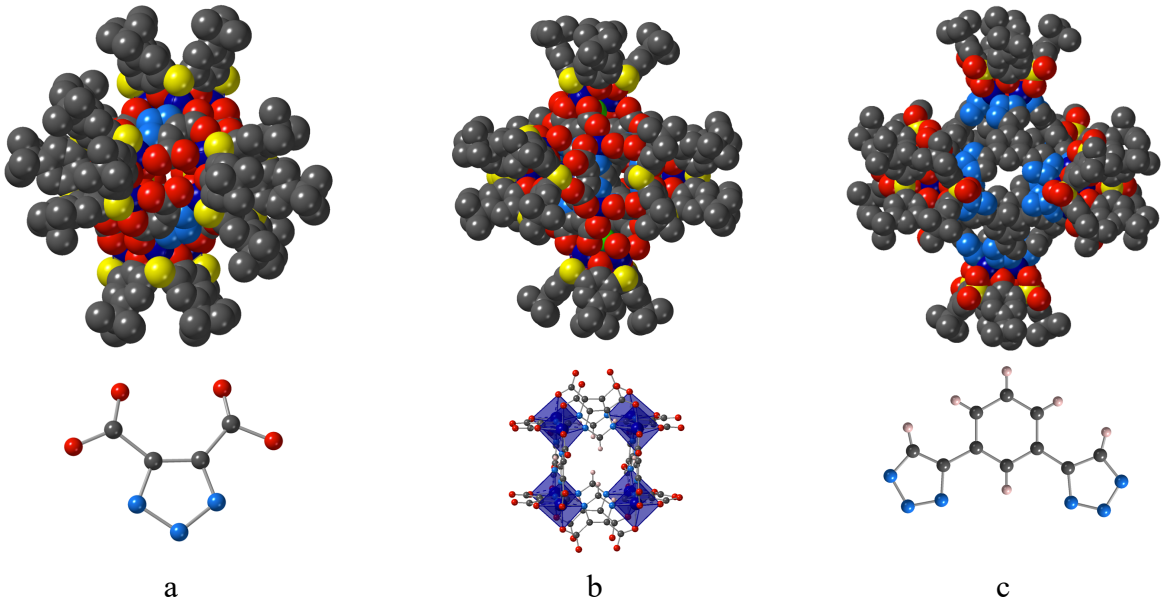

a b c

Figure 48: A portion of the X-ray structure of anionic octahedral cages of formula (a) $[Co_4(TCA)(SO_4)]_6(L)_6(HCOO)_6^{12-}$ (L =1H-1,2,3-triazole-4,5-dicarboxylate anion), (b) $\{Co_{26}\}$ $[Co^{II}_{18}(\mu_3\text{-}Cl)_6(H2O)_{12}(TCA)_6(Co^{II}_8\text{-}(IDC)_{12}]^{6-}$ and (b) $[M^{II}_{24}(\mu_4\text{-}OH)_4(SO_2TCA)_6BDT]_8]^{6-}$ (M = Co, Fe) (L = 1,3-bis(1H 1,2,3-triazol-5-yl)benzene anion). H atoms and solvent molecules are not presented for the sake of clarity. Adapted from Ref. [29b], [133] and [107].

4.3.4. The use of tritopic symmetrical metal-organic carboxylate linkers

This is the only example of metallic based tritopic ligand used for the formation of octahedral $\{M_{24}Co_8\}$-MOCs, that was reported by our team.

A Co^{III}-dipyrrine carboxylate complex (Co^{III}-dipyr) combined with H_4SO_2TCA, leads to the formation of racemate supramolecular octahedral containers $M_{24}Co_8$ [M^{II}_{24}(μ_4-H_2O)$_6$(SO_2TCA)$_6$(Co^{III}-dipyr)$_8$] (M=Co, Ni), with an inner cavity of *ca.* 19 Å (Figure 49) [134]. The compounds reveal interesting gas sorption properties with highly selective adsorption of C_2-hydrocarbon gases *versus* CH_4 (§ 6. 2. and table 2).

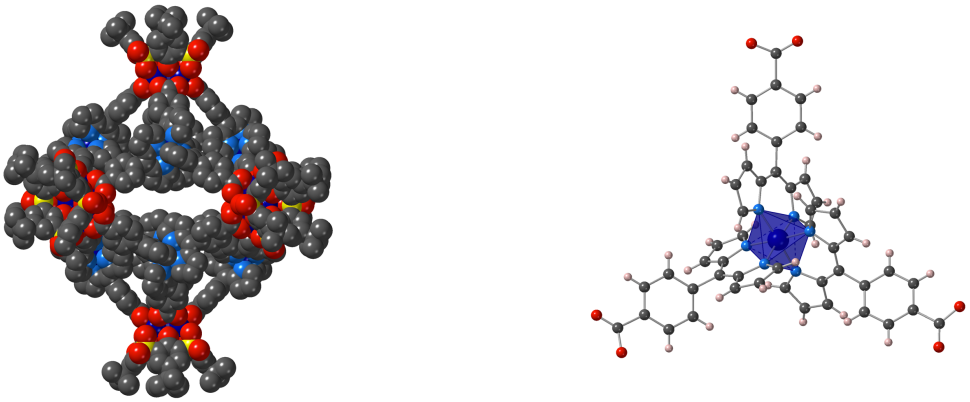

Figure 49: A portion of the X-ray structure of neutral octahedral {$M_{24}Co_8$}-MOCs of formula [M^{II}_{24}(μ_4-H_2O)$_6$(SO_2TCA)$_6$(Co^{III}-dipyr)$_8$] (M=Co, Ni) (Co^{III}-dipyr =Co^{III}-dipyrrine carboxylate complex). Solvent molecules are not presented for the sake of clarity. Adapted from Ref. [134].

4.3.5. The use of tritopic deformed organic carboxylate linkers

The possibility to control the distortion of the octahedral cages is illustrated by using of 5-[(4-carboxybenzyl) amino]-isophthalate anion ($BBDC^{2-}$) (also combined with *cis,cis*-cyclohexane-1,3,5-tricarboxylate anion CTC^{2-}). Two tetragonal- and trigonal-elongated octahedral coordination containers of formula [Co^{II}_{24}(μ_4-H_2O)$_6$(SO_2TCA)$_6$($BBDC$)$_6$(CTC)$_2$] and [Co^{II}_{24}(μ_4-H_2O)$_6$(SO_2TCA)$_6$($BBDC$)$_8$], (Figure 50 a-b) were obtained [122]. [Co^{II}_{24}(μ_4-H_2O)$_6$(SO_2TCA)$_6$($BBDC$)$_8$], displays two types of apertures: four small openings with dimensions of *ca*. 1.0 × 2.3 Å, similar to those observed in its BTC-based analogue [121], and eight much longer windows (length of *ca*. 8.6 Å). [Co^{II}_{24}(μ_4-H_2O)$_6$(SO_2TCA)$_6$($BBDC$)$_6$(CTC)$_2$] also displays two types of windows, containing six small apertures (*ca*. 1.0 × 2.3 Å) and six elongated portals (*ca*. 8.6 × 1.7 Å). The combination of both Brønsted-acidic (μ_4-H_2O) and Brønsted-basic (–NH–) centres promoted the acid-base dual catalytic reactivity toward the Knoevenagel condensation catalysis (§ 6. 3. and table 3).

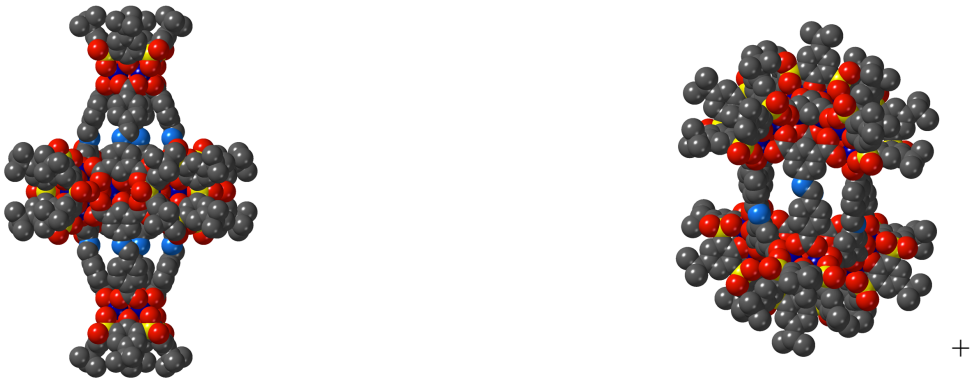

a b

Figure 50: A portion of the X-ray structure of neutral octahedral deformed cages based on (a) tetragonal elongated [$Co^{II}_{24}(\mu_4\text{-}H_2O)_6(SO_2TCA)_6(BBDC)_8$] and (b) trigonal elongated [$Co^{II}_{24}(\mu_4\text{-}H_2O)_6(SO_2TCA)_6(BBDC)_6(CTC)_2$]. H atoms and solvent molecules are not presented for the sake of clarity. Adapted from Ref. [122].

4.3.6. The use of tetratopic carboxylate linkers

Another example of formation of deformed octahedron-shaped cage was provided using the tetratopic (R-/S-) enantiopure 4,4′,6,6′-*tetrakis*-(4-benzoic acid)-1,1′-s-pinol phosphonate anion (PA), behaving as the triangular panelling ligand. The generated neutral chiral cage, with inner cavity of 21 × 21 × 32 $Å^3$ presented the formula [$M^{II}_{24}(\mu_4\text{-}H_2O)_6(SO_2TCA)_6(HPA)_8$] (M = Co, Ni) and intermolecular H-bonded assembly due to interaction of *exo* orientated COOH binding sites, leading to formation of unique robust and porous 3D molecular network in the crystalline phase (Figure 51) [135]. The cage cavity features a large internal volume (~3339 $Å^3$), containing two kinds of apertures: the large one of 12 ×19 $Å^2$ and the small one of 10 × 15 $Å^2$, leading to the highest porous thiacalix[4]arene based MOCs (SA = 1239 m^2g^{-1}), and their gas sorption properties were evaluated (§ 6. 2. and table 2). In addition, its chiral character was explored for high performance enantioselective catalysis (§ 6. 3. and table 3).

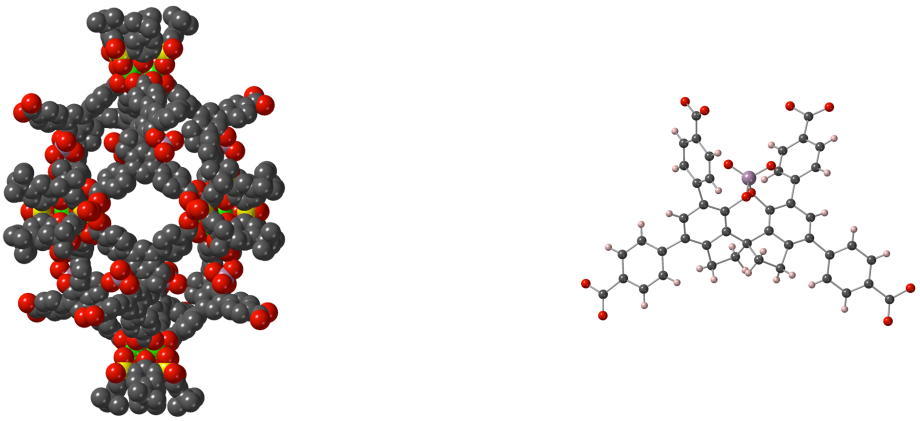

Figure 51: A portion of the X-ray structure of the neutral chiral octahedral cage of formula [$M^{II}_{24}(\mu_4\text{-}H_2O)_6(SO_2TCA)_6(HPA)_8$] (M=Co, Ni) (HPA = 4,4′,6,6′-tetrakis(4-benzoic acid)-1,1′-spinol phosphonate) . Solvent molecules are not presented for the sake of clarity. Adapted from Ref. [135].

5. Atypical geometries for high nuclearity clusters and cages

The use of small, unsymmetrical or more sophisticated ligands for the formation of high nuclearity TCA based species leads to unusual geometries of the finite objects, some of them being cages. And for the observed geometries (different from square or octahedral cages that are rationalizable, as shown in § 4) the prediction of the final geometry is not always possible.

All the presented compounds are obtained in solvothermal conditions using three types of ligands: only H_4TCA, H_4DTCA or H_4SO_2TCA (see Figures 2 and 34) have been used for the formation of the cages.

5.1. Homometallic TCA based compounds using O donor linkers

The use of H_4TCA combined with short oxalic acid, $M(AcO)_2$ in basic conditions leads to two $\{M_9\}$ isostructural compounds with the core of formula $[M^{II}_9(HTCA)_3(ox)_3Cl_3(H_2O)_6]$ (M = Co, Ni) [136]. The compounds are built from the fusion of 3 $[M^{II}_3HTCA]^{3-}$ (partially deprotonated $HTCA^{3-}$ species) by ox^{2-} and chlorine anions. It forms very tight triangular-shaped species (Figure 52 a), that present efficient abilities for the reduction of 2, 4-dinitrophenol (§ 6. 3. and table 3).

A cluster presenting a similar shape was observed by the reaction of more coordinating H_4SO_2TCA, 2,5-thiophenedicarboxylic acid (H_2TDC) and $CoCl_2$, with the formation of a $\{Co_{12}\}$ anionic compound of formula $[Co^{II}_{12}(SO_2TCA)_3(TDC)_6Cl_3]$ (Figure 52 b) [137]. The compound results from the linking of 3 $[Co^{II}_4(\mu_4\text{-}H_2O)SO_2TCA]^{4+}$ shuttlecock-like units by TDC^{2-} and chlorine anions. While using a nickel salt, a neutral $\{Ni_{24}\}$-MOC of formula $Ni^{II}_{24}(SO_2TCA)_6(TDC)_{12}(H_2O)_6$ species was obtained, presenting a trigonal prism shape, resulting from the fusion of 2 Ni_{12} species, analogous to the above described Co_{12} compound, by TDC^{2-} anions (without Cl-anions) (Figure 52 c) with a cavity diameter of *ca.* 10.3 Å. In the cavity of this compound, behaving as a cage, Pt metallic nanoclusters were confined, by the reduction (by the cage) of a H_2PtCl_6 solution. The resulting $Pt@Ni_{24}$ compound exhibits high electrocatalytic activity toward hydrogen evolution reaction (§ 6. 3. and table 3) [137].

A deformed tetrahedral example was provided by the combination of H_4TCA, $CoCl_2$, 5-sulfoisophthalic acid sodium salt in basic conditions, it leads to a $\{Co_{16}\}$ compound presenting the formula $[Co^{II}_4Cl(TCA)(CH_3OH)]_4(SIP)_4(HCOO)_2$ (Figure 52 d), where SIP = 5-sulfoisophthalic acid. The compound presents a tetrahedral shape, and results from the fusing of $[Co^{II}_4(\mu_4\text{-}Cl)TCA]^{3+}$ shuttlecock-like units by 5-sulfoisophthalate and acetate anions [138]. It is interesting to note that the used ligand is an isophtalate derivative, and in this case, no square-like compound is observed. The magnetic properties of the compound were evaluated (§ 6. 1. 1. and table 1).

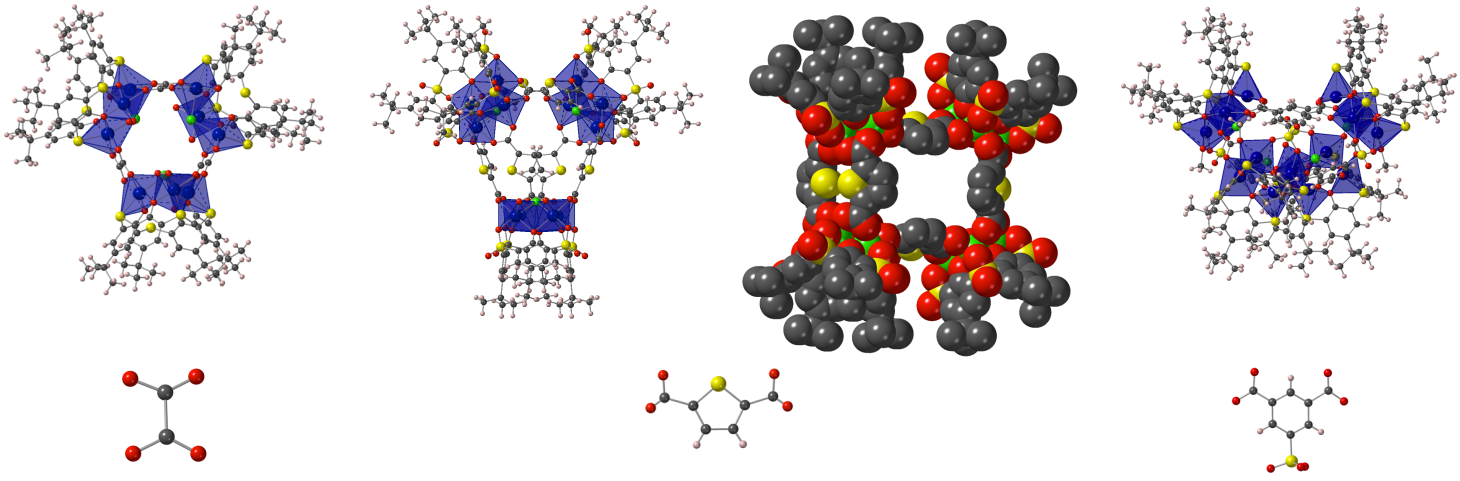

a b c d

Figure 52: A portion of the X-ray structure of the neutral clusters based on TCA and SO_2TCA (a) $\{M_9\}$ triangular -shaped compound of formula $[M^{II}_9(HTCA)_3(ox)_3Cl_3(H_2O)_6]$ (M = Co, Ni) (b) $\{Co_1\}_2$ triangular -shaped compound of formula $[Co^{II}_{12}(SO_2TCA)_3(TDC)_6Cl_3]$ (c) trigonal prism -shaped $\{Ni_{24}\}$-MOC of formula $Ni^{II}_{24}(SO_2TCA)_6(TDC)_{12}(H_2O)_6$ and (d) deformed tetrahedron-shaped $\{Co_{16}\}$ compound $[Co^{II}_4Cl(TCA)(CH_3OH)]_4(SIP)_4(HCOO)_2$. Solvent molecules are not presented for the sake of clarity. Adapted from Ref. [136], [137] and [138].

5.2. Homometallic TCA based clusters using N donor linkers

The use of N donor linkers yielded series of three $\{Co_{14}\}$ compounds, by the combination of upper rim dealkylated H_4DTCA (Figure 2), $Co^{II}Cl_2$ (or $Co^{II}(Ac)_2$) and HAD (HAD = adenine) (and sometimes DMA [139]. This leads to the formation of deformed triangular or trigonal-shaped $\{Co_{14}\}$ compounds of formula: $[Co^{II}_{14}(DTCA)_3(AD)_6(HAD)_2Cl_7(HCOO)_3]$, $[Co_{14}(DTCA)_3(AD)_6Cl_4(HCOO)_6(H_2O)]$ and $[Co^{II}_{14}(DTCA)_3(AD)_6(OH)_3(CH_3COO)_7(H_2O)_2]$, where deprotonated/partially deprotonated adenine, acetate and hydroxo anions are bridging 3 $[DTCACo_4]^{4-}$ units (Figure 53 a-c). In addition, as observed for each compound, 2 Co^{2+} species (in different environment) are also involved in the bridging. The gas sorption properties of these compounds (§ 6. 2. and table 2) were measured.

The same nuclearity was observed while mixing H_4TCA, $Co^{II}Cl_2$ and 1H-tetrazole (HTz): a $\{Co_{14}\}$ trigonal cluster of formula $[Co^{II}_{14}(TCA)_3Cl_3(Tz)_{12}(H_2O)_6]$ was formed (Figure 53 d) [140], with the fusing of $[Co^{II}_4(TCA]^{4+}$ shuttlecock-like species by $[Co^{II}(OH_2)_3Tz_3]^{2+}$ species. While annealing the cluster into Co_9S_8 NPs, products of different compositions are obtained and used as electrode for supercapacitors (§ 6. 5. 1.).

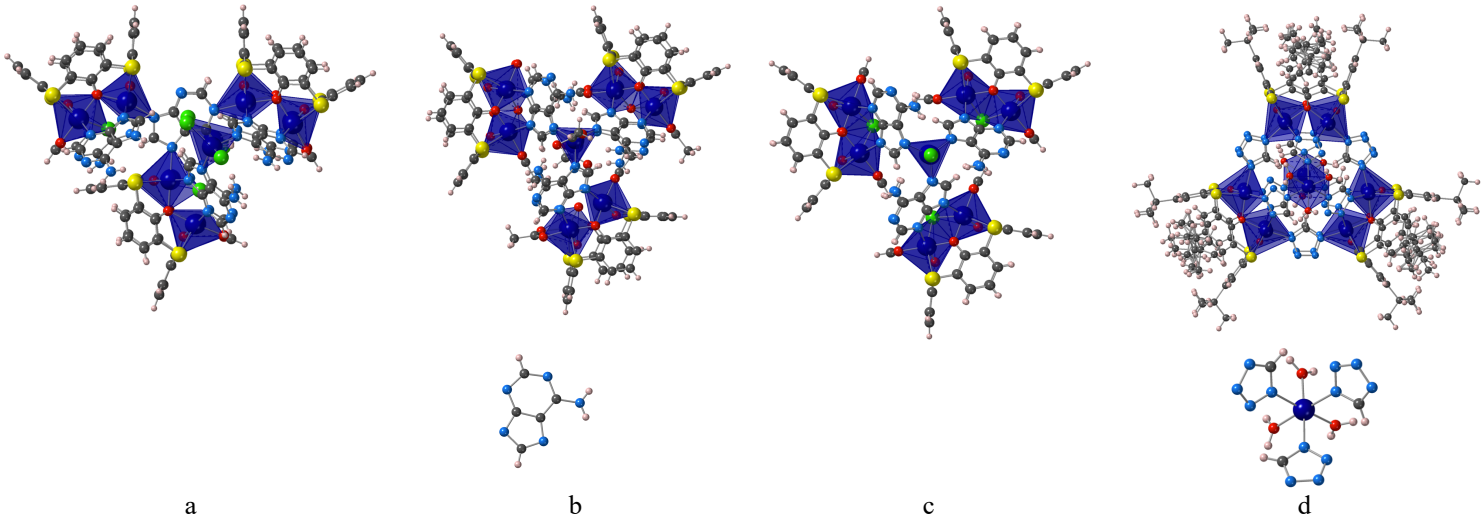

Figure 53: A portion of the X-ray structure of the $\{Co_{14}\}$ cationic clusters, obtained using N donor ligands and TCA and DTCA (a)-(c) deformed triangular-shaped cluster of formula $[Co^{II}_{14}(DTCA)_3(AD)_6(HAD)_2Cl_7(HCOO)_3]$, $[Co^{II}_{14}(DTCA)_3(AD)_6Cl_4(HCOO)_6(H_2O)]$ and $[Co^{II}_{14}(DTCA)_3(AD)_6(OH)_3(CH_3COO)_7(H_2O)_2]$ and (d) $\{Co_{14}\}$ trigonal cluster $[Co^{II}_{14}(TCA)_3Cl_3(Tz)_{12}(H_2O)_6]$ Solvent molecules are not presented for the sake of clarity. Adapted from Ref. [139] and [140].

A very interesting $\{Co_{32}\}$ tetragonal prismatic cluster has been obtained while mixing H_4TCA, $Co(Ac)_2$, 1,3-dicyanobenzene and NaN_3. The compound adopts the formula $[Co^{II}_4(TCA)Cl]_8L_4(N_3)_8Cl_8$ (H_2L = *in situ* generated 1,3-*bis*-(2*H*-tetrazol-5-yl)benzene), where $[Co^{II}_4(TCA]^{4+}$ shuttlecock-like units are bridged by chloro-, azido- and the *in situ* generated L

anions (Figure 54) [141]. It forms a porous cage with a cavity size of *ca.* 6.0 × 6.0 × 10.4 $Å^3$, exhibiting tetragonal arrangement, which porosity was confirmed by gas sorption measurements (§ 6. 2. and table 2).). Within its cavity, the Au metallic nanoclusters were confined (Au@Co_{32}), by the reduction of a $HAuCl_4$ solution with $NaBH_4$ [142] and larger metallic clusters have been formed outside the cages (Au/Co_{32}) The resulting Au@Co_{32} compound exhibits high electrocatalytic activity towards nitroarene reduction and organic dye decomposition (§ 6. 3. and table 3).

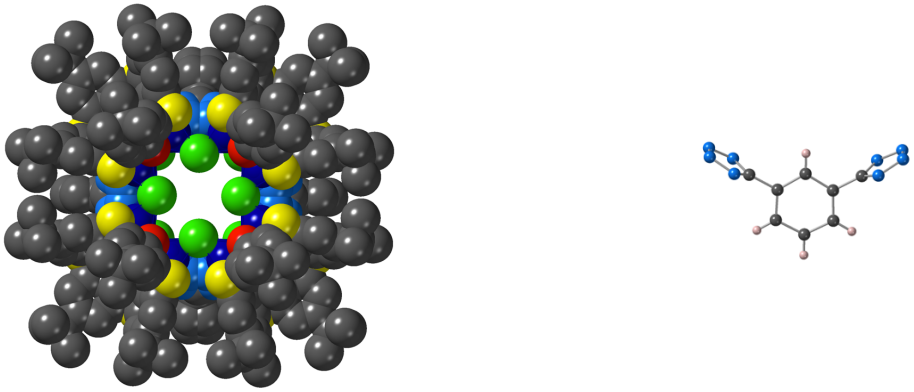

Figure 54: A portion of the X-ray structure of TCA based Co_{32} tetragonal prismatic cluster of formula $[Co_4(TCA)Cl]_8L_4(N_3)_8Cl_8$ (L= *bis*-tetrazolyl derivative). Solvent molecules are not presented for the sake of clarity. Adapted from Ref. [141].

5.3. Homometallic TCA based clusters using isophtalate derivatives N/O donor linkers

The use of N/O donor linkers yielded compounds presenting also high nuclearity. For the formation of the presented compounds, only H_4TCA has been used. Some of the compounds are obtained when two different ligands are mixed.

5.3.1. Using imidazole-4,5-dicarboxylic acid (H_3IDC)

Two reported compounds are based on the use of imidazole-4,5-dicarboxylic acid (H_3IDC). They differ by their synthetic conditions, but their components are analogous.

A V -shaped $\{Ni_{14}\}$ clusters of formula $Ni^{II}_{14}(TCA)_6(IDC)_2(H_2O)_3(DMF)Cl_2$ (Figure 55 a) [143] was formed by fusing two deformed $[TCA_2Ni_4]$ sandwich like units with two $[Ni^{II}_4TCA]^{4+}$ shuttlecock-like species, additional Ni^{2+} cations, IDC^{3-} and bridging chloro anions. The magnetic properties of the compounds were measured (§ 6. 1. 1. and table 1).

The combination of H_4TCA, $Ni^{II}Cl_2$ and H_3IDC yielded the formation of a Ni_{36} open icosahedron-shaped cage of formula $Ni^{II}_{36}Cl_{12}(H_2TCA)_{12}(IDC)_{12}$ (Figure 55 b) [133] with cavity diameter of 13.9 Å. The formation of this cage was based on the coordination of 12 $[Ni^{II}_3H_2TCA]^{2+}$ (partially deprotonated TCA) units with 12 imidazole-4,5-dicarboxylate. The oxygen reduction reaction (ORR) activity of this compound has been evaluated (§ 6. 3. and table 3).

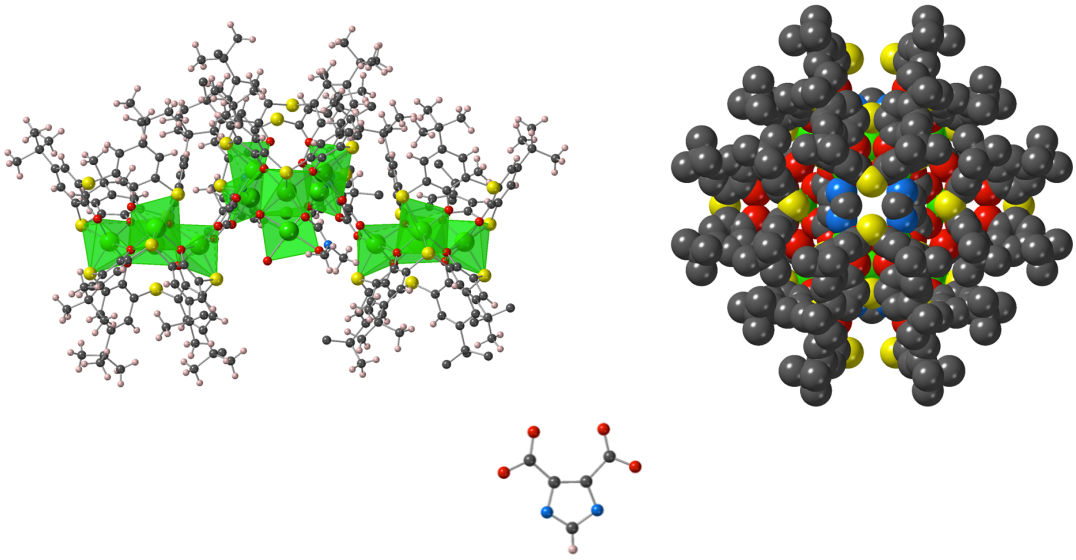

a b

Figure 55: A portion of the X-ray structure of high nuclearity neutral compounds obtained from H_4TCA, imidazole-4,5-dicarboxylate anion (IDC) and Ni^{2+}, leading to (a) a of V -shaped $\{Ni_{14}\}$ cluster $Ni^{II}_{14}(TCA)_6(IDC)_2(H_2O)_3(DMF)Cl_2$ (b) Ni_{36} open icosahedron -shaped cage of formula $Ni^{II}_{36}Cl_{12}(H_2TCA)_{12}(IDC)_{12}$. Solvent molecules are not presented for the sake of clarity. Adapted from Ref. [143] and [133]

5.3.2. Using imidazole-4,5-dicarboxylic acid and an ancillary ligand

A series of four Ni_{14} compounds was obtained by mixing H_4TCA, $NiCl_2$ and imidazole-4,5-dicarboxylic acid (H_3IDC) and an additional ligand: isophthalic acid (H_2BDC), 1,3,5-benzenetricarboxylic acid (H_2TDC), 5-(5-fluoropyridin-3-yl)isophthalic acid (H_2FPBDC) and 5-(pyrimidin-5-yl) isophthalic (H_2PBDC) [143].

The V-shaped compounds appear to all have the same $Ni^{II}_{14}(TCA)_6(IDC)_2(H_2O)_2(DMF)$ core (Figure 56 a-d) and were resulting from the linking of two deformed $[TCA_2Co_4]$ sandwich like units by two $[Ni^{II}_4TCA]^{4+}$ shuttlecock-like species, additional Co^{2+} cations, IDC^{3-} and the corresponding carboxylate anion, leading thus to a series of compounds of formula: $Ni^{II}_{14}(TCA)_6(IDC)_2(H_2O)_2(DMF)_2(BDC)$, $Ni^{II}_{14}(TCA)_6(IDC)_2(H_2O)_2(DMF)_2(BTC)$, $Ni^{II}_{14}(TCA)_6(IDC)_2(H_2O)_2(DMF)_2(FPBDC)$, $Ni^{II}_{14}(TCA)_6(IDC)_2(H_2O)_2(DMF)_2(PBDC)$. The magnetic properties of the series were measured (§ 6. 1. 1. and table 1).

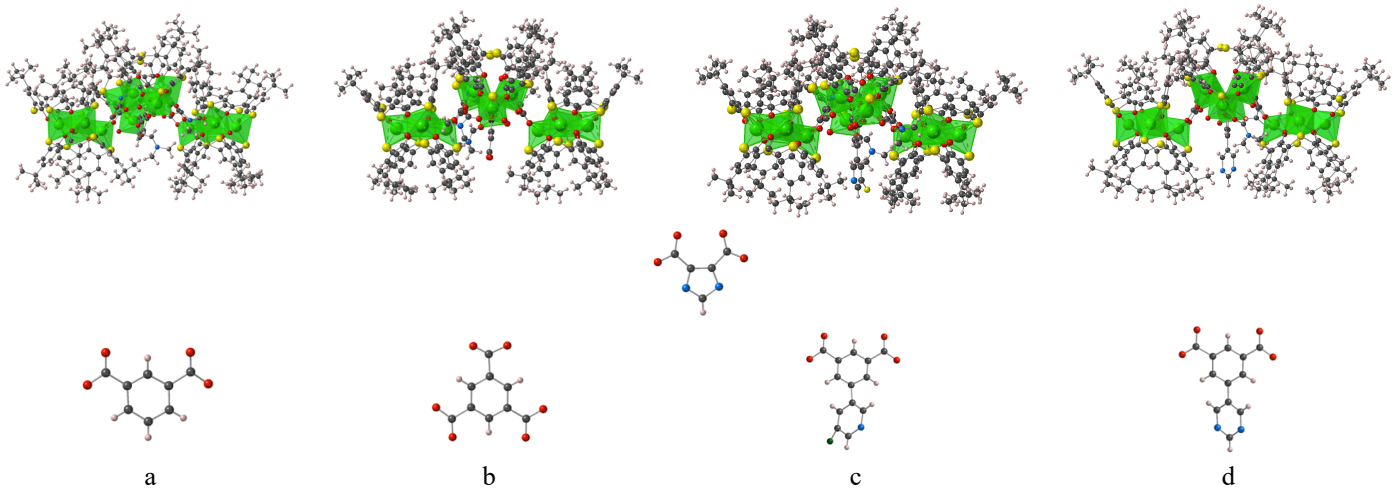

a b c d

Figure 56: A portion of the X-ray structure of a series of four V -shaped $\{Ni_{14}\}$ species assembled from TCA, two deformed $[TCA_2Co_4]$ sandwich like units formed by two $[Ni^{II}_4TCA]^{4+}$ shuttlecock-like species, additional Co^{2+} cations, IDC^{2-} and the corresponding carboxylate anion (a) BDC $Ni^{II}_{14}(TCA)_6(IDC)_2(H_2O)_2(DMF)_2(BDC)$ (b) BTC $Ni^{II}_{14}(TCA)_6(IDC)_2(H_2O)_2(DMF)_2(BTC)$ (c) FPBDC $Ni^{II}_{14}(TCA)_6(IDC)_2(H_2O)_2(DMF)_2(FPBDC)$ and (d) PBDC $Ni^{II}_{14}(TCA)_6(IDC)_2(H_2O)_2(DMF)_2(PBDC)$. Solvent molecules are not presented for the sake of clarity. Adapted from Ref. [143].

5.3.3. Using isophtalic derivatives

As reported in [96], while mixing H_4TCA 5-(pyridin-3-yl)isophthalic acid or 5-(5-fluoropyridin-3-yl)isophthalic acid with Co^{2+} cations leads to the formation of square-like cages (§4. 3. 3). Using the same components, but different synthetic conditions (presence of tetramethylammonium hydroxide), two isostructural $\{Co_{16}\}$ deformed tetrahedral clusters of formula $[Co^{II}_4(TCA)Cl]_4(L)_4(HCOO)_4(H_2O)_4]$ were obtained (Figure 57 a-b) [96], resulting from the fusing of 4 $[Co^{II}_4(\mu_4\text{-}Cl)TCA]^{3+}$ shuttlecock-like species with L. The compounds exhibit selective sorption of organic dyes (§ 6. 4. and table 4).

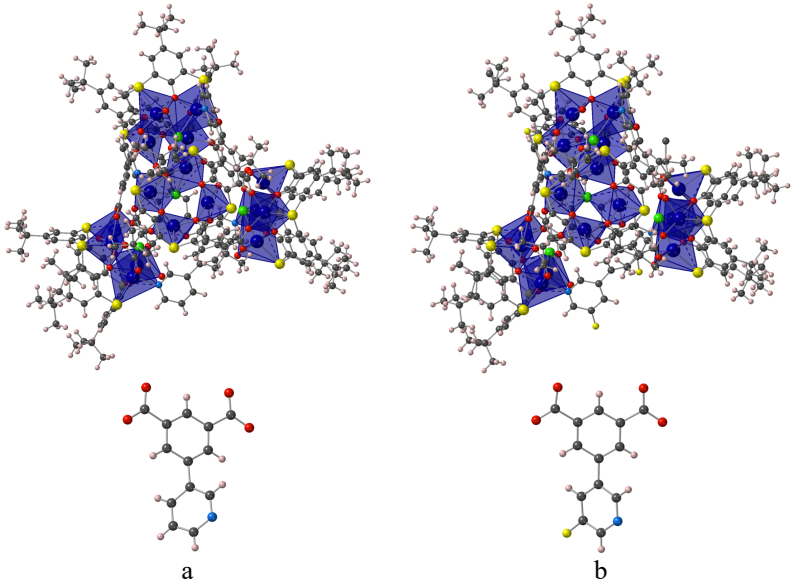

Figure 57: A portion of the X-ray structure of the clusters based on TCA and the use of N/O donor bridging ligands (a and) (b) two isostructural $\{Co_{16}\}$ deformed tetrahedron clusters of formula$[Co^{II}_4(TCA)Cl]_4(L)_4(HCOO)_4(H_2O)_4]\}$ (L = 5-(pyridin-3-yl)isophthalate or 5-(5-fluoropyridin-3-yl)isophthalate. Solvent molecules are not presented for the sake of clarity. Adapted from Ref. [96] and [133].

5.4. Heterometallic TCA based clusters using O donor linkers

In relation with the heterometallic clusters presented in § 2.2.2.d., there is an interesting report of a series of heterometallic $Na_4Ni^{II}_{24}Ln^{III}_4$ cages based on the use of different rigid O donor dicarboxylic ligands of different lengths (Figure 58 a-d) [144]: 1,4-Benzenedicarboxylic acid (H_2BDC) or terephtalic acid, 2,6-naphthalenedicarboxylic acid (H_2NDC), 4,4′-biphenyldicarboxylic acid (H_2BPDC) and 2,2′-bipyridine-5,5′-dicarboxylic acid (H_2BIPY). A series of cationic compounds of general formula $[Na_4Ni^{II}_{24}Ln^{III}_4(TCA)_6L_3(CO_3)_6(OH)_8Cl_4(H_2O)_{10}]^{10+}$ (L =BDC, NDC, BPDC and BIPY, and Ln = Dy except for BDC where Ln = Dy and Tb) were reported and they were the stepwise results of the fusing of already reported $[Na_2Ni^{II}_{12}Ln^{III}_2(TCA)_3(CO_3)_3(OH)_4(Cl)_2(OAc)_6(dma)_4]^{2+}$

units [59] by L ligands of different lengths. In this case, due to the presence of bimetallic species, the octahedral cages were not observed. The magnetic properties (§ 6. 1. 1. and table 1) and gas sorption properties (§ 6. 2. and table 2) of these interesting cages were reported.

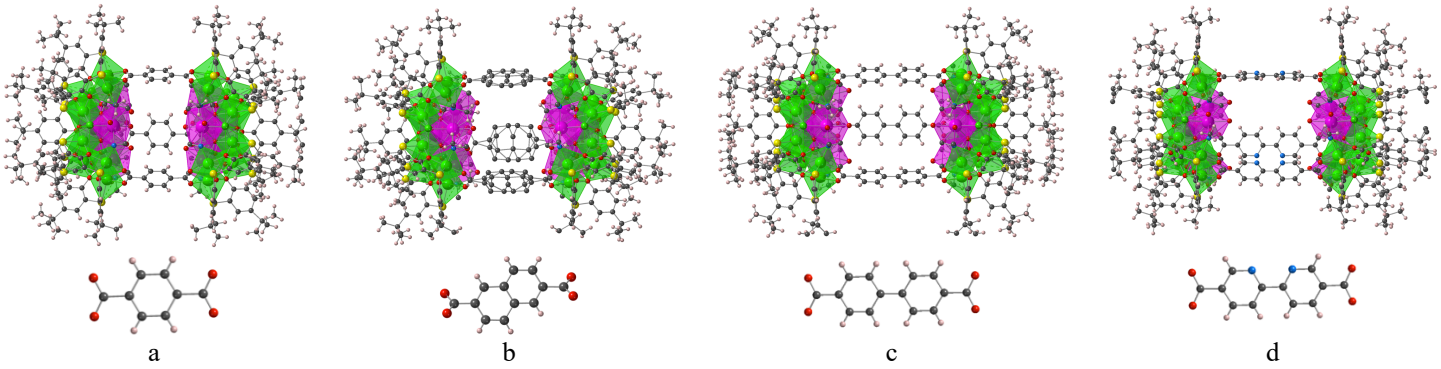

Figure 58: A portion of the X-ray structure of the cationic $Na_4Ni^{II}_{24}Ln^{III}_4$ cages based on the use of $[Na_2Ni^{II}_{12}Ln^{III}_2(TCA)_3(CO_3)_3(OH)_4(Cl)_2(OAc)_6(dma)_4]^{2+}$ units and L ligands, with general formula $[Na_4Ni^{II}_{24}Ln^{III}_4(TCA)_6L_3(CO_3)_6(OH)_8Cl_4(H_2O)_{10}]^{10+}$ (a) L =BDC (b) L = NDC (c) L = BPDC and (d) L = BIPY. Solvent molecules are not presented for the sake of clarity and (b) presents disordered naphthalene moieties. Adapted from Ref. [144]

5.5. Super-high nuclearity cages using isophtalate derivatives N/O donor linkers

Finally, a giant cage-like clusters of very high nuclearity will be presented here below.

A $\{Ni_{40}\}$-MOC was obtained by mixing H_4TCA, $Ni^{II}Cl_2$ and 5-(pyridin-4-yl)isophthalic acid (H_2PIP), presenting the formula $[Ni^{II}_4(TCA)]_{10}(Cl)_6(PIP)_{16}(HPIP)_{0.775}(HCOO)_{1.225}(CO_3)_{0.9868}(Me_2NCOO)_{1.0132}(DMF)_{0.93924}$ where 10 $[Ni^{II}_4(\mu_4\text{-}Cl)TCA]^{3+}$ shuttlecock-like species were fused with PIP^{2-} and $HPIP^-$ (deprotonated and partially deprotonated), carbonate and formate anions (Figure 59 a) [145] with a cavity diameter of 16.7 Å. The formed cage can be seen as a <u>hexadecahedron</u> (faces occupied by PIP^{2-} anions) with a gyroelongated square bipyramidal geometry (J17 Johnson solid). The gas sorption properties of this $\{Ni_{40}\}$ cage were evaluated (§ 6. 2. and table 2).

The $\{M_{48}\}$-MOCs were obtained from the combination of H_4TCA, $M^{II}Cl_2$ (M = Co, Ni) and 5-(1*H*-tetrazol-1-yl) isophthalic acid (L). This leads to two isostructural compounds of formula $[M^{II}_{48}(TCA)_{12}(L)_{18}Cl_{12}(H_2O)_6]$ (M = Co, Ni) [146], build from the bridging of 12 $[M^{II}_4ClTCA]^{3+}$ shuttlecock-like units by L^{2-} (Figure 59 b) with a cavity diameter of 22.3 Å. It can be described as a merohedral convex icosahedron with 18 triangular faces or as a <u>deformed icosahedron</u> with 20 triangular faces. The sorption of small molecules was studied (§ 6. 2. and table 2).

Finally, the highest reported nuclearity cluster involving calix[4]arene derivatives was $\{M_{72}\}$-MOCs, obtained from the combination of H_4TCA, MCl_2 (M = Co, Fe, Ni) and diisophthalic acid ($H_4TADIPA$), leading to isostructural anionic compounds of formula $(M^{II}_{72}Cl_{18}(TCA)_{18}(TADIPA)_{16}(H_2O)_8(HCOO)_4$ (M = Co, Fe, Ni), where 16 $[M^{II}_4(\mu_4\text{-}Cl)TCA]^{3+}$ shuttlecock-like units are fused by formate and L^{2-} anions [147] (Figure 59 c) with a cavity size of 30.3 × 32.8 × 12.3 $Å^3$. The <u>deformed hexadecahedron</u> can described as a

compressed double-decker hexagonal prism. these polynuclear species were used for stabilization of Pd nanoparticles inside the pores, leading to composite material Pd@Co_{72}, and were involved in the hydrogen evolution reaction (HER) (§ 6. 3. and table 3).

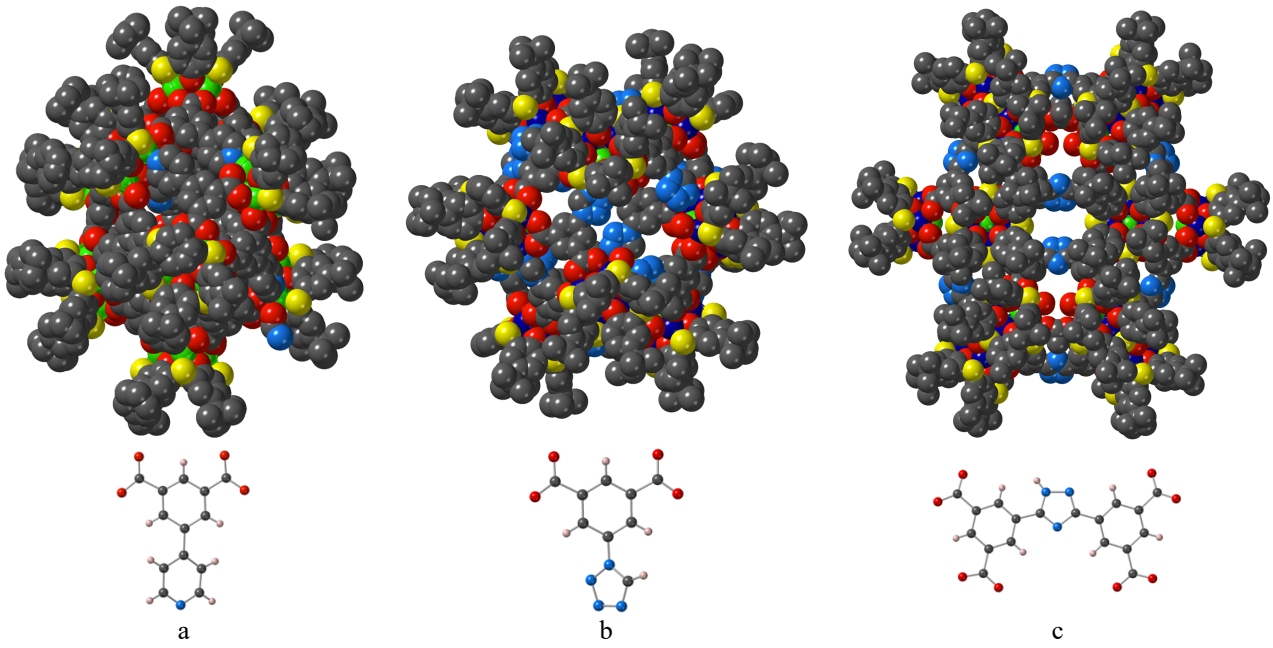

Figure 59: A portion of the X-ray structure of the highest nuclearity cluster complexes observed for cages based on TCA and used of N/O bridging ligands (a) {Ni_{40}}-MOC, a hexadecahedron (faces occupied by PIP^{2-} anions) with a gyroelongated square bipyramidal geometry of formula $[Ni^{II}_4(TCA)]_{10}(Cl)_6(PIP)_{16}(HPIP)_{0.775}(HCOO)_{1.225}(CO_3)_{0.9868}(Me_2NCOO)_{1.0132}(DMF)_{0.93924}$ (b) {Co_{48}}-MOC merohedral convex icosahedron with 18 triangular faces or as a deformed icosahedron with 20 triangular faces of formula $[M^{II}_{48}(TCA)_{12}(L)_{18}Cl_{12}(H_2O)_6]$ (M = Co, Ni) and (c) {Co_{72}}-MOC deformed hexadecahedron can be seen as a compressed double-decker hexagonal prism pressed from the top and bottom hexagonal faces of formula $(M^{II}_{72}Cl_{18}(TCA)_{18}(TADIPA)_{16}(H_2O)_8(HCOO)_4$ (M = Co, Fe, Ni). Solvent molecules are not presented for the sake of clarity. Adapted from Ref. [145], [146] and [147].

6. Application of the finite thiacalix[4]arene based supramolecular species

6.1. Magnetic and optical properties

6.1.1 Magnetic properties

The magnetic properties of the calix[4]arene compounds are well documented. As already mentioned, Brechin *et al.* reported in 2009 on the calix[4]arene coordination abilities for the formation of Single Molecules Magnets [24], and later, in 2020, a comprehensive review has been published by Fuller *et al.* summarising the recent achievements in this field [25].

The magnetic properties of thiacalix[4]arene based complexes are found to be relatively classical in terms of quantification of the magnetic interaction between paramagnetic ions, and no further applications of these species have been described. The properties of the formed high nuclear species and cages are almost based on the properties of the $[M^{II}_4(\mu_4\text{-X})YTCA]^{n+}$ shuttlecock-like square species [28 c, e, f] (Y = -, D, P, SO_2, see figure 3 and M = paramagnetic cation), that, depending on the nature of the M^{II} ion, display different behaviour: weak antiferromagnetic coupling between Mn(II) (J = -5.57 cm^{-1}) or Fe(II) (J = -4 cm^{-1}). Increasing

the nuclearity lead sometimes to complex behaviours. The results are gathered in table 1, presented below.

Table 1: Comparison of the observed magnetic properties in high nuclearity thiacalix[4]arene based clusters and cages.

Compound	**Type of compound**	**Paramagnetic Metals involved**		**Reported interactions between M**	**Reference**
$[Co^{II}_8(SO_2TCA)_2(CAM)_2(\mu_4\text{-}H_2O)_2Cl_4]$ $[Co^{II}_8(SO_2TCA)_2(CAM)_3(\mu_4\text{-}Cl)_2(CH_3OH)_2(dma)_2]$	Pocket-like	Co_8	Co(II)	Antiferromagnetic	[83]
$[M^{II}_9(HTCA)_3(ox)_3Cl_3(H_2O)_6]$ (M = Co, Ni)	triangular-shaped M_9 species	M_9	Co(II) Ni(II)	Antiferromagnetic	[136]
$[Fe^{II}_{10}TCA_4Cl_{14}]$	Fused sandwiches	Fe_{10}	Fe(II)	Antiferromagnetic	[28e]
$[Co^{II}_{10}(TCA)_4(N_3)_4]$	Fused sandwiches	Fe_{10}	Co(II)	-	[29a]
$[M^{II}_{12}(PTCA)_3(HCOO)_3(\mu_6\text{-}CO_3)_2(\mu\text{-}Mtta)(\mu\text{-}Mtta)_2(\mu_4\text{-}Mtta)_2(Py)_4]$ (M = Ni or Co)	Deformed cage	M_{12}	Co(II) Ni(II)	Antiferromagnetic	[66]
$[Co^{II}_{12}(SO_2TCA))_4(5\text{-}NH_2\text{-}tz)_8(CH_3OH)_8]$	Square	Co_{14}	Co(II)	Antiferromagnetic	[67]
$[Na_2M^{II}_{12}(PTCA)_3(O_3PPh)_6(\mu\text{-}H_2O)(\mu\text{-}Cl)_2]$ (M = Ni, Co) $[Na_4M^{II}_{16}(SO_2TCA)_4(O_3PPh)_8(\mu_4\text{-}OH)_4(CH_3OH)_4]$ (M = Ni, Co)	Deformed Nanospheres	M_{12} M_{16}	Co(II) Ni(II)	Antiferromagnetic	[63]
$[Co^{II}_{14}(OH)_2\text{-}(SO_2TCA)_4(5\text{-}ph\text{-}tz)_{10}(5\text{-}ph\text{-}tzH)_2(CH_3OH)_2]$	Deformed cage	Co_{14}	Co(II)	Antiferromagnetic	[67]
$Ni^{II}_{14}(TCA)_6(IDC)_2(H_2O)_3(DMF)Cl_2$ $Ni^{II}_{14}(TCA)_6(IDC)_2(H_2O)_2(DMF)_2(BDC)$ $Ni^{II}_{14}(TCA)_6(IDC)_2(H_2O)_2(DMF)_2(BTC)$ $Ni^{II}_{14}(TCA)_6(IDC)_2(H_2O)_2(DMF)_2(FPBDC)$ $Ni^{II}_{14}(TCA)_6(IDC)_2(H_2O)_2(DMF)_2(PBDC)$	Seesaws	Ni_{14}	Ni(II)	strong antiferromagnetic	[143]
$[Mn^{II}_{14}(SO_2TCA)_3(tBuPO_3)_6(\mu_4\text{-}OH)_3Cl(H_2O)(CH_3OH)]$ $[Mn^{II}_{16}(SO_2TCA)_3(PhPO_3)_7(HPO_4)(\mu_4\text{-}OH)_3Cl(H_2O)(CH_3OH)_4]$	Deformed Nanospheres	Mn_{14} Mn_{16}	Mn(II)	Antiferromagnetic	[64]
$[Co^{II}_4Cl(TCA)(CH_3OH)]_4(SIP)_4(HCOO)_2$	Tetrahedral cage	Co_{16}	Co(II)	Antiferromagnetic	[138]
$[Co^{II}_{16}(TCA)_4(\mu_4\text{-}Cl)_4(HCOO)_2(\mu\text{-}Mtta)_6(\mu\text{-}Mtta)_8]$	metallamacrocycle	Co_{16}	Co(II)	Antiferromagnetic	[66]
$[Ni^{II}_{18}Na_6(TCA)_6(3\text{-}S\text{-}trz)_6Cl_6(H_2O)_6]$	Flying saucer-like	Ni_{18}	Ni(II)	Antiferromagnetic	[57]
$[Co^{II}_{20}(TCA)_5(\mu\text{-}H_2O)(\mu_3\text{-}OH)_4(HPO_4)_8]$ $[Co^{II}_{24}\text{-}(TCA)_6(PO_4)_8(\mu_4\text{-}Cl)_6]$	Deformed Nanospheres	Co_{20} Co_{24}	Co(II)	Antiferromagnetic	[62] [63]
$[Co^{II}_4(TCA)(trz)_2Cl_2(CH_3OH)(H_2O)]_6$	Metallamacrocyle	Co_{24}	Co(II)	Antiferromagnetic	[73]
$[Co^{II}_{24}(SO_2TCA)_8(trz)_{16}(CH_3OH)_8]$	Metallamacrocyle	Co_{24}	Co(II)	Antiferromagnetic	[75]
$[Mn^{II}_{24}(TCA)_6(\mu_3\text{-}OH)_8(\mu\text{-}Cl)_3(\mu_5\text{-}CO_3)_6\text{-}(CH_3CH_2OH)_6]$	Nanosphere	Mn_{24}	Mn(II)	strong antiferromagnetic	[60]
$[Co^{II}_{24}(TCA)_6(MO_4)_8Cl_6][HPM_{12}O_{40}]$ (M = Mo and W)	Nanosphere	Co_{24}	Co(II)	Antiferromagnetic	[55]
$[Co^{II}_{24}(TCA)_6(\mu_4\text{-}Cl)_6(1,4\text{-}BDC)_{12}]$	Octahedral Cage	Co_{24}	Co(II)	Antiferromagnetic	[108]
$[[Co^{II}_4(TCA)(\mu\text{-}Cl)]_2[Co^{II}_4(TCA)(\mu\text{-}SO_4)]_4(bpdc)_8]^{2-}$	Octahedral Cage	Co_{24}	Co(II)	Antiferromagnetic	[116]
$[Co^{II}_{27}(TCA)_6(3\text{-}SH\text{-}trz)_8(di\text{-}S\text{-}trz)_4(CO_3)_{0.25}(SO_3)_{0.75}Cl_{10}(OH)_2(CH_3OH)_2(H_2O)_4]$ $[Co^{II}_{28}(TCA)_6(3\text{-}SH\text{-}trz)_8(di\text{-}S\text{-}trz)_4(SO_4)Cl_{10}(OH)_4(CH_3OH)_4(H_2O)_6]$ $[Co^{II}_{28}(TCA)_6(trz)_{16}(CO_3)Cl_{11}(OH)_3(CH_3OH)_2(H_2O)_6]$	Flying saucer-like	Co_{27} Co_{28}	Co(II)	Antiferromagnetic	[57]
$[Co^{II}_4(TCA)Cl]_8L_4(N_3)_8Cl_8$	Deformed Nanosphere	Co_{32}	Co(II)	Antiferromagnetic	[141]
$[Co^{II}_{24}Co^{III}_8(\mu_3\text{-}O)_{24}(H_2O)_{24}(TCA)_4]$	Nanosphere	Co_{32}	Co(II)	Antiferromagnetic	[50]
$[Nd^{III}_{10}(SO_2TCA)_4(MePO_3)_4(Cl)_2(OH)_4(H_2O)_2(DMF)_8(MeOH)_2]$ $[Nd^{III}_{11}(SO_2TCA)_3(PhPO_3)_6(Cl)_2(OH)_6(DMF)_{12}]$ $[Nd^{III}_{19}(SO_2TCA)_5(PhPO_3)_5(CO_3)_6(HCOO)_7(OH)_8(H_2O)_7(DMF)_{12}]$	Deformed Nanospheres	Nd_{10} Nd_{11} Nd_{19}	Nd(III)	Antiferromagnetic And weak Ferromagnetic	[65]
$[Na_2Ni^{II}_{12}Ln^{III}_2(TCA)_3(\mu_7\text{-}CO_3)_3(\mu_3\text{-}OH)_4(\mu_3\text{-}Cl)_2\text{-}(OAc)_6(dma)_4]$ (Ln = Dy or Tb)	vertex-fused tricubane cores	$Ni_{12}Ln_2$	Ni(II) Ln(III)	SMM behaviour Antiferromagnetic	[59]
$[Na_4Ni^{II}_{24}Ln^{III}_4(TCA)_6L_3(CO_3)_6(OH)_8Cl_4(H_2O)_{10}]^{10+}$ (L =BDC, NDC, BPDC and BIPY, and Ln = Dy except for BDC where Ln = Dy and Tb)	Double vertex-fused tricubane cores	$Ni_{24}Ln_4$	Ni(II) Ln(III)	Antiferromagnetic slow magnetic relaxation behaviour	[144]

6.1.2 Optical properties

The optical properties of thiacalix[4]arene based clusters and cages mainly concerns the decorated Au (or Ag) NPs. As already reported, the absorption of such species (Ag_{35} ($[Ag_{35}(H_2TCA)_2(TCA)(C{\equiv}CBu^t)_{16}](SbF_6)_3$ or isostructural Ag_{34} and $Ag_{33}Ag$ ($[Ag_{34}(TCA)_3(C{\equiv}CBu^t)_9(tfa)_4(CH_3OH)_3]SbF_6$ and $[Ag_{33}Au(TCA)_3(C{\equiv}CBu^t)_9(tfa)_4(CH_3OH)_3]SbF_6$), figures 4 b-d) in solution depends on the number and nature of metallic atoms in the core [39], [40]. This was also supported by calculations. The higher nuclearity compounds for example $\{Ag_{88}\}$ ($Ag_{88}(TCA)_8(EtS)_{32}(OAc)_8$]) exhibited a wide visible light absorption, which promoted a photocurrent response, when illuminated [43]. An analogous behaviour was observed in case of the heterometallic NPs of formula $[Ag_{18}(Mo_2O_5PTCA)_6]$, $[Ag_{18}S(Mo_2O_5(PTCA)_2)_2]$ [45] or $[(Mo_6O_{22})@H_3Ag_{49}(MO_3)_9(MoO_4)$-$(TCA)_6(iPrS)_{18}(CH_3CN)_2(H_2O)]$ [47]. The highest nuclearity cluster, $\{Ag_{155}\}$ ($Ag_{155}(CyS)_{40}(TCA)_5Cl_2$) also exhibited intense absorption in the visible region, together with photothermal effect up to 60°C [44] (§ 6. 5. 2.).

The mixed *4d-3s* compounds of formula $Mo_8Na_8(\mu_3\text{-}O)_{12}(\mu\text{-}O)_4$-$(TCA)_2(H_2TCA)_4(CH_3OH)_4]$ and $[Mo_8Na_8(\mu_4\text{-}O)_4(\mu_3$-$O)_8(\mu O)_4(TCA)_2(H_2TCA)_4(CH_3OH)_5(H_2O)$ showed UV-vis absorption up to 700 nm with band gaps between 1.98 eV and 1.75 eV [56], caused by the Mo-S interactions, as established by DFT calculations.

The emission properties have been also reported for some of the compounds. The $[H_2Cd^{II}_{24}(TCA\text{-}O_2)_6(PO_5)_6Cl_8(DMF)_6]$ $\{Cd_{24}\}$ cluster exhibits emission properties (around 385 nm) when irradiated at 325 nm that are modified after its photocatalytic activity [61].
Lanthanide based high nuclearity clusters displayed, as expected, photoemission ability. The $\{Nd_{10}\}$ ($[Nd^{III}_{10}(SO_2TCA)_4(MePO_3)_4(Cl)_2(OH)_4(H_2O)_2(DMF)_8(MeOH)_2]$), $\{Nd_{11}\}$ ($[Nd^{III}_{11}(SO_2TCA)_3(PhPO_3)_6(Cl)_2(OH)_6(DMF)_{12}]$) and $\{Nd_{19}\}$ ($[Nd^{III}_{19}(SO_2TCA)_5(PhPO_3)_5(CO_3)_6(HCOO)_7(OH)_8(H_2O)_7(DMF)_{12}]$) complexes have shown NIR intense emission, associated with the characteristic bands of the Nd(III) cation, at RT when irradiated at 375 nm [65].

6.2. Gas storage and separation

The presented results were obtained on the basis of analysis of solid-gas sorption.

The pioneering work on compounds, containing calix[n]arene derivatives, reported by Atwood *et al.*, revealed that calix[4]arene nonporous supramolecular structure are able to absorb N_2, O_2, CO, CO_2, C_2H_2, CH_4 and nitrogen oxides with some degree of selectivity [148]. After that, a lot of studies, concerning Coordination polymers based on calix[4]arene have been performed [14].

In this part, the data about the sorption properties of the clusters and cages based on thiacalix[4]arene building blocks, towards rather small gas and solvent molecules, are gathered in Table 2. The obtained results correlate rather well with those reported for other metal-organic cages, recently reviewed by Bloch *et al.*, especially concerning the octahedral $\{M_{24}\}$ and square-like $\{M_{16}\}$ species [149]. It was established that octahedral cages $[[Co^{II}_4(TCA)(\mu$-$Cl)]_2[Co^{II}_4(TCA)(\mu\text{-}SO_4)]_4(bpdc)_8]^{2-}$ [116] and $[M^{II}_{24}(\mu_4\text{-}H_2O)_6(SO_2TCA)_6(HPA)_8]$ (M=Co and Ni) [135] exhibit the highest surface area (table 2).

Table 2: Comparison of the observed gas sorption properties in high nuclearity thiacalix[4]arene based clusters and cages.

Compound	Type of compound	BET surface (N_2) m^2g^{-1}	Type of isotherm	Adsorption of other gas/solvents	Reference
$[Co^{II}_8(TCA)_2(CAM)_2(\mu_4\text{-}H_2O)_2Cl_4]$ $[Co^{II}_8(SO_2TCA)_2(CAM)_3(\mu_4\text{-}Cl)_2(CH_3OH)_2(dma)_2]$	Pocket-like Co_8	455, 317	Type I	H_2, CO_2 and CH_4	[83]
$[(SO_2TCA)_2Ni^{II}_8(\mu\text{-}H_2O)_2][(MDB)_4]$	Pocket -like Co_8	835	Type I	CO_2/O_2 and CO_2/N_2 adsorption selectivity Solvents: Benzene, MeOH	[89]
$[(SO_2TCA)_2Co^{II}_8(\mu\text{-}OH)_2][(NDC)_4]$	Pocket -like Co_8	247	Type I	H_2, CO_2	[85]
$[(SO_2TCA)_2M^{II}_8(\mu\text{-}X)_2][(TPCD)_4]$ (M = Mg, Mn, Co, and Ni; X = OMe; H_2O)	Pocket -like M_8	485 (Mg), 399 (Mn) 596 (Co) 619 (Ni)		CO_2 H_2 (mmol/g) 3.84 (Ni) 3.87 (Co)	[92] [150]
$(dccalix)_2(SO_2TCA)_2(M^{II}_3(\mu\text{-}OH_2)_2)_2(DMF)_2$ (M = Co and Ni)	Pocket -like M_6	77 (Co) 132 (Ni)		Solvents: H_2O, MeOH, EtOH and $CH_3C(O)CH_3$	[93]
$[(SO_2TCA)_2Co^{II}_8(\mu\text{-}H_2O)_2][(NDC\text{-}X)_4]$ (X = Br, H)	Pocket -like Co_8	300 (X = Br)	Type I	I_2 adsorption	[86]
$[Co_{14}(DTCA)_3(AD)_6Cl_4(HCOO)_6(H_2O)]$ $[Co_{14}(DTCA)_3(AD)_6(OH)_3(CH_3COO)_7(H_2O)_2]$	Co_{14}	80 227			[139]
$[[(TCA)_4Co^{II}_{16}(\mu\text{-}Cl_4)](IP)_8^{4-}[(CH_3)_4N^+]_4$	Square-like Co_{16}	409	Type I		[94]
$[(SO_2TCA)_4Ni^{II}_{16}(\mu\text{-}H_2O)_4][(1,3\text{-}BDC)_8]$ $[(SO_2TCA)_4Co^{II}_{16}(\mu\text{-}H_2O)_4][(5\text{-}SO_3\text{-}1,3\text{-}BDC)_8]$	Square-like Ni_{16}	803 (1,3-BDC) 446 (5-SO_3-1,3-BDC)	Type I	O_2, CO_2, Solvents: Benzene, MeOH H_2 (mmol/g) 3.30	[97] [150]
$H_4[(TCA)_4Co^{II}_{16}(\mu\text{-}Cl)_4][(L')_8]\}$	Square-like Co_{16}	230	Type I		[96]
$[(SO_2TCA)_4M^{II}_{16}(\mu\text{-}H_2O)_4][L_8]$ (M = Co, Ni) 5-methyl-1,3-benzenedicarboxylate anion = L1 5- bromo-1,3-benzenedicarboxylate anion = L2 5-sulfo-1,3-benzenedicarboxylate anion = L3 5-propoxy-1,3-benzenedicarboxylate anion = L4 5-heptoxyoxyisophthalate anionc = L5	Square-like M_{16}	442 (Ni, L1) 596 (Ni, L2) 238 (Co, L3) 403 (Ni, L4) 22 (Co, L5)		CO_2 H_2 (mmol/g) 4.39	[99] [150]
$[Zn^{II}_4(SO_2TCA)(\mu_4\text{-}OH)]_4\text{-}(5\text{-}Me\text{-}im\text{-}1,3\text{-}BDC)_8Cl_8$	Square-like Zn_{16}		Type I	CO_2	[101]
$[(SO_2TCA)_4Co^{II}_{16}(\mu\text{-}H_2O)_4][(5\text{-}Pr\text{-}1,3\text{-}BDC)_8]$ $[(SO_2TCA)_4Co^{II}_{16}(\mu\text{-}H_2O)_4][(5\text{-}N_3\text{-}1,3\text{-}BDC)_8]$	Square-like Co_{16}	426 37	Type II		[100]
$[(SO_2TCA)_4Co^{II}_{16}(\mu_4\text{-}OH)_4][BDT]_8]^{4-}$	Square-like Co_{16}	307	Type I	H_2, CO_2 and CH_4	[107]
$[(SO_2TCA)_4M^{II}_{16}(\mu\text{-}H_2O)_4][(5\text{-}N\text{-}1,3\text{-}BDC)_8]$(M = Co or Mg) (5-Ac-1,3-BDC = 5-amino isophthalate anion), $(SO_2TCA)_4Co^{II}_{16}(\mu\text{-}H_2O)_4][(5\text{-}Ac\text{-}1,3\text{-}BDC)_8]$ (5-Ac-1,3-BDC = 5-Acetylamide isophthalate anion)) $(SO_2TCA)_4Mg^{II}_{16}(\mu\text{-}H_2O)_4][(5\text{-}hex\text{-}1,3\text{-}BDC)_8]$ 5-Hexanoylamide isophthalate anion)	Square-like M_{16}	19-349	Type I	N_2 CO_2	[102]
$[Co^{II}_4(\mu_4\text{-}Cl)(TCA)_6(1,4\text{-}BDC)_{12}]^{6-}$	Octahedral Co_{24}	512	Type I	H_2, CO_2	[108]
$[Fe^{II}_{24}(\mu_4\text{-}Cl)_6(TCA)_6(1,3,5\text{-}BTC)_8]^{6-}$ $[Fe^{II}_{24}(\mu_4\text{-}Cl)_6(SO_2TCA)_6(1,3,5\text{-}BTC)_8]^{6-}$ $[Fe^{II}_{24}(\mu_4\text{-}Cl)(SO_2TCA)_6(1,4\text{-}BDC)_{12}]^{6-}$ $[Fe^{II}_{24}(\mu_4\text{-}Cl)_6(SO_2TCA)_6(TATB)_8]^{6-}$	Octahedral Fe_{24}	217 - 511 879	Type I	Ar, N_2, CO_2 (354) separation of C_2/C_3-hydrocarbons	[109]
$[[Co^{II}_4(TCA)(\mu\text{-}Cl)]_2[Co^{II}_4(TCA)(\mu\text{-}SO_4)]_4(bpdc)_8]^{2-}$	Octahedral Cage	1211	Type I	N_2 CO_2	[116]
$[Co^{II}_{24}(\mu_4\text{-}Cl)_6(TCA)_6(1,3,5\text{-}BTB)_8]^{6-}$ $[Co^{II}_{24}(\mu_4\text{-}Cl)_6(PTCA)_6(1,3,5\text{-}BTB)_8]^{6-}$	Octahedral Co_{24}	605 568	Type I	$N_2 + I_2$	[117]
$[M^{II}_{24}(\mu_4\text{-}H_2O)(SO_2TCA)_6(1,4\text{-}BDC)_{12}]$ (M = Co, Ni)	Octahedral M_{24}	523 (SO_2TCA) (M = Ni) 423 (SO_2TCA) (M = Co)	Type	N_2, O_2 O_2/N_2 adsorption selectivity for	[110] [150]

				$[Ni^{II}_4(\mu_4\text{-}H_2O)(^{tpen}SO_2TCA)_6(1,4\text{-}BDC)_{12}]$ H_2 (mmol/g) 3.41 (Ni)	
$[M^{II}_{24}(\mu\text{-}H_2O)_6(SO_2TCA)_4][L_{12}]$ (M = Co, Ni) 2-methyl-1,4-benzenedicarboxylate anion= L1 2-bromo-1,4-benzenedicarboxylate anion= L2 2,5-dihydroxy-1,4-benzenedicarboxylate anion= L3	Octahedral M_{24}	437 (Ni, L1) 410 (Ni, L2) 592 (Ni, L3)		CO_2 H_2 (mmol/g) 2.5 (Ni, L2) 3.41 (Ni, L3) 2.5 (Ni, L2)	[99] [150]
$[Zn^{II}_{24}(\mu_4\text{-}H_2O)_6(SO_2TCA)_6(2\text{-}NH_2\text{-}1,4\text{-}BDC)_{12}]$ $[(Fe_{24}Cl_6(TCA)_6(L1)_8)]^{6-}$ $[(Fe_{24}Cl_6(SO_2TCA)_6(L1)_8)]^{6-}$ $[(Fe_{24}Cl_6(SO_2TCA)_6(L2)_8)]^{6-}$ $[(Fe_{24}Cl_6(SO_2TCA)_6(L3)_{12})]^{6-}$ trimesate anion= L1 terephthalate anion= L2 triazine-trisbenzoate anion = L3	Octahedral Fe_{24}	850 (L1, TCA) 363 (L1, SO_2TCA) 511 (L2, SO_2TCA) 879 (L3, SO_2TCA)		CO_2 Xe/Kr separation H_2 (mmol/g) 3.44 (L2, SO_2TCA) 3.03 (L1, SO_2TCA) 3.85 (L3, SO_2TCA)	[113] [150]
$[Co^{II}_{24}(\mu_4\text{-}H_2O)_6(SO_2TCA)_6(BTE)_8]$	Octahedral Co_{24}	928 770	Type I	N_2 sorption I_2 sorption	[120]
$[(Co_{24}(\mu_4\text{-}OH)_6(SO_2TCA)_6(OH)_6(L)_8)]^{6-}$ L1 = 4,4′,4″-(benzene-1,3,5-triyl-tris(benzene-4,1-diyl))tribenzoate anion L2 = 4,4′,4″-benzene-1,3,5-triyl-tribenzoate anion	Octahedral Co_{24}	558 (L1) 410 (L2)			[123]
$[Ni^{II}_{24}(\mu_4\text{-}H_2O)_6(DTBSO_2TCA)_6(1,3,5\text{-}BTC)_8]$	Octahedral Ni_{24}	230 (SO_2TCA)		CO_2/N_2 sorption selectivity	[121]
$[M^{II}_{24}(\mu_4\text{-}OH)_4(SO_2TCA)_6BDT]_8]^{6-}$ (M = Co, Fe)	Octahedral M_{24}	488 (Fe) 559 (Co)	Type I	H_2, CO_2 and CH_4	[107]
$[[Co_4(TCA)(SO_4)]_6(L)_6(HCOO)_6]^{12-}$ 1H-1,2,3-triazole-4,5-dicarboxylate anion	Deformed octahedral Co_{24}	542	Type I	N_2, H_2	[29b]
$[M^{II}_{24}(\mu_4\text{-}H_2O)_6(SO_2TCA)_6(HPA)_8]$ (M=Co and Ni)	Deformed octahedral M_{24}	1239 (Co) 1192 (Ni)	Type I	N_2	[135]
$[M^{II}_{24}(\mu_4\text{-}H_2O)_6(SO_2TCA)_6(Co^{III}\text{-dipyr})_8]$ (M=Co, Ni) (Co^{III}-dipyr = Co^{III}-dipyrrine carboxylate complex	Octahedral $M_{24}Co_8$	417 (Ni) 462 (Co)		CO_2, CH_4, C_2H_2, C_2H_4 and C_2H_6	[134]
$[Zn^{II}_{24}(\mu_4\text{-}H_2O)_6(SO_2TCA)_6(MnL)_{12}]$	Octahedral $Zn_{24}Mn_{12}$	185		N_2 CO_2	[116]
$[Co_{20}(TCA)_5(\mu\text{-}H_2O)(\mu_3\text{-}OH)_4(HPO_4)_8]$	Co_{20}	388	Type I		[62]
$[Co^{II}_{30}(TCA)_6(pdc)_{12}(MeO)_6(MeOH)_8(H_2O)_6]$ $[Co^{II}_{30}(TCA)_6(pdc)_{12}(MeO)_6(H_2O)_{12}]$	Co_{30} metallamacrocycles	384 591	Type I	N_2	[76]
$[Na_4Ni^{II}_{24}Ln^{III}_4(TCA)_6L_3(CO_3)_6(OH)_8Cl_4(H_2O)_{10}]^{10+}$ (L =BDC, NDC, BPDC and BIPY, and Ln = Dy except for BDC where Ln = Dy and Tb)	$Na_4Ni_{24}Ln_4$	746 (L =BDC, Ln =Dy) 778 (L =NDC, Ln =Dy) 828 (L =BPDC, Ln =Dy) 868 (L =BIPY, Ln =Dy)		H_2	[144]
$[Co^{II}_4(TCA)Cl]_8L_4(N_3)_8Cl_8$ L = 1,3-bis(2H-tetrazol-5-yl)benzene)	Deformed Nanosphere Co_{32}	665			[141]
$[Ni^{II}_4(TCA)]_{10}(Cl)_6(PIP)_{16}(HPIP)_{0.775}(HCOO)_{1.225}(CO_3)_{0.9868}(Me_2NCOO)_{1.0132}(DMF)_{0.939}$ H_2PIP = 5-(pyridin-4-yl)isophthalic acid	Deformed Nanosphere Ni_{40}	646		CO_2, CH_4, C_2H_6, and C_3H_8 CH_4/C_3H_8 selectivity	[145]
$[M^{II}_{48}(TCA)_{12}(L)_{18}Cl_{12}(H_2O)_6]$ (M = Co, Ni)	Merohedral icosahedral Co_{48}	582		CO_2, CH_4, C_2H_4, C_2H_6, and C_3H_8 CH_4/C_3H_8 selectivity	[146]

6.3. Catalysis and Photocatalysis

The geometries and presence of metals in such high nuclearity supramolecular clusters and cages make them good candidate for catalysis and sometimes photocatalysis [151].

Recent advances in Porous Coordination Cage catalysed reactions were thoroughly reviewed in 2019 [7]. The use of thiacalix[4]arene derivatives for the formation of catalytically active clusters has been exhaustively documented in 2021 [152,153]. Herein, we present the summary of the catalytic activity exhibited by the species, described in this review, showing their strong ability to be involved in many different reactions. The obtained results are gathered in the table 3.

Table 3: Comparison of the observed catalytic properties for high nuclearity thiacalix[4]arene based clusters and cages

Compound	Type of compound	Explore catalytic reaction	Efficiency	Reference
$[Ag_{21}\text{-}(TCA)_3(O_2PPh_2)_6]S_bF_6$	Decorated NPs icosahedral kernel Ag_{21}	reduction of 2,4-nitrophenol		[38]
$[M_9(HTCA)_3(ox)_3Cl_3(H_2O)_6]$ (M = Co, Ni)	triangular-shaped M_9 species	reduction of 2,4-nitrophenol	High efficiency	[136]
$[(Mo_6O_{22})@H_3Ag_{49}(MO_3)_9(MoO_4)\text{-}(TCA)_6(iPrS)_{18}(CH_3CN)_2(H_2O)]$	polymolybdate-templated $\{Ag_{49}Mo_{16}\}$	electrocatalytic CO_2 reduction	44.75% CO faradaic efficiency	[47]
$[Co^{II}_{24}Na_4(\mu_4\text{-}Cl)_6(TCA)_6(2,4,6\text{-}PTC)_8]^{2-}$	Octahedral cage Co_{24}	Photocatalytic CO_2 reduction	High selectivity Co/Cu	[119]
$[(SO_2TCA)_2M^{II}_8(\mu\text{-}OH)_2][(CBPy)_4]$ (M = Co and Ni)	Barrel-like M_8	electrocatalytic oxygen evolution reaction (OER)	overpotential of 0.290 V at 10 mA cm−2	[90]
$[Co^{II}_{26}(TCA)_6\text{-}(HL)_4Cl_4(HCOO)_4(CH_3O)_2(OH)_2(DMF)_{10}(H_2O)_5]$ $[Ni^{II}_{28}(TCA)_6(HL)_6(PO_4)_2(\mu_3\text{-}O)_2Cl_2(CH_3OH)_{14}(H_2O)_2(DMF)_8][(CH_3NH_2CH_3)_4]$	Co_{26} Ni_{28} metallacycle	electrocatalytic oxygen evolution reaction (OER)	overpotential of 0.364 V (Co26) at 10 mA cm^{-2}	[68]
$[(SO_2TCA)_4Fe^{II}_8Co^{II}_8(\mu\text{-}H_2O)_4][BTT]_8$	Square-like $Fe^{II}_8Co^{II}_8$	electrocatalytic oxygen evolution reaction (OER)	overpotential of 0.285V at 10 mA cm−2	[106]
$(NH_4)[M_4^{II}(TCA)Cl[(Mo^{V}O_2)_2S(CH_3O)]_4]$ (M = Co or Ni)	Cluster M_4Mo_8	electrocatalytic oxygen evolution reaction (OER)	ultra-stable 366.8 mV at 40.0 mA cm−2 for more than 150 hours	[53]
$[Co^{II}_{18}(\mu_3\text{-}Cl)_6(H_2O)_{12}(TCA)_6(Co^{II}_8\text{-}(IDC)_{12}]^{6-}$ $Ni^{II}_{36}Cl_{12}(H_2TCA)_{12}(IDC)_{12}$	Co_{26} Octahedral cage Ni_{36}	electrocatalytic oxygen evolution reaction (OER)	E1/2 of 0.786 V	[133]
$[Ni_{18}Cl_6(TCA)_6(MNA)_6]$	Ni_{18} metallacycle	electrocatalytic Glucose Oxidation	peak potentials of +0.3 and +0.46 V	[77]
$[Ni_{20}(TCA)_5(L)_5(SO_4)_5Cl_5]^{5-}$	Ni_{20} metallacycle	electrocatalytic Glucose Oxidation	oxidative peak at +0.40 V and a reductive peak at +0.33 V	[29c]
$[Ni^{II}_4(TCA)]_2[(Mo^{V}_5Mo_3{}^{VI}O_{24})(PO_4)]$ $[Ni^{II}_4(TCA)]_2[(Mo^{V}_5Mo^{VI}_3O_{24})(OH)(CO_3)]$	Ni_8Mo_8 heterometallic cluster	electrocatalytic Glucose Oxidation	distinguishable electrochemical sensing and electrocatalytic performances for glucose	[54]
$M@[Ni^{II}_{18}Cl_6(TCA)_6(MNA)_6]$ M = Au, Pd, Ir, Ru, Rh, Pt	Ni_{18} metallacycle	hydrogen evolution reaction (HER).	AuPd@ shows excellent HER	[77]
$[H_2Cd^{II}_{24}(TCA\text{-}O_2)_6(PO_5)_6Cl_8(DMF)_6]$	Co_{24} cluster	hydrogen evolution reaction (HER)	HE value 47.75 μmol HE rate 1.36 mmol g −1 h−1	[61]
$Ni^{II}_{24}(SO_2TCA)_6(TDC)_{12}(H_2O)_6$ $Pt@Ni_{24}$	Ni_{24} trigonal prismatic cage	hydrogen evolution reaction (HER)	current density of 10 mA· cm−2·μg−1 Pt at the potential of −0.48 V	[137]
$[(SO_2TCA)_2Co^{II}_8(\mu\text{-}H_2O)_2][(CBAB)_4]$ $[(SO_2TCA)_2Co^{II}_8(\mu\text{-}H_2O)_2][(MDB)_4]$ $[(SO_2TCA)_2Ni^{II}_8(\mu\text{-}H_2O)_2][(ADBD)_4]$	Pocket -like M_8	Knoevenagel condensation of 2-naphthaldehyde and malononitrile	0% 14% 92%	[87]
$[(SO_2TCA)_2Ni^{II}_8(\mu\text{-}H_2O)_2][(ADBD)_4]$ $[(SO_2TCA)_2Zn^{II}_8(\mu\text{-}H_2O)_2][(MDB)_4]$	Pocket -like M_8	Knoevenagel condensation of aldehydes and malononitrile	Up to 95% with aldehydes of size fitting the one of the pocket	[88]

$[[Co_4(\mu_4\text{-}OH)(SO_2TCA)]_6(BTB)_8]^{6-}$ $[[Co_4(\mu_4\text{-}OH)(SO_3SO_2TCA)]_6(BTB)_8]^{30-}$	Octahedral cage Co_{24}	Knoevenagel condensation of aldehydes and malononitrile	Catalytic cycle is provided	[125]
$[Co^{II}_{24}(\mu_4\text{-}H_2O)_6(SO_2TCA)_6(BBDC)_6(CTC)_2]$ $[Co^{II}_{24}(\mu_4\text{-}H_2O)_6(SO_2TCA)_6(BBDC)_8]$	Octahedral cage Co_{24}	Knoevenagel condensation of 1,3-indanedione and aromatic aldehydes.	Efficiency depends on the size of the aromatic aldehyde	[122]
$[Zn^{II}_4(SO_2TCA)(\mu_4\text{-}OH)]_4$-(5-Me-im-1,3-BDC)$_8Cl_8$	Square-like Zn_{16}	formylation reaction of morpholine with CO2	Compound adsorbed on phenylsilane, can be recycled and high yield	[101]
$[(SO_2TCA)_4Co^{II}_{16}(\mu\text{-}H_2O)_4][AQ]_8$	Square-like Co_{16}	[2 + 2] photocycloaddition of chalcones in syn-HH cyclobutanes	440 nm irradiation, high yield and stereoselectivity	[105]
$[Zn^{II}_{24}(\mu_4\text{-}H_2O)_6(SO_2TCA)_6(MnL)_{12}]$	Octahedral $Zn_{24}Mn_{12}$	* oxidative kinetic resolution of racemic secondary alcohols * epoxidation of olefins	oxidative kinetic resolution of racemic secondary alcohols with good conversions (52-62%) excellent-to-high enantio- selectivities (81–99.1% ee)	[116]
$[M^{II}_{24}(\mu_4\text{-}H_2O)_6(SO_2TCA)_6(HPA)_8]$ (M=Co and Ni)	Octahedral cage M_{24}	Asymmetric [3 + 2] coupling of indoles with quinone monoamine Friedel–Crafts alkylation of indole with aryl aldimines	enantioselectivities up to 99.9% ee Recyclibility	[135]
$[Co^{II}_{24}(\mu_4\text{-}H_2O)_6(SO_2TCA)_6$(2-Im-1,4-BDC)$_{12}]^{12+}$	Octahedral cationic cage Co_{24}	cycloaddition reaction of CO2 on epichlorohydrin	More than 90% yield can be recycled	[114]
$[Co^{II}_{24}(\mu_4\text{-}H_2O)_6(SO_2TCA)_6$(1,4-AQDC)$_{12}]$	Octahedral cage Co_{24}	[2 + 2] photocycloaddition of chalcones in syn-HH cyclobutanes	440 nm irradiation, low yield and stereoselectivity	[105]
$[[Co^{II}_4(\mu_4\text{-}H_2O)\text{-}(SO_2TCA)]_6(BTB)_8]^{6-}$ $[Co^{II}_{24}(\mu_4\text{-}OH)_6((SO_3)SO_2TCA)_6(BTB)_8]^{30-}$ Co NPs@Co_{24}	Octahedral cage Co_{24} Co NPs@Co_{24}	Hydrolysis of ammonia-borane	High catalytic activity	[124]
$[Co^{II}_{24}(\mu_4\text{-}OH)_6((SO_3)SO_2TCA)_6(BTB)_8]^{30-}$ Ru NPs@Co_{24}	Octahedral cage Co_{24} Ru NPs@Co_{24}	Hydrolysis and methanolysis of borane ammonia	High catalytic activity	[127]
$[Co^{II}_{24}(\mu_4\text{-}OH)_6((SO_3)SO_2TCA)_6(BTB)_8]^{30-}$ Ru/Rh/Pd/Co/Ni/Cu NPs@Co_{24}	Octahedral cage Co_{24} NPs@Co_{24}	Methanolysis and hydrolysis of ammonium borane	High catalytic activity	[128]
$[M^{II}_9(HTCA)_3(ox)_3Cl_3(H_2O)_6]$ (M = Co, Ni)	triangular-shaped M_9 species	*hydrogenation of other nitroarene derivatives *reduction of nitrobenzene		[136]
$[(SO_2TCA)_2Co^{II}_8(\mu\text{-}H_2O)_2][(CBAB)_4]$ $[(SO_2TCA)_2Co^{II}_8(\mu\text{-}H_2O)_2][(MDB)_4]$	Pocket-like M_8	Rhodamine B isomerization		[87]
'$[Co^{II}_4(\mu_4\text{-}OH)(SO_3SO_2TCA)]_6(BTB)_8]^{30-}$ $[Ru(bpy)_3]^{2+}$@Co_{24}	Octahedral cage Co_{24} $[Ru(bpy)_3]^{2+}$@Co_{24}	photo-degradation of methylene blue (MB)	High catalytic activity and recycling Catalytic cycle is provided	[126]
$[M^{II}_9(HTCA)_3(ox)_3Cl_3(H_2O)_6]$ (M = Co, Ni)	triangular-shaped M_9 species	Catalytic degradation of (MB)	High efficiency	[136]
Au@$[Co^{II}_4(TCA)Cl]_8L_4(N_3)_8Cl_8$ H_2L = *in situ* generated 1,3-bis(2H-tetrazol-5-yl)benzene	Co_{32} tetragonal prismatic	Catalytic degradation of dye		[142]
$[M^{II}_{24}(\mu_4\text{-}H_2O)_6(SO_2TCA)_6(PPT)_8]$ (M = Co, Zn and Ni)	Octahedral cage M_{24}	photo-induced oxidations: * Photocatalytic selective oxidation of thioethers (M=Zn) * Photocatalytic oxidative coupling reactions of amines (M=Ni) * autoxidation of aldehydes(M=Co)	Specificity depending on the nature of the metal	[132]
$[Cu^{II}_{12}(TCA)_3Cl_3(PhPO_3)_{12}(H_2O)_2]^{3-}$ $[Cu^{II}_{16}(TCA)_4Cl_4(PhPO_3)_8]^{4-}$	Cu_{12} and Cu_{16} metallamacrocycles	Sulfide oxidation		[72]

6.4. Molecular sensing

Due to intrinsic porosity and accessible chemical sites for binding the guest molecules, the coordination cages and clusters are able to be involved in molecular recognition processes, which can be used for molecular sensing or separation performances. Several properties are reported, based mostly on liquid-liquid or solid-liquid extraction data, that are gathered in Table 4.

Table 4: Comparison of the molecular sensing abilities in solution of high nuclearity thiacalix[4]arene based clusters.

Compound	Type of compound	Recognized molecules	Comments	Reference
$(CrO_4)_2Cl_6@Ag_{46}(PTCA)_6(iPrS)_{12}(CH_3CN)_6]$	Ag_{46}	methyl orange (MO) methylene blue (MB) rhodamine B (RhB)	Specificity for MB and RhB (UV measurements)	[42]
$[(SO_2TCA)_2Co^{II}_8(\mu\text{-}H_2O)_2][(MDB)_4]$ $[(SO_2TCA)_2Co^{II}_8(\mu\text{-}H_2O)_2][(CBAB)_4]$	Pocket -like Co_8	methyl orange (MO) methylene blue (MB) eosin Y (EY)	Full extraction of MB And selectivity from MB-MO mixtures (UV measurements)	[87]
$[(SO_2TCA)_2M^{II}_8(\mu\text{-}OH)_2][(NDC)_4]$ (M = Co, Ni)	Pocket -like M_8	methylene blue (MB) eosin Y (EY)	Efficient separation of MB from the MB–EY	[85]
$[(SO_2TCA)_4Ni^{II}_{16}(\mu\text{-}H_2O)_4][(1,3\text{-}BDC)_8]$ $[(SO_2TCA)_4Ni^{II}_{16}(\mu\text{-}H_2O)_4][(5\text{-}SO_3\text{-}1,3\text{-}BDC)_8]$	Square-like Ni_{16}	methylene blue (MB)	Liquid/liquid and also solid-liquid extraction	[97]
$H_4\{[(TCA)_4Co^{II}_{16}(\mu\text{-}Cl)_4][(L')_8]\}$	Square-like Co_{16}	methylene blue (MB) rhodamine B (RhB)		[96]
$[Co^{II}_{32}Cl_8(TCA)_8(pdc)_8(H_2O)_{16}]$	metallacycle Co_{32}	methyl blue (MB), disodium fluorescein (Na_2Fl) rhodamine B (RhB)	Large absorption of RhB Selectivity for RhB over Na_2Fl	[76]
$[Co^{II}_{24}(\mu_4\text{-}H_2O)_6(SO_2TCA)_6(2,3\text{-dihydroxy-}1,4\text{-}BDC)_{12}]$	Octahedral cage Co_{24}	methyl blue (MB), eosin Y (EY) rhodamine B (RhB)	high adsorption capacity of MB Excellent selective separation performance of MB/EY or MB/RhB dye mixtures	[112]
$[Co^{II}_{24}(\mu_4\text{-}OH)\text{-}(SO_2TCA)_6(BTB)_8]^{6-}$ $[Co^{II}_{24}(\mu_4\text{-}H_2O)\text{-}(SO_3SO_2TCA)_6(BTB)_8]^{30-}$	Octahedral cage Co_{24}	Rhodamine B Methylene Blue Methyl Orange Eosin Y		[125]
$[M^{II}_4(\mu_4\text{-}H_2O)(SO_2TCA)_6(1,4\text{-}BDC)_{12}]$ (M = Co, Ni) $[M^{II}_4(\mu_4\text{-}H_2O)(^{tpen}SO_2TCA)_6(1,4\text{-}BDC)_{12}]$ (M = Co, Ni) $[M^{II}_4(\mu_4\text{-}H_2O)(^{tpen}SO_2TCA)_6(1,4\text{-}BDC)_{12}]$ (M = Co, Ni)	Octahedral cage M_{24}	methylene blue (MB) Aspirin	Absorption of 7 eq of MB and 30 eq of aspirin in solution And more at the solid/liquid interface	[110]
$[[Co^{II}_4(\mu_4\text{-}H_2O)\text{-}(SO_3SO_2TCA)]_6(BTB)_8]^{30-}$ $[Ru(bpy)_3]^{2+}@Co_{24}$	Octahedral cage Co_{24} $[Ru(bpy)_3]^{2+}$ $@Co_{24}$	methylene blue (MB)		[126]
Pocket-like M_8	Pocket-like Zn_8	13 aromatic amines	specific recognition of 2-picolylamine	[91]
$[(SO_2TCA)_4M^{II}_{16}(\mu\text{-}H_2O)_4][PIP]_8$ (M = Co, Zn)	Square-like M_{16}	proton (from trifluoroacetic acid)		[104]
$[Co_4(TCA)(SO_4)]_6(L)_6(HCOO)_6A$ $A = (C_2H_5)_3NH^+$ L = 1H-1,2,3-triazole-4,5-dicarboxylate anion	Deformed octahedral Co_{24}	Hg^{2+}	Selective adsorption of Hg^{2+} Adsorption of 330 mgg^{-1} High removal efficiency	[29b]
$[Mg^{II}_{24}(\mu_4\text{-}H_2O)_6(TCA)_6(1,3,5\text{-}BTC)_8]$	Octahedral Mg_{24}	Fe^{3+}, MnO_4^-, nitrobenzene (NB) 2,4-dinitrophenol (2,4-DNP)	Selective sensing of Fe^{3+} and MnO_4^- ions Selective sensing of NB and 2,4-DNP among nitro aromatics	[118]

6.5. Other properties

In this section there are reported other properties that thiacalix[4]arene based high nuclearity clusters and cages are able to exhibit.

6.5.1 Energy storage/production application

There are few examples concerning the direct use of thiacalix[4]arene based high nuclearity clusters in energy storage/production devices.

For the neutral octahedral cage $[Mn^{II}_{24}(\mu_4\text{-}H_2O)_6(SO_2TCA)_6(1,3,5\text{-}BTC)_8$, a moderate gravimetric capacitance of 75 F g^{-1} as electrode material in energy storage devices was investigated [154].

The electrochemical behaviour and energy storage mechanism as flexible supercapacitors of series of octahedral Coordination cages with different cavity sizes have been investigated: octahedral compounds $[[(M^{II}_4(\mu_4\text{-}H_2O)(SO_2TCA)]_6(Ln)_8]$ (L1 = trimesate, L2 = 4, 4', 4''-s-triazine-2, 4, 6-triyltribenzoate (TATB), L3 = 1，3，5-*tris*-(4'-carboxy[1，1'-biphenyl]-4-yl)benzene and L4 3,3''-diamino-5'-(3-amino-4-(ethoxycarbonyl)phenyl)-[1,1':3',1''-terphenyl]-4,4''-dicarboxylate and M = Co, Mn or Mg). Especially $[M^{II}_{24}(\mu_4\text{-}OH_2)_6(SO_2TCA)_6(TATB)_8]$ (M = Co, Ni) exhibit a high molecular capacitance of 2510 F $mmol^{-1}$ at 0.5 A g^{-1} and rare activation feature, resulting in an unprecedented 115% capacitance retention after 10000 cycles [129].

For example, when annealing at 650°C under N_2 the $\{Co_{24}\}$ $[Co^{II}_4(TCA)(trz)_2Cl_2(CH_3OH)(H_2O)]_6$ metallamacrocycle [73], Co_9S_8 nanoparticles have been obtained. They have displayed excellent rate performance, coulomb efficiency and cyclic stability when used as modified electrode material additive for ion Li-batteries [74].

The high nuclear $[Co^{II}_{14}(TCA)_3Cl_3(Tz)_{12}(H_2O)_6]$ compound, when annealed, also forms stable Co_9S_8 nanoparticles. This compound was tested as supercapacitor by embedding in a composite electrode, displaying the capacitances of 83.7% at 2 A g^{-1} and 70.0% at 5 A g^{-1} (303.3 Fg^{-1}). In addition, the electrode showed high charge-discharge reversibility with a capacity retention of 96.3% and average columbic efficiency of 98.2% after 1000 cycles at 2.0 A g^{-1} [140].

The $Pb^{II}_8Ti^{IV}_7(\mu_2\text{-}O)_6(OH)_6\text{-}(TCA)_6](OH)_2$ cluster an heterometallic highly symmetrical and soluble Pb/Ti cluster [58], was used as film in a perovskite solar cell device displaying a power conversion efficiency of *ca*. 15%, that was stable for more than 500 hrs (with 70% of efficiency).

6.5.2 Photothermal effect

The photothermal effect has been also documented several times for thiacalix[4]arene based high nuclearity clusters, showing their high efficiency.

The decorated Ag-NP Ag_{155} ($Ag_{155}(CyS)_{40}(TCA)_5Cl_2$) was in depth investigated concerning its atomic scaled electronic/hole distribution, and this leads to an intense photothermal effect [44]. This effect was also observed for the reported $[Ag_{72}]$ cluster [48].

The $\{Ni_{16}\}$ $[(TCA)_4Ni^{II}_{16}(\mu\text{-}Cl)_4][(5\text{-}NH_2\text{-}1,3\text{-}BDC)_8]$ square-like cage [94,155] was post-synthetically modified by reaction with ferrocene (Fc) aldehyde affording $[Ni_{16}\text{-}Fc\text{-}x]$ complexes (x = 1, 2, 4, 8). The $[Ni_{16}\text{-}Fc\text{-}x]$ (x=4,8), that exhibit synergistic photothermal

conversion properties, due to the presence of the ferrocene inside the cavities, but also to the charge transfer between Fc groups and {Ni_{16}} clusters.

In the heterometallic {Cu_{12}} $[Cu^{I}_{3}(HTCA)]_2[Cu^{I}_{6}(2\text{-}PyS)_6]$ cluster, the electron and hole distribution showed that Cu_{12} is an efficient photothermal conversion material both in the solid state and in water/N,N-dimethylformamide solvents [69].

6.5.3 Drug molecules adsorption/transport

Finally, the drugs adsorption properties were evidenced for thiacalix[4]arene based high nuclearity cages. Moreover, some studies went a step further by providing drug transport and delivery, performed by these coordination species.

The square-like {Zn_{16}} compound of formula $[(SO_2TCA)_4Zn^{II}_{16}(\mu\text{-}H_2O)_4][PMTC]_4$ was used for the encapsulation of anti-inflammatory drugs: including naproxen (NPX), diclofenac sodium (DCF), and aspirin (APhe). This was revealed by systematic host-guest studies using NMR technics. The drug release process was found to be pH responsive. The cages, loaded with drugs, have demonstrated a very good biostability and biocompatibility [101].

Some of reported octahedral cages, displaying large inner cavity size, have been also tested for this application purpose.

The anionic octahedral cages $[(Co_{24}(\mu_4\text{-}OH)_6(SO_2TCA)_6(BTB)_8)]^{6-}$ (BTB = 1,3,5-*tris*(4-carboxyphenyl)benzene) and $[Co^{II}_{24}(\mu_4\text{-}OH)_6(SO_2TCA)_6(BBC)_8]^{6-}$ (BBC =4,4′,4″-(benzene-1,3,5-triyl-*tris*-(benzene-4,1-diyl))tribenzoate) were studied as ibuprofen (Ibu) guest receptor by NMR and IR spectroscopies. The drug release was proved by dialyzing the Ibu-loaded samples against phosphate buffered saline solution, and showed that 67% of the loaded drug was released within 7 hours [123].

The neutral octahedral cage $[Co^{II}_{24}(\mu_4\text{-}H_2O)_6(SO_2TCA)_6(1,3,5\text{-}BTC)_8]$ was investigated towards the recognition of some well-known gastric proton pump inhibitors such as (R)-(+)-rabeprazole sodium (**D1**) and (S)-(−)-pantoprazole sodium (**D2**) [156]. It was revealed that the encapsulation of the drug occurs sequentially, first within the *endo* cavity of the cage, then with the participation of the *exo* cavities of sulfonylcalix[4]arene backbones, and, finally, leading to the cooperative binding, involving interactions *via exo* MOCs cavities interaction. The encapsulation of guest molecules and drugs into the *endo* cavity of the cage was measured and strong binding affinity was revealed (3.04×10^5 M^{-1} and 2.81×10^5 M^{-1} for **D1** and **D2**, respectively).

The neutral {Co_{24}} octahedral cage $[Co^{II}_{24}(\mu_4\text{-}H_2O)_6(SO_2TCA)_6(PPT)_8]$ (PPT = tribenzoate derivative of N-phenylene-phenothiazine) have demonstrated the highest drug delivery ability into the cells among its counterparts, studied up to date. The anticancer (+)camptothecin drug was deposited inside the cage cavity for molecular transportation into a series of cancel cells (HeLa cells, SKOV3 ovarian carcinoma cells, H1299 human lung cancer cells, and HepG2 liver hepatocellula). The *in vitro* and *in vivo* experiments demonstrated that the camptothecin-cage complex was able to permeate into the nuclei, demonstrating a rather high cytotoxycity effect towards all studied tumor cells, especially against HeLa cell series with IC_{50} = 0.09 ± 12 μM [130] [131]. The encapsulated drug complex displayed superior cytotoxicity towards multiple cancer cells over the free drug. This has been also demonstrated later, using the same neutral {Co_{24}} octahedral cage $[Co^{II}_{24}(\mu_4\text{-}H_2O)_6(SO_2TCA)_6(PPT)_8]$, where the cell entry mechanism, disassembly, and cytotoxicity have been deeply investigated [157].

These examples are first promising preliminarily studies for the use of such species for drug transport and delivery.

7. CONCLUSION AND OUTLOOKS

In the field of fascinating discrete coordination species generated using Thiacalix[4]arene derivatives, the state of the art of current achievements in design and applications obtained during last years, is provided in this review. It is important to note, that in all the reported cases, the *cone* conformation of the macrocyclic ligands is observed, leading to the formation of $[M^{II}_4(\mu_4\text{-}X)YTCA]^{3+}$ (X = Cl, OH), $[M^{II}_4(\mu_4\text{-}H_2O)YTCA]^{4+}$ or $[M^{II}_3(\mu_4\text{-}X)YTCA]^{+}$ (X = Cl, OH), $[M^{II}_3(\mu_4\text{-}H_2O)YTCA]^{3+}$ (Y = -, D, P, SO_2, see figure 3) shuttlecock-like units, that are the basis of the formation of the presented discrete species. It has been also shown that the diversity of example has increased by switching from TCA derivatives to SO_2TCA macrocycle, displaying much stronger coordination ability towards a large array of metal ions.

However, the remarkable binding affinity of TCA towards "soft" metal ions such as Ag(I) and Au(I), resulting from the involvement of sulphur atoms in the coordination, produced a number of exciting examples of Metal NPs, displaying strong M-M interactions, and held by TCA derivatives together with other organic co-ligands. NPs with up to 155 atoms have been revealed using XRD, giving rise to compounds that also exhibit specific optical and catalytic properties.

Then, using no specific ligands or coordinating anions, the formations of spherical M_{24} or M_{32} species was observed. Variation of the nuclearity and shapes of these oxo-clusters could be reached by adding some small linkers (small inorganic coordinating anions like CO_3^{2-}, CH_3COO^-, $HCOO^-$, phosphate, etc..). In contrast, the formation of wheel-like metallamacrocycles was observed while using multitopic small coordinating linkers (malonate, phenylphosphonate, risedronate, pyrazole-3,5-dicarboxylate, 2-mercaptonicotinate or 1,3,4-thiadiazole-2,5-dithiolate anions). In this case, the assembly of shuttlecock-like units bound by linkers led to ring-like architectures with up to 32 metals within the metallamacrocycle.

The rationalization of the formed species appears more obvious with the formation of pocket-like cages of general formula $[M^{II}_n(TCA)_2L_m]^{p-}$ (or $[M^{II}_n(SO_2TCA)_2L_m]^{p-}$) (n = 6 or 8 and m = 2, 3 or 4), where L is a flexible ligand bearing two terminal carboxylate coordinating groups. In contrast, the square-like coordination assemblies of general formula $[M^{II}_n(TCA)_4L_8]^{p-}$ (or $[M^{II}_n(SO_2TCA)_4L_8]^{p-}$) (n = 12 or 16) where L is a rigid linker, bearing isophtalate or a tetrazolate anionic scaffold. Due to geometry factor it was revealed that the square-like species display larger pores compared to pocket-like architectures, and they were extensively studied for their gas adsorption properties.

The rationalisation reached its peak with the formation of octahedral cages. The octahedral cages of general formula $[M^{II}_{24}(\mu_4\text{-}X)_6(YTCA)_6L_{12}]^{6-}$ (X = Cl or OH) or $[M^{II}_{24}(\mu_4\text{-}H_2O)_6(YTCA)_6L_{12}]$ (Y = -, D, P, SO_2, see figure 3) for edge-linked species were reproducibly obtained by the use of rigid terephthalate-based linkers and also one metal-organic linker. For the formation of $[M^{II}_{24}(\mu_4\text{-}X)_6(YTCA)_6L_8]^{6-}$ (X = Cl or OH) $[M^{II}_{24}(\mu_4\text{-}H_2O)_6(YTCA)_6L_8]$ (Y = -, D, P, SO_2, see figure 3) (face-panelled species) the rigid linkers, displaying the triangular disposition of binding sites (generally carboxylate) such trimesate or CTC, BTC triazine -based

ligands etc were also used to reproducibly obtain the coordination cages of octahedral geometry. The formed compounds present large cavities, and exhibit interesting molecular recognition properties, as well as gas sorption and catalysis.

For the other used ligands (less symmetrical, less rigid) or the combination of ligands, the obtained compounds (cages and high nuclearity clusters), the serendipity plays a significant role for the formation of high nuclearities clusters, as well as the synthetic conditions, presence of other species in the medium etc.

The obtained coordination species have been intensively studied for their intriguing sorption properties, host-guest chemistry and related catalytic, storage/separation and sensing activities and can be helpful in application in many different fields.

Despite the rapid development of porous materials with controlled cavity size and properties, especially coordination cages, presented in this review, several challenges remain in this field. For example, the exploration of similar species involving lanthanide metals would certainly lead to species with tuneable magnetic/optical properties. Some attempts have been already paid when the formed polynuclear thiacalix[4]arene based species were linked by carboxylic moieties, leading to polymeric structure [158,159].

The formation of such porous coordination compounds has found application in the field of drug delivery, which has been already successfully studied *in vitro* and *in vivo*. By modifying the upper rim of thiacalix[4]arene platform as well as of the substituents, located at the side position of the used linkers, one may achieve the selectivity in cell membrane permeability, leading to decrease of the side effects, emerging upon the anti-cancer therapy, this is a very important issue for the use of such species.

Finally, the possibility to combine different properties in only one material and, thus, to construct various multifunctional systems make these fascinating coordination species especially appealing objects for further investigation by paving the way for innovative applications across diverse fields.

8. ACKNOWLEDGMENTS

This work was supported by the University of Strasbourg, a Doctoral Vernadski scholarship from French Embassy (I. V. K.), the CNRS, the Fondation Jean-Marie Lehn and the Russian Science Foundation (grant 19-73-20035).

9. REFERENCES

[1] J. M. Lehn, Eur. Rev. 17 (2009) 263-280 10.1016/j.ccr.2017.12.005

[2] (a) H. Qian, M. Zhu, Z. Wu, R. Jin Quantum Sized Gold Nanoclusters with Atomic Precision Acc. Chem. Res. 45 (2012) 1470-1479 10.1021/ar200331z; (b) H. Yu, B. Rao, W. Jiang, S. Yang, M. Zhu The photoluminescent metal nanoclusters with atomic precision Coord. Chem. Rev. 378 (2019) 595-617 10.1016/j.ccr.2017.12.005

[3] V. Chiozzi, F. Rossi Inorganic–organic core/shell nanoparticles: progress and applications Nanoscale Adv. 2 (2020) 5090-5105 10.1039/D0NA00411A

[4] R. Jin, Quantum Sized, Thiolate-Protected Gold Nanoclusters. Nanoscale 2 (2010) 343-362 10.1039/B9NR00160C.

[5] (a) A. Dolbecq, E. Dumas, C. R. Mayer, P. Mialane Hybrid Organic-Inorganic Polyoxometalate Compounds: From Structural Diversity to Applications Chem. Rev. 110 (2010) 6009-6048 10.1021/cr1000578; (b) D-L. Long, R. Tsunashima, L. Cronin. Polyoxometalates: Building Blocks for Functional Nanoscale Systems Angew. Chem., Int. Ed. 49 (2010) 1736-1758 10.1002/anie.200902483; (c) Ma, P. T.; Hu, F.; Wang, J. P.; Niu, J. Y. Carboxylate covalently modified polyoxometalates: From synthesis, structural diversity to applications. Coord. Chem. Rev. 378 (2019) 281-309 10.1016/j.ccr.2018.02.010

[6] (a) D. J. Tranchemontagne, Z. Ni, M. O'Keeffe, O. M. Yaghi, Reticular Chemistry of Metal-Organic Polyhedra Angew. Chem., Int. Ed. 47 (2008) 5136-5147 10.1002/anie.200705008; (b) T. R. Cook, P. J. Stang, Recent Developments in the Preparation and Chemistry of Metallacycles and Metallacages *via* Coordination Chem. Rev. 115 (2015) 7001-7045 10.1021/cr5005666; (c) E.-S. M. El-Sayed, D. Yuan, Metal-Organic Cages (MOCs): From Discrete to Cage-based Extended Architectures. Chem. Lett. 49 (2020) 28-53 10.1246/cl.190731; (d) S. Pullen, J. Tessarolo, G. H. Clever Increasing structural and functional complexity in self-assembled coordination cages Chem. Sci. 12 (2021) 7269-7293 10.1039/D1SC01226F; (e) C. T. McTernan, J. A. Davies, J. R. Nitschke Beyond Platonic: How to Build Metal-Organic Polyhedra Capable of Binding Low-Symmetry, Information-Rich Molecular Cargoes Chem. Rev.122 (2022) 10393-10437 10.1021/acs.chemrev.1c00763

[7] (a)Y. Fang, J. A. Powell, E. Li, Q. Wang, Z. Perry, A. Kirchon, X. Yang, Z. Xiao, C. Zhu, L. Zhang, F. Huang, H-C. Zhou Catalytic reactions within the cavity of coordination cages Chem. Soc. Rev. 48 (2019) 4707-4730 10.1039/C9CS00091G; (b) J. E. M. Lewis Molecular engineering of confined space in metal–organic cages Chem. Commun. 58 (2022) 13873-13886 10.1039/D2CC05560K.

[8] (a) H. Kumagai, M. Hasegawa, S. Miyanari, Y. Sugawa, Y. Sato, T. Hori, S. Ueda, H. Kamiyama, S. Miyano Facile synthesis of p-tert-butylthiacalix[4]arene by the reaction of p-tert-butylphenol with elemental sulfur in the presence of a base Tetrahedron Lett. 38 (1997) 3971-3974 10.1016/S0040-4039(97)00792-2; (b) H. Akdas, L. Bringel, E. Graf, M. W. Hosseini, G. Mislin, J. Pansanel, A. De Cian, J. Fischer Thiacalix[4]arenes: Synthesis and structural analysis of thiacalix[4]arene and of *p-tert*-butylthiacalix[4]arene Tetrahedron Lett. 39 (1998) 2311-2314 10.1016/S0040-4039(98)00067-7.

[9] P. Rao, M. W. Hosseini, A. De Cian, J. Fischer Synthesis and structural analysis of mercaptothiacalix[4]arene Chem. Commun. (1999) 2169-2170 10.1039/A906058H

[10] S. Shinkai Calix[4]arenes - the third generation of supramolecules Tetrahedron 49 (1993) 8933-9150 10.1016/S0040-4020(01)91215-3.

[11] (a) C.D. Gutsche in Calix[4]arenes Revised: Monographs in Supramolecular Chemistry Vol. 6 The Royal Society of Chemistry Cambridge (1998); (b) Calix[4]arenes (Eds. Z. Asfari, V. Böhmer, J. Harrowfield, J. Vicens) Kluwer Academic Dordrecht (2001); (c) Calix[4]arenes and Beyond (Eds. P. Neri, J. Sessler, M-X.Wang) Springer International Publishing (2016).

[12] N. Morohashi, F. Narumi, N. Iki, T. Hattori, S. Miyano Thiacalix[4]arenes Chem. Rev. 106, (2006) 5291-5316 10.1021/cr050565j

[13] M. Zhao, J. Lv, D-S. Guo Promising advances of thiacalix[4]arene in crystal structures RSC Adv. 7 (2017) 10021-10050 10.1039/C6RA25616C

[14] A. Ovsyannikov, S. Solovieva, I. Antipin, S. Ferlay Coordination Polymers based on calix[4]arene derivatives: Structures and properties Coord. Chem. Rev. 352 (2017) 151-186 10.1016/j.ccr.2017.09.004

[15] C. Aronica, G. Chastanet, E. Zueva, S. A. Borshch, J. M. Clemente-Juan, D. Luneau A Mixed-Valence Polyoxovanadate(III,IV) Cluster with a Calix[4]arene Cap Exhibiting Ferromagnetic V(III)-V(IV) Interactions J. Am. Chem. Soc. 130 (2008) 2365-2371 10.1021/ja078030q

[16] G. Karotsis, S. Kennedy, S. J. Dalgarno, E. K. Brechin Calix[4]arene supported enneanuclear Cu(II) clusters Chem. Commun. 46 (2010) 3884-3886 10.1039/C0CC00011F

[17] S. M. Taylor, R. D. McIntosh, S. Piligkos, S. J. Dalgarno, E. K. Brechin Calix[4]arene supported clusters: a dimer of [$Mn^{III}Mn^{II}$] dimers Chem. Commun. 47 (2011) 1440-1442 10.1039/C0CC04466K

[18] S. M. Taylor, R. D. McIntosh, C. M. Beavers, S. J. Teat, S. Piligkos, S. J. Dalgarno, E. K. Brechin Calix[4]arene-supported clusters: employment of complementary cluster ligands for the construction of a ferromagnetic [Mn_5] cage Chem. Commun. 48 (2012) 11190-11192 10.1039/C2CC35944H

[19] L. R. B. Wilson, M. Coletta, R. Jose, G. Rajaraman, S. J. Dalgarno, E. K. Brechin Oxidation state variation in bis-calix[4]arene supported decametallic Mn clusters Dalton Trans. 50 (2021) 17566-17572 10.1039/D1DT03410C

[20] Y-Q. Tian, Y-S. Cui, W-D. Yu, C-Qiao Xu, X-Y. Yi, J. Yan, J. Li, C. Liu An ultrastable Ti-based metallocalixarene nanocage cluster with photocatalytic amine oxidation activity Chem. Commun. 58 (2022) 6028-6031 10.1039/D2CC01740G

[21] A. F. A. Alshamrani, O. Santoro, T. J. Prior, M. A. Alamri, G. J. Stasiuk, M. R. J. Elsegood, C. Redshaw Scandium calix[n]arenes (n = 4, 6, 8): structural, cytotoxicity and ring opening polymerization studies Dalton Trans. 50 (2021) 8302-8306 10.1039/D1DT01330K

[22] S. Sanz, R. D. McIntosh, C. M. Beavers, S. J. Teat, M. Evangelisti, E. K. Brechin, S. J. Dalgarno Calix[4]arene-supported rare earth octahedra Chem. Commun. 48 (2012) 1449-1451 10.1039/C1CC14603C

[23] (a) G. Karotsis, M. Evangelisti, S. J. Dalgarno, E. K. Brechin A Calix[4]arene 3d/4f Magnetic Cooler Angew. Chem. Int. Ed. 48 (2009) 9928-9931 10.1002/anie.200905012 (b) S. Sanz, K. Ferreira, R. D. McIntosh, S. J. Dalgarno, E. K. Brechin Calix[4]arene-supported $Fe^{III}_2Ln^{III}_2$ clusters Chem. Commun. 47 (2011) 9042-9044 10.1039/C1CC13055B

[24] G. Karotsis, S. J. Teat, W. Wernsdorfer, S. Piligkos, S. J. Dalgarno, E. K. Brechin Calix[4]arene-Based Single-Molecule Magnets Angew. Chem. Int. Ed. 48 (2009) 8285-8288 10.1002/anie.200904094

[25] R. O. Fuller, G. A. Koutsantonis, M. I. Ogden Magnetic properties of calix[4]arene-supported metal coordination clusters Coord. Chem. Rev. 402 (2020) 213066 10.1016/j.ccr.2019.213066

[26] S. Pasquale, S. Sattin, E. C. Escudero-Adán, M. Martínez-Belmonte, J. de Mendoza Giant regular polyhedra from calix[4]arene carboxylates and uranyl Nat Commun 3 (2012) 785 10.1038/ncomms1793

[27] T. Kajiwara, N. Iki, M. Yamashita Transition metal and lanthanide cluster complexes constructed with thiacalix[n]arene and its derivatives Coord. Chem. Rev. 251 (2007) 1734-1746 10.1016/j.ccr.2007.01.001

[28] (a) G. Mislin, E. Graf, M. W. Hosseini, A. Bilyk, A. K. Hall, J. M. Harrowfield, B. W. Skelton, A. H. White Thiacalix[4]arenes as cluster keepers: synthesis and structural analysis of a magnetically coupled tetracopper(ii) square Chem. Commun. (1999) 373-374 10.1039/A809184F; (b) H. Akdas, E. Graf, M. W. Hosseini, A. De Cian, A. Bilyk, B. W. Skelton, G. A. Koutsantonis, I. Murray, J. M. Harrowfield, A. H. White Koilands from thiophiles: mercury(II) clusters from thiacalix[4]arenes Chem. Commun. (2002) 1042-1043 10.1039/B201379G; (c) C. Desroches, G. Pilet, S. A. Borshch, S. Parola, D. Luneau Tetranuclear Manganese(II) Complexes of Thiacalix[4]arene Macrocycles with Trigonal Prismatic Six-Coordinate Geometries: Synthesis, Structure, and Magnetic Properties Inorg. Chem. 44 (2005) 9112-9120 10.1021/ic050507g; (d) T. Kajiwara, T. Kobashi, R. Shinagawa, T. Ito, S. Takaishi, M. Yamashita, N. Iki Highly Symmetrical Tetranuclear Cluster Complexes Supported by p-tert- Butylsulfonylcalix[4]arene as a Cluster-Forming Ligand Eur. J. Inorg. Chem. (2006) 1765-1770 10.1002/ejic.200501086; (e) C. Desroches, G. Pilet, P. Á. Szilágyi, G. Molnár, S. A. Borshch, A. Bousseksou, S. Parola, D. Luneau Tetra- and Decanuclear Iron(II) Complexes of Thiacalix[4]arene Macrocycles: Synthesis, Structure, Mössbauer Spectroscopy and Magnetic Properties Eur. J. Inorg. Chem. (2006) 357-365 10.1002/ejic.200500640; (f) M. Lamouchi, E. Jeanneau, A. Pillonnet, A. Brioude, M. Martini, O. Stéphan, F. Meganem, G. Novitchi, D. Luneau, C. Desroches Tetranuclear manganese(II) complexes of sulfonylcalix[4]arene macrocycles: synthesis, structure, spectroscopic and magnetic properties Dalton Trans. 41 (2012) 2707-2713 10.1039/C2DT11786J; (g) Y. Suffren, N. O'Toole, A. Hauser, E. Jeanneau, A. Brioude, C. Desroches Discrete polynuclear manganese(ii) complexes with thiacalix[4]arene ligands: synthesis, structures and photophysical properties Dalton Trans. 44 (2015) 7991-8000 10.1039/C5DT00827A; (h) C. Lecourt, Y. Suffren, E. Jeanneau, D. Luneau, C. Desroches Mono-, Di-, and Tetranuclear Manganese(II) Complexes with *p*-Phenylsulfonylcalix[4]arene Macrocycles as Ligand Antennas: Synthesis, Structures, and Emission Properties Cryst. Growth Des 22, (2022) 2279-2288 10.1021/acs.cgd.1c01348; (i) M-L. Xu, C-X. Wang, H-H. Hou, S-Y. Wan, Y-S. Kang, W-L. Shan Assembly of three sulfonylcalix[4]arene-based multinuclear complexes: Tunable structures and guest encapsulation properties Inorganic Chemistry Communications 142 (2022) 109643 10.1016/j.inoche.2022.109643

[29] (a) Y. Bi, W. Liao, G. Xu, R. Deng, M. Wang, Z. Wu, S. Gao, H. Zhang Three p-tert-Butylthiacalix[4]arene-Supported Cobalt Compounds Obtained in One Pot Involving In Situ Formation of N_6H_2 Ligand Inorg. Chem. 49 (2010) 7735-7740 10.1021/ic1005105; (b) K. Li, W. Liao Two sulfur and nitrogen-rich cobalt–thiacalix[4] arene compounds for the selective mercury removal from aqueous solutions CrystEngComm 22 (2020) 7668-7672 10.1039/D0CE01209B; (c) K. Li, Z. Zhuang, W. Chen, W. Liao Anion-Directed Assembly of Nickel-

Calix[4]arene Complexes: Constructing Isolated {Ni_8}, {Ni_{20}}, {Ni_{24}}, and {Ni_{32}} Clusters Cryst. Growth Des. 20 (2020) 4164-4168 10.1021/acs.cgd.0c00426

[30] (a) A. Bilyk, A. K. Hall, J. M. Harrowfield, M. W. Hosseini, B. W. Skelton, A. H. White A Unique Rare-Earth Cluster within a Calix[4]arene Sandwich: Parallels in the Chemistry of Cyclosiloxanes and Calix[4]arenes Aust. J. Chem. 53 (2000) 895-898 10.1071/CH00152; (b) T. Kajiwara, K. Katagiri, M. Hasegawa, A. Ishii, M. Ferbinteanu, S. Takaishi, T. Ito, M. Yamashita, N. Iki Conformation-Controlled Luminescent Properties of Lanthanide Clusters Containing p-tert-Butylsulfonylcalix[4]arene Inorg. Chem. 45 (2006) 4880-4882 10.1021/ic060397t; (c) Y. Bi, X-T. Wang, W. Liao, X. Wang, R. Deng, H. Zhang, S. Gao Thiacalix[4]arene-Supported Planar Ln_4 (Ln = Tb^{III}, Dy^{III}) Clusters: Toward Luminescent and Magnetic Bifunctional Materials Inorg. Chem. 48 (2009) 11743-11747 10.1021/ic9017807; (d) C-M. Liu, D-Q. Zhang, X. Hao, D-B. Zhu Syntheses, Crystal Structures, and Magnetic Properties of Two p-tert-Butylsulfonylcalix[4]arene Supported Cluster Complexes with a Totally Disordered $Ln_4(OH)_4$ Cubane Core Cryst. Growth Des. 12 (2012) 2948-2954 10.1021/cg300173t; (e) J-Y. Ge, X. Duan, J-P. Ma, S. Huang, J. Du, P. Wang Thiacalix[4]arene-Supported Tetranuclear Tb^{III} and Eu^{III} Compounds: Synthesis, Structure, Luminescence, and Magnetism Z. Anorg. Allg. Chem. 645 (2019) 416-421 10.1002/zaac.201800356

[31] J-Y. Ge, J. Ru, F. Gao, Y. Song, X-H. Zhou, J-L. Zuo Pentanuclear lanthanide pyramids based on thiacalix[4]arene ligand exhibiting slow magnetic relaxation Dalton Trans. 44 (2015) 15481-15490 10.1039/C5DT02062J;

[32] T. Kajiwara, H. Wu, T. Ito, N. Iki, S. Miyano Octalanthanide Wheels Supported by p-tert-Butylsulfonylcalix[4]arene Angew. Chem. Int. Ed. 43 (2004) 1832-1835 10.1002/anie.200353449

[33] Z. Li, D. Wang, Z. Zhou, G. Zhao, Q. Li, Y. Bi, Z. Zheng Thiacalix[4]arene-Sandwiched Sandglass-like Ln_9 Clusters (Ln = Tb and Eu): Insights into the Selective Luminescence Quenching Properties by p-Nitrobenzene Derivatives Inorg. Chem. 61 (2022) 20814-20823 10.1021/acs.inorgchem.2c03107

[34] (a) Y. Bi, Y. Li, W. Liao, H. Zhang, D. Li A Unique Mn_2Gd_2 Tetranuclear Compound of p-tert-Butylthiacalix[4]arene Inorg. Chem. 47 (2008) 9733-9735 10.1021/ic801086n; (b) Y. Bi, X-T. Wang, B-W. Wang, W. Liao, X. Wang, H. Zhang, S. Gao, D. Li Two $Mn^{II}_2Ln^{III}4$ (Ln = Gd, Eu) hexanuclear compounds of *p*-tert-butylsulfinylcalix[4]arene Dalton Trans. (2009) 2250-2254 10.1039/B817515B; (c) N. Iki, M. Ohta, T. Tanaka, T. Horiuchi, H. Hoshino A supramolecular sensing system for Ag^I at nanomolar levels by the formation of a luminscent Ag^I-Tb^{III}–thiacalix[4]arene ternary complex New J. Chem. 33 (2009) 23-25 10.1039/B816596C; (d) N. Iki, S. Hiro-oka, T. Tanaka, C. Kabuto, H. Hoshino Highly Efficient Near-Infrared-Emitting Lanthanide(III) Complexes Formed by Heterogeneous Self-Assembly of Ag^I, Ln^{III}, and Thiacalix[4]arene-p-tetrasulfonate in Aqueous Solution (Ln^{III} = Nd^{III}, Yb^{III}) Inorg. Chem. 51 (2012) 1648-1656 10.1021/ic2019583; (e) N. Iki, T. Tanaka, H. Hoshino The role of cadmium(II) bridges in the self-assembly with lanthanide(III) and thiacalix[4]arene (TCAS) to selectively form a luminescent ternary $Cd^{II}_2.Tb^{III}_2.TCAS_2$ complex Inorg. Chim. Acta 397 (2013) 42-47 10.1016/j.ica.2012.11.016; (f) K. Su, F. Jiang, J. Qian, M. Wu, K. Xiong, Y. Gai, M. Hong Thiacalix[4]arene-Supported Kite-Like Heterometallic Tetranuclear $Zn^{II}Ln^{III}_3$ (Ln = Gd, Tb, Dy, Ho) Complexes Inorg. Chem. 52 (2013) 3780-3786 10.1021/ic302367q; (g) S. M. Aldoshin, N. A. Sanina, S. E. Solov'eva, I. S. Antipin, A. I. Dmitriev, R. B. Morgunov, D. V. Korchagin, G. V. Shilov, A. N. Utenyshev, K. V. Bozhenko Thiacalix[4]arene-containing M_2Ln_2 complexes (M = Mn^{II}, Co^{II}; Ln = Eu^{III}, Pr^{III}): synthesis, structure, and magnetic properties Russ. Chem. Bull. 63 (2014) 1465-1474 10.1007/s11172-014-0622-7; (h) X. Zhu, W. Liao 3d-4f coordination compounds of water-soluble sulfonylcalix[4]arenetetrasulfonate in cone conformation Polyhedron 111 (2016) 185-189 10.1016/j.poly.2016.03.040; (i) S. M. Aldoshin, I. S. Antipin, M. V. Kniazeva, D. V. Korchagin, R. B. Morgunov, A. S. Ovsyannikov, A. V. Palii, N. A. Sanina, G. V. Shilov, S. E. Solovieva Synthesis, Structure and Magnetic Properties of Mn_2Tb_2 Tetranuclear Complex with *p*-tert-Butylthiacalix[4]arene Isr. J. Chem. 60 (2020) 600-606 10.1002/ijch.201900155

[35] (a) Q. Lenne, A. Mattiuzzi, I. Jabin, N. Le Poul, Y. R. Leroux, C. Lagrost Functionalizing Gold Nanoparticles with Calix[4]arenes Monolayers for Enhancing Selectivity and Stability in ORR Electrocatalysis Adv. Mater. Interfaces. 7 (2020) 2001557; (b) P. Padnya, V. Gorbachuk, I. Stoikov The Role of Calix[n]arenes and Pillar[n]arenes in the Design of Silver Nanoparticles: Self-Assembly and Application Int. J. Mol. Sci. 21 (2020) 1425 10.3390/ijms21041425; (c) M. Retout, B. Cornelio, G. Bruylants, I. Jabin Bifunctional Calix[4]arene-Coated Gold Nanoparticles for Orthogonal Conjugation Langmuir 38 (2022) 9301-9309 10.1021/acs.langmuir.2c01122

[36] (a) N. de Silva, J-M. Ha, A. Solovyov, M. M. Nigra, I. Ogino, S. W. Yeh, K. A. Durkin, A. Katz A bioinspired approach for controlling accessibility in calix[4]arene-bound metal cluster catalysts Nature Chem., 2 (2010), 1062-1068 10.1038/nchem.860; (b) J-M. Ha, A. Solovyov, A. Katz Accessibility in Calix[8]arene-Bound Gold

Nanoparticles: Crucial Role of Induced-Fit Binding J. Phys. Chem. C 114 (2010) 16060-16070 10.1021/jp104122m; (c) X. Chen, H. Häkkinen Protected but Accessible: Oxygen Activation by a Calix[4]arene-Stabilized Undecagold Cluster J. Am. Chem. Soc. 135 (2013) 12944-12947 10.1021/ja4059074

[37] (a) T. R. Tshikhudo, D. Demuru, Z. Wang, M. Brust, A. Secchi, A. Arduini, A. Pochini, Molecular recognition by calix[4]arene-modified gold nanoparticles in aqueous solution. Angew. Chem. Int. Ed. 44 (2005) 2913-2916 10.1002/anie.200462909; (b) J. Hassinen, P. Pulkkinen, E. Kalenius, T. Pradeep, H. Tenhu, H. Häkkinen, R. H. A. Ras Mixed-Monolayer-Protected Au_{25} Clusters with Bulky Calix[4]arene Functionalities J. Phys. Chem. Lett. 5 (2014) 585-589 10.1021/jz500052h

[38] Z-J. Guan, R-L. He, S-F. Yuan, J-J. Li, F. Hu, C-Y. Liu, Q-M. Wang Ligand Engineering toward the Trade-Off between Stability and Activity in Cluster Catalysis Angew. Chem. Int. Ed. 61 (2022) e2021169 10.1002/anie.202116965

[39] Z-J. Guan, J-L. Zeng, Z-A. Nan, X-K. Wan, Y-M. Lin, Q-M. Wang Thiacalix[4]arene: New protection for metal nanoclusters Sci. Adv. 2 (2016) e1600323 10.1126/sciadv.1600323

[40] Z-J. Guan, F. Hu, S-F. Yuan, Z-A. Nan, Y-M. Lin, Q-M. The stability enhancement factor beyond eight-electron shell closure in thiacalix[4]arene- protected silver clusters Chem. Sci. 10 (2019) 3360-3365 10.1039/C8SC03756F

[41] W-X. Xie, C-H. Xue, M. Liu, K. Zhou, H-H. Gu, J-Y. Ji, B-K. Chen, N. Liu, Y-F. Bi Thiacalix[4]arene-protected alkynyl Ag_n (n = 9, 18) nanoclusters: syntheses, structural characterizations, photocurrent responses and fluorescence properties Dalton Trans. 52 (2023) 13405-13412 10.1039/D3DT02285D

[42] R. K. Gupta, L. Li, Z. Wang, B-L. Han, L. Feng, Z-Y. Gao, C-H. Tung, D. Sun Regulating the assembly and expansion of the silver cluster from the Ag_{37} to Ag_{46} nanowheel driven by heteroanions Chem. Sci. 14, (2023) 1138-1144 10.1039/D2SC06436G

[43] Z. Wang, H-F. Su, Y-W. Gong, Q-P. Qu, Y-F. B, C-H. Tung, D. Sun, L-S. Zheng hierarchically assembled 88-nuclei silver-thiacalix[4]arene nanocluster Nat. Commun. 11 (2020) 308 10.1038/s41467-019-13682-5

[44] Z. Wang, F. Alkan, C. M. Aikens, M. Kurmoo, Z-Y. Zhang, K-P. Song, C-H. Tung, D. Sun An Ultrastable 155-Nuclei Silver Nanocluster Protected by Thiacalix[4]arene and Cyclohexanethiol for Photothermal Conversion Angew. Chem., Int. Ed. 61 (2022) e202206742 10.1002/anie.202206742

[45] Z. Wang, L. Li, L. Feng, Z-Y. Gao, C-H. Tung, L-S. Zheng, D. Sun Solvent-Controlled Condensation of $[Mo_2O_5(PTC4A)_2]^{6-}$ Metalloligand in Stepwise Assembly of Hexagonal and Rectangular Ag_{18} Nanoclusters Angew. Chem. Int. Ed. 61 (2022) e202200823 10.1002/anie.202200823

[46] Z. Wang, H-F. Su, L-P. Zhang, J-M. Dou, C-H. Tung, D. Sun, L. Zheng Stepwise Assembly of Ag_{42} Nanocalices Based on a Mo^{VI}-Anchored Thiacalix[4]arene Metalloligand ACS Nano 16 (2022) 4500-4507 10.1021/acsnano.1c10905

[47] S-Qi. Li, L-F. Dai, Y-Q. Tian, Y-X. Yi, J. Yan, C. Liu Polymolybdate-guided assembly of a thiacalix[4]arene-protected Ag nanocluster for electrocatalytic CO_2 reduction Chem. Commun. 59 (2023) 575-578 10.1039/D2CC05692E

[48] Z. Wang, Y-J. Zhu, O. Ahlstedt, K. Konstantinou, J. Akola, C-H. Tung, F. Alkan, D. Sun Three in One: Three Different Molybdates Trapped in a Thiacalix[4]arene Protected Ag_{72} Nanocluster for Structural Transformation and Photothermal Conversion Angew. Chem. Int. Ed. 63 (2024) e202314515 10.1002/anie.202314515

[49] N. Frank, A. Dallmann, B. Braun-Cula, C. Herwig, C. Limberg Mercaptothiacalix[4]arenes Steer 24 Copper(I) Centers to form a Hollow- Sphere Structure Featuring Cu_2S_2 Motifs with Exceptionally Short Cu···Cu Distances Angew. Chem. Int. Ed. 59 (2020) 6735-6739 10.1002/anie.201915882

[50] Y. Bi, X-T. Wang, W. Liao, X. Wang, X. Wang, H. Zhang, S. Gao A $\{Co_{32}\}$ Nanosphere Supported by p-tert-Butylthiacalix[4]arene J. Am. Chem. Soc. 131 (2009) 11650-11651 10.1021/ja9034939

[51] A. Bilyk, J. W. Dunlop, R. O. Fuller, A. K. Hall, J. M. Harrowfield, M. W. Hosseini, G. A. Koutsantonis, I. W. Murray, B. W. Skelton, R. L. Stamps, A. H. White Systematic Structural Coordination Chemistry of p-tert-Butyltetrathiacalix[4]arene: Further Complexes of Transition-Metal Ions Eur. J. Inorg. Chem. (2010) 2106-2126 10.1002/ejic.200901071

[52] A. Gehin, S. Ferlay, J. M. Harrowfield, D. Fenske, N. Kyritsakas, M. W. Hosseini Giant Core−Shell Nanospherical Clusters Composed of 32 Co or 32 Ni Atoms Held by 6 p-tert-Butylthiacalix[4]arene Units Inorg. Chem. 51 (2012) 5481-5486 10.1021/ic300550v

[53] M. Zhang, M. Chen, Y. Bi, L. Huang, K. Zhou, Z. Xu, Z. Zheng A bimetallic Co_4Mo_8 cluster built from Mo_8 oxothiomolybdate capped by a Co_4-thiacalix[4] arene unit: the observation of the Co–Mo synergistic effect for binder-free electrocatalysts J. Mater. Chem. A 7 (2019) 12893-12899 10.1039/C9TA01603A

[54] M. Wang, Y. Guo, G. Zhao, B. Chen, Y. Bi Ni_4-thiacalix[4]arene sandwiched Mo_8 polyoxometalate bimetallic nanoclusters for electrocatalytic glucose oxidation Chin. Chem. Lett. 34 (2023) 107365 10.1016/j.cclet.2022.03.088

[55] Y. Bi, S. Du, W. Liao p-tert-Butylthiacalix[4]arene-supported high-nuclearity $\{Co_{24}M_8\}$ (M = Mo or W) nanospheres and the hybrids with Keggin polyoxometalates Chem. Commun. 47 (2011) 4724-4726 10.1039/C0CC05574C

[56] X. Hang, Y. Yu, Z. Wang, Y. Bi Thiacalix[4]arene-Supported MoNa Clusters: Crystal Transition and Mo-S Coordination on Visible-Light Absorption Cryst. Growth Des. 20 (2020) 7934-7940 10.1021/acs.cgd.0c01204

[57] S. Wang, Y. Bi, W. Liao Constructing calix[4]arene-supported high nuclearity Co_{27}, Co_{28} and $Ni_{18}Na_6$ clusters with triazoles as co-bridges CrystEngComm,17 (2015) 2896-2902 10.1039/C5CE00314H

[58] S. Zhou, C. Li, H. Fu, J. Cao, J. Zhang, L. Zhang Lead-Doped Titanium-Oxo Clusters as Molecular Models of Perovskite-Type $PbTiO_3$ and Electron-Transport Material in Solar Cells Chem. Eur. J. 26 (2020) 6894-6898 10.1002/chem.202000911

[59] S K. Xiong, X. Wang, F. Jiang, Y. Gai, W. Xu, K. Su, X. Li, D. Yuan, M. Hong Heterometallic thiacalix[4]arene-supported $Na_2Ni^{II}_{12}Ln^{III}_2$ clusters with vertex-fused tricubane cores (Ln = Dy and Tb) Chem. Commun. 48 (2012) 7456-7458 10.1039/c2cc32360e

[60] K-C. Xiong, F-L. Jiang, Y-L. Gai, D-Q. Yuan, D. Han, J. Ma, S-Q. Zhang, M-C. Hong Chlorine-Induced Assembly of a Cationic Coordination Cage with a m5- Carbonato-Bridged Mn^{II} Core Chem. Eur. J. 18 (2012) 5536-5540 10.1002/chem.201200125

[61] C. Shi, M. Zhang, X. Hang, Y. Bi, L. Huang, K. Zhou, Z. Xu, Z. Zheng Assembly of thiacalix[4]arene-supported high-nuclearity Cd_{24} cluster with enhanced photocatalytic activity Nanoscale 10 (2018) 14448-14454 10.1039/C8NR03474E

[62] K. Su, F. Jiang, J. Qian, M. Wu, Y. Gai, J. Pan, D. Yuan, M. Hong Open Pentameric Calix[4]arene Nanocage Inorg. Chem. 53 (2014) 18-20 10.1021/ic4024184

[63] K. Su, F. Jiang, J. Qian, Y. Gai, M. Wu, S. M. Bawaked, M. Mokhtar, S. A. AL-Thabaiti, M. Hong Generalized Synthesis of Calix[4]arene-Based High-Nuclearity M_{4n} Nanocages (M = Ni or Co; n = 2-6) Cryst. Growth Des. 14 (2014) 3116-3123 10.1021/cg5003836

[64] K. Su, F. Jiang, J. Qian, J. Pan, J. Pang, X. Wan, F. Hu, M. Hong Self-assembly of two high-nuclearity manganese calix[4]arene-phosphonate clusters: diamond-like Mn_{16} and drum-like Mn_{14} RSC Adv. 5 (2015) 33579-33585 10.1039/C5RA02530C

[65] K. Su, F. Jiang, M. Wu, J. Qian, J. Pang, D. Yuan, M. Hong Syntheses, structures, luminescence and magnetic properties of three high-nuclearity neodymium compounds based on mixed sulfonylcalix[4]arene- phosphonate ligands CrystEngComm 18 (2016) 4921-4928 10.1039/C6CE00092D

[66] K. Xiong, F. Jiang, Y. Gai, Z. He, D. Yuan, L. Chen, K. Su, M. Hong Self-Assembly of Thiacalix[4]arene-Supported Nickel(II)/Cobalt(II) Complexes Sustained by in Situ Generated 5-Methyltetrazolate Ligand Cryst. Growth Des. 12 (2012) 3335-3341 10.1021/cg300483c

[67] C-M. Liu, D-Q. Zhang, X. Hao, D-B. Zhu Calix[4]arene-Supported Polynuclear Cobalt(II) Cluster Complexes Tuned by Substitution Groups of the Second Bridging Ligands Eur. J. Inorg. Chem. (2012) 4210-4217 10.1002/ejic.201200682

[68] M. Chen, M. Zhang, X. Wang, Y. Bi, B. Chen, Z. Zheng Thiacalix[4]arene-Supported Irregular Co_{26} and Ni_{28} High-Nuclearity Clusters with Pyridyl-Diphosphonates: Strategies to Create Active Metal Sites and Fabricate Multicomponent Materials Inorg. Chem. 58 (2019) 6276-6282 10.1021/acs.inorgchem.9b00495

[69] Z. Zhou, L. Xu, G. Zhao, K. Zhou, B. Chen, Y. Bi An ultra-stable Cu^I_{12} cluster built from a Cu^I_6 precursor sandwiched by two Cu^I_3-thiacalix[4]arene units for efficient photothermal conversion Inorg. Chem. Front. 10 (2023) 3230-3236 10.1039/D3QI00479A

[70] (a) A. Caneschi, A. Cornia, A. C. Fabretti, S.Foner, D. Gatteschi, R. Grandi, L. Schenetti Synthesis, Crystal Structure, Magnetism, and Magnetic Anisotropy of Cyclic Clusters Comprising six Iron(III) Ions and

Entrapping Alkaline Ions Chem. Eur. J.2 (1996) 1379-1387 10.1002/chem.19960021109; (b) J. A. Whiteford, C. V. Lu, P. J. Stang Molecular Architecture via Coordination: Self-Assembly, Characterization, and Host−Guest Chemistry of Mixed, Neutral-Charged, Pt−Pt and Pt−Pd Macrocyclic Tetranuclear Complexes. X-ray Crystal Structure of Cyclobis[[cis- Pt(dppp)(4-ethynylpyridine)$_2$][cis-Pd^{2+}(PEt$_3$)$_2^{2-}$OSO$_2$CF$_3$]] J. Am. Chem. Soc. 119 (1997) 2524-2533 10.1021/ja9635286; (c) R. W. Saalfrank, I. Bernt, E. Uller, F. Hampel Template-Mediated Self Assembly of Six- and Eight-Membered Iron Coronates Angew Chem., Int. Ed. Engl. 37 (1997) 2482-2485 10.1002/anie.199724821; (d) R. Piotrowski, K. Polborn, G. Hilt, K. Severin A Self-Assembled metallamacrocyclic ionophore with ohgh affinity and selectivity for Li^+ and Na^+ J. Am. Chem. Soc. 123 (2001) 2699-2700 10.1021/ja005804t

[71] T. Kajiwara, K. Katagiri, S. Takaishi, M. Yamashita, N. Iki A Dodecalanthanide Wheel Supported by p-tert-Butylsulfonylcalix[4]arene Chem. Asian J. 1 (2006) 349-351 10.1002/asia.200600057

[72] W-L. Mu, L. Wu, W-D. Yu, X-Y. Yi, J. Yan, C. Liu Atomically accurate structural tailoring of thiacalix[4]arene-protected copper(ii)-based metallamacrocycles, Dalton Trans. 52 (2023) 5438-5442 10.1039/D3DT00455D

[73] Y. Bi, G. Xu, W. Liao, S. Du, X. Wang, R. Deng, H. Zhang, S. Gao Making a [Co$_{24}$] metallamacrocycle from the shuttlecock-like tetranuclear cobalt-calix[4]arene building blocks properties Chem. Commun. 46 (2010) 6362-6364 10.1039/C0CC01844A

[74] X. Han, A. Feixue, X. Wang, B. Chen, L. Wang, Y. Bi Thiacalix[4]arene-supported Co$_{24}$ nanocluster derived octahedral Co$_9$S$_8$ nanoparticles in N-doped carbon for superior Li-ion storage Polyhedron 171 (2019) 279-284 10.1016/j.poly.2019.07.027

[75] C-M. Liu, D-Q. Zhang, X. Hao, D-B. Zhu Nestlike C$_4$-Symmetric [Co$_{24}$] Metallamacrocycle Sustained by p-tert-Butylsulfonylcalix[4]arene and 1,2,4-Triazole Chem. Eur. J. 17 (2011) 12285-12288 10.1002/chem.201101607

[76] K. Zhang, S-W. Du A novel series of giant cobalt-calix[4]arene macrocycles: ring-expansion and modulation of pore apertures through recrystallization Dalton Trans. 50 (2021) 6181-6187 10.1039/D1DT00556A

[77] S. Wang, X. Gao, X. Hang, X. Zhu, H. Han, X. Li, W. Liao, W. Chen Calix[4]arene-Based {Ni18} Coordination Wheel: Highly Efficient Electrocatalyst for the Glucose Oxidation and Template for the Homogenous Cluster Fabrication J. Am. Chem. Soc. 140 (2018) 6271-6277 10.1021/jacs.7b13193

[78] P. P. Cholewa, S. J. Dalgarno Metal–organic calix[4]arene capsules: the evolution of controlled assembly CrystEngComm 16, (2014) 3655-3666 10.1039/C3CE42169D

[79] C. M. A. Gangemia, A. Pappalardoa, G. T. Sfrazzetto Assembling of Supramolecular Capsules with Resorcin[4]arene and Calix[n]arene Building Blocks Curr. Org. Chem. 19 (2015) 2281-2308 10.2174/1385272819666150608221916

[80] Y. Liang, E. Li, K. Wang, Z-J. Guan, H-H. He, L. Zhang, H-C. Zhou, F. Huang, Y. Fang Organo-macrocycle-containing hierarchical metal–organic frameworks and cages: design, structures, and applications Chem. Soc. Rev. 51 (2022) 8378-8405 10.1039/D2CS00232A

[81] Y. Bi, S. Du, W. Liao Thiacalixarene-based nanoscale polyhedral coordination cages Coord. Chem. Rev. 276 (2014) 61-72 10.1016/j.ccr.2014.06.011

[82] H. Tan, S. Du, Y. Bi, W. Liao Two 2D Metal-Calix[4]arene Aggregates Incorporating Pre-Designed Coordination Nanocages. Chem. Commun. 49 (2013) 8211-8213 10.1039/C3CC42259C

[83] K. Su, F. Jiang, J. Qian, J. Pang, F. Hu, S. M. Bawaked, M. Mokhtar, S. A. Al-Thabaitic, M. Hong Bridging different Co$_4$–calix[4]arene building blocks into grids, cages and 2D polymers with chiral camphoric acid CrystEngComm. 17 (2015) 1750-1753 10.1039/C4CE02186J

[84] M. V. Kniazeva, A. S. Ovsyannikov, A. I. Samigullina, D. R. Islamov, A. T. Gubaidullin, P. V. Dorovatovskii, V. A. Lazarenko, S. E. Solovieva, I. S. Antipin, S.Ferlay, Impact of Flexible Succinate Connectors on the Formation of Tetrasulfonylcalix[4]Arene Based Nano-Sized Polynuclear Cages: Structural Diversity and Induced Chirality Study. CrystEngComm 24 (2022) 628-638 10.1039/D1CE01482J

[85] C.-Z. Sun, T.-P. Sheng, F.-R. Dai, Z.-N. Chen Sulfonylcalixaren-Based Ortho -Dicarboxylate-Bridged Coordination Containers for Guest Encapsulation and Separation. Cryst. Growth Des.19 (2019) 1144-1148 10.1021/acs.cgd.8b01633

[86] J.-Y. Liu, T.-P. Sheng, C. Li, Z. Wang, F.-R.; Dai, Z.-N Chen Iodine Adsorption *via* Porous Molecular Solids Based on Coordination Containers Derived from Naphthalene-1,8-Dicarboxylate. Cryst. Growth Des. 22 (2022) 3182-3189 10.1021/acs.cgd.2c00039

[87] F.-R. Dai, Y. Qiao, Z. Wang, Designing Structurally Tunable and Functionally Versatile Synthetic Supercontainers. Inorg. Chem. Front. 3 (2016) 243-249 10.1039/C5QI00212E

[88] Y. Qiao, L. Zhang, J. Li, W. Lin, Z. Wang, Switching on Supramolecular Catalysis *via* Cavity Mediation and Electrostatic Regulation. Angew. Chem. 128 (2016) 12778-12782 10.1002/anie.201606847.

[89] L.-J. Cheng, X.-X. Fan, Y.-P. Li, Q.-H. Wei, F.-R. Dai, Z.-N. Chen, Z. Wang, Engineering Solid-State Porosity of Synthetic Supercontainers *via* Modification of Exo-Cavities. Inorg. Chem. Commun. 78 (2017) 61-64 10.1016/j.inoche.2017.03.005

[90] N. Bhuvaneswari, K. P. Annamalai, F.-R. Dai, Z.-N. Chen, Pyridinium Functionalized Coordination Containers as Highly Efficient Electrocatalysts for Sustainable Oxygen Evolution. J. Mater. Chem. A 5 (2017) 23559-23565 10.1039/C7TA05797K.

[91] N. Bhuvaneswari, F.-R. Dai, Z.-N. Chen, Sensitive and Specific Guest Recognition through Pyridinium-Modification in Spindle-Like Coordination Containers. Chem. Eur. J. 24 (2018), 6580-6585 10.1002/chem.201705210

[92] M. R. Dworzak, C. A. Rowland, G. P. A. Yap, E. D. Bloch, Controlling Phase in Low-Nuclearity Calix[4]arene-Capped Porous Coordination Cages with Ligand Functionalization. CrystEngComm 24 (2022) 6315-6319 10.1039/D2CE00861K

[93] M. V. Kniazeva, A. S. Ovsyannikov, B. Nowicka, N. Kyritsakas, A. I. Samigullina, A. T. Gubaidullin, D. R. Islamov, P. V. Dorovatovskii, E. V. Popova, S. R. Kleshnina, S. E. Solovieva, I. S. Antipin, S. Ferlay Porous nickel and cobalt hexanuclear ring-like clusters built from two different kind of calix[4]arene ligands – new molecular traps for small volatile molecules CrystEngComm. 24 (2022) 330-340 10.1039/D1CE01361K

[94] M. Liu, W. Liao, Bridging Calix[4]arene-Based {Co_4} Units into a Square or Belt with Aromatic Dicarboxylic Acids. CrystEngComm 14 (2012) 5727-5729 10.1039/C2CE25692D

[95] D. Wang, M. Zhu, G. Zhao, B. Chen, Y. Bi, Post-Modified Thiacalix[4]Arene-Based Ni_{16}-NH_2 Cluster by Ferrocene for Synergistic Photothermal Conversion Property Inorg. Chim. Acta 555 (2023) 121587 10.1016/j.ica.2023.121587

[96] X. Hang, S. Wang, X. Zhu, H. Han, W. Liao pH-dependent formation of different coordination cages based on Co_4-TC_4A secondary building units and bridging ligands CrystEngComm 18 (2016) 4938-4943 10.1039/C6CE00028B

[97] F.-R. Dai, D. C. Becht, Z. Wang, Modulating Guest Binding in Sulfonylcalix[4]arene-Based Metal-Organic Supercontainers. Chem. Commun. 50 (2014) 5385-5387 10.1039/C3CC47420H

[98] C. M. Montone, M. R. Dworzak, G. P. A. Yap, E. D. Bloch Covalent modification of surfaces with porous metal–organic materials J. Mater. Chem. A, 11 (2023) 23888-23894 10.1039/D3TA04662A

[99] M. R. Dworzak, M. M. Deegan, G. P. A. Yap, E. D. Bloch, Synthesis and Characterization of an Isoreticular Family of Calix[4]arene-Capped Porous Coordination Cages. Inorg. Chem. 60 (2021) 5607-5616 10.1021/acs.inorgchem.0c03554

[100] M. R. Dworzak, C. M. Montone, N. I. Halaszynski, G. P. A. Yap, C. J. Kloxin, E. D. Bloch, Rapid Post-Synthetic Modification of Porous Coordination Cages with Copper-Catalyzed Click Chemistry. Chem. Commun. 59 (2023) 8977-8980 10.1039/D3CC02015K

[101] C.; He, Y.-H.; Zou, D.-H.; Si, Z.-A.; Chen, T.-F.; Liu, R.; Cao, Y.-B.Huang, A Porous Metal-Organic Cage Liquid for Sustainable CO_2 Conversion Reactions. Nat Commun 14 (2023) 3317 10.1038/s41467-023-39089-x.

[102] M. R. Dworzak, J. Sampson, C. M. Montone, K. J. Korman, G. P. A. Yap, E. D. Bloch, Postsynthetic Modification of Calixarene-Based Porous Coordination Cages. Chem. Mater. 36 (2024) 752-758 10.1021/acs.chemmater.3c02187.

[103] C. He, X. Chen, C.-Z. Sun, L.-Y. Zhang, W. Xu, S. Zhang, Z. Wang, F.-R. Dai, Decahexanuclear Zinc(II) Coordination Container Featuring a Flexible Tetracarboxylate Ligand: A Self-Assembly Supermolecule for

Highly Efficient Drug Delivery of Anti-Inflammatory Agents. ACS Appl. Mater. Interfaces 13 (2021) 33812-33820 10.1021/acsami.1c06311

[104] C.-Z. Sun, L.-J. Cheng, Y. Qiao, L.-Y. Zhang, Z.-N. Chen, F.-R. Dai, W. Lin, Z. Wang, Stimuli-Responsive Metal–Organic Supercontainers as Synthetic Proton Receptors. Dalton Trans. 47 (2018) 10256-10263 10.1039/C8DT01900B

[105] Y. Jin, H. Jiang, X. Tang, W. Zhang, Y. Liu, Y. Cui, Coordination-Driven Self-Assembly of Anthraquinone-Based Metal-Organic Cages for Photocatalytic Selective [2 + 2] Cycloaddition. Dalton Trans. 50 (2021) 8533-8539 10.1039/D1DT00652E

[106] X. Hang, X. Wang, M. Wang, M. Chen, Y. Bi, Thiacalix[4]arene-Based $\{Co/Fe\}_{16}$ Coordination Clusters: Bimetallic Synergistic Effect for an Enhanced Oxygen Evolution Reaction. Inorg. Chem. Front. 10 (2023) 926-933 10.1039/D2QI01885C

[107] A. Dey, M. R. Dworzak, K. D. P. Korathotage, M. Ghosh, J. Hoq, C. M. Montone, G. P. A. Yap, E. D. Bloch Increasing the Stability of Calixarene-Capped Porous Cages Through Coordination Sphere Tuning Dalton (2024), *under press*. 10.1039/D3DT03365A

[108] K. Xiong, F. Jiang, Y. Gai, D. Yuan, L. Chen, M. Wu, K. Su, M. Hong. Truncated octahedral coordination cage incorporating six tetranuclear-metal building blocks and twelve linear edges, Chem. Sci. 3 (2012) 2321-2325 10.1039/C2SC20264F

[109] M. M. Deegan, T. S. Ahmed, G. P. A. Yap, E. D. Bloch Structure and redox tuning of gas sorption properties in calix[4]arene-supported Fe(II)-based porous cages Chem. Sci. 11 (2020) 5273-5279 10.1039/D0SC01833C

[110] F-R. Dai, U. Sambasivam, A. J. Hammerstrom, Z. Wang Synthetic Supercontainers Exhibit Distinct Solution versus Solid State Guest-Binding Behavior J. Am. Chem. Soc. 136 (2014) 7480-7491 10.1021/ja502839b

[111] N. L. Netzer, F-R. Dai, Z. Wang, C. Jiang pH-Modulated Molecular Assemblies and Surface Properties of Metal-Organic Supercontainers at the Air-Water Interface Angew. Chem. Int. Ed. 53 (2014) 10965-10969 10.1002/ange.201406733

[112] C-X. Wang, N. Si, L. Wen, H-Y.Zan, X-X. Wang, W-L. Shan, A sulfonylcalix[4]arene-based metal–organic cage with octahedral porous structure for guest adsorption and separation Inorg. Chem. Commun. 153 (2023) 110874 10.1016/j.inoche.2023.110874

[113] W-L. Shan, M-L. Xu, H-H. Hou, P. Zhao, Q-Y. Zhang, M-J. Yin, F. Luo Sulfonylcalix[4]arene-based metal-organic polyhedra with hierarchical porous structures for efficient Xe/Kr separation. Nano Res. 16 (2023) 2536-2542 https://doi.org/10.1007/s12274-022-4909-y

[114] H. Y. Tong, J. Liang, Q. J. Wu, Y. H. Zou, Y. B. Huang R. Cao, Soluble imidazolium-functionalized coordination cages for efficient homogeneous catalysis of CO_2 cycloaddition reactions, Chem. Commun. 57 (2021) 2140-2143 10.1039/D0CC08098E

[115] H. Tan, S. Du, Y. Bi, W. Liao Two Elongated Octahedral Coordination Cages Constructed by M4-TC4A Secondary Building Units (M = Co^{II} and Fe^{II}) and 2,2′-Bipyridine-4,4′-dicarboxylic Acids Inorg. Chem. 53 (2014) 7083-7085 10.1021/ic501012e

[116] C. Tan, J. Jiao, Z. Li, Y. Liu, X. Han, Y. Cui Design and Assembly of a Chiral Metallosalen-Based Octahedral Coordination Cage for Supramolecular Asymmetric Catalysis Angew. Chem. Int. Ed. 57 (2018) 2085-2090 10.1002/anie.201711310

[117] M. Liu, W. P. Liao, C. Hu, S. C. Du, H. J. Zhang Calix[4]arene-Based Nanoscale Coordination Cages Angew. Chem., Int. Ed., 51 (2012) 1585-1588 10.1002/anie.201106732

[118] J. Zhang, Y. Deng, S. Wang, J. Yang, S. Hu A calix[4]arene-based coordination cage as an efficient luminescent sensor for Fe^{3+}, MnO_4^-, NB and 2,4-DNP in aqueous medium CrystEngComm 25 (2023) 1495-1500 10.1039/D2CE01508K

[119] Y. Guo, J. Li, G. Zhao, B. Chen, X. Hang, Y. Bi Post-synthetic atomically precise single-CuII sites in a thiacalix[4]arene-supported octahedral $Na@Co_{24}$ cluster: the Cu-Co synergistic effect for selective photocatalytic conversion of CO_2 to CO Chem. Commun. 59 (2023) 5591-5594 10.1039/D3CC01230A

[120] S. Du, C. Hu, J-C. Xiao, H. Tana, W. Liao A giant coordination cage based on sulfonylcalix[4]arene Chem. Commun. 48 (2012) 9177-9179 10.1039/C2CC34265K

[121] F-R. Dai, Z. Wang Modular Assembly of Metal−Organic Supercontainers Incorporating Sulfonylcalix[4]arenes J. Am. Chem. Soc. 134 (2012) 8002-8005 10.1021/ja300095j

[122] T-P. Sheng, C. He, Z. Wang, G-Z. Zheng, F-R. Dai, Z-N. Chen Precise Assembly and Supramolecular Catalysis of Tetragonal- and Trigonal-Elongated Octahedral Coordination Containers CCS Chem. 4 (2022) 1098-1107 10.31635/ccschem.021.202100987

[123] S. Du, T-Q. Yu, W. Liao, C. Hu Structure modeling, synthesis and X-ray diffraction determination of an extra-large calix[4]arene-based coordination cage and its application in drug delivery Dalton Trans. 44 (2015) 14394-14402 10.1039/C5DT01526J

[124] Y. Fang, Z. Xiao, J. Li, C. Lollar, L. Liu, X. Lian, S. Yuan, S. Banerjee, P. Zhang, H-C. Zhou Formation of a Highly Reactive Cobalt Nanocluster Crystal within a Highly Negatively Charged Porous Coordination Cage Angew. Chem. Int. Ed. 57 (2018) 5283-5287 10.1002/anie.201712372

[125] C. Liang, J. Yuan, C. Zhu, Y. Fang Surface charges of porous coordination cage tune the catalytic reactivity of Knoevenagel condensation Catal. Today 400-401 (2022) 89-94 10.1016/j.cattod.2021.11.008

[126] Y. Fang, Z. Xiao, A. Kirchon, J. Li, F. Jin, T. Togo, L. Zhang, C. Zhu, H-C. Zhou Bimolecular proximity of a ruthenium complex and methylene blue within an anionic porous coordination cage for enhancing photocatalytic activity Chem. Sci. 10 (2019) 3529-3534 10.1039/C8SC05315D

[127] Y. Fang, J. Li, T. Togo, F. Jin, Z. Xiao, L. Liu, H. Drake, X. Lian, H-C. Zhou Ultra-Small Face-Centered-Cubic Ru Nanoparticles Confined within a Porous Coordination Cage for Dehydrogenation Chem. 4 (2018) 555-563 10.1016/j.chempr.2018.01.004

[128] Y. Fang, H-C. Zhou Metal nanoparticles encapsulated within charge tunable porous coordination cages for hydrogen generation reaction Catalysis Today 374 (2021) 12-19 10.1016/j.cattod.2020.10.030

[129] K. K. Liu, Z. J. Guan, M. Ke, Y. Fang, Bridging the Gap between Charge Storage Site and Transportation Pathway in Molecular-Cage-Based Flexible Electrodes ACS Central Science 9 (2023) 805-815 10.1021/acscentsci.3c00027

[130] Y. Fang, X. Lian, Y. Huang, G. Fu, Z. Xiao, Q. Wang, B. Nan, J-P. Pellois, H-C. Zhou Investigating Subcellular Compartment Targeting Effect of Porous Coordination Cages for Enhancing Cancer Nanotherapy Small 14 (2018) 1802709 10.1002/smll.201802709

[131] Y. Liang, Y. Fang, Y. Cui, H. C. Zhou, A stable biocompatible porous coordination cage promotes *in vivo* liver tumor inhibition Nano Res. 14 (2021) 3407-3415 10.1007/s12274-021-3646-y

[132] J-P. Yuan, Z-J. Guan, H-Y. Lin, B. Yan, K-K. Liu, H-C. Zhou, Y. Fang Modeling the Enzyme Specificity by Molecular Cages through Angew. Chem. Int. Ed. (2023) e202303896 10.1002/anie.202303896

[133] X. Hang, W. Yang, S. Wang, H. Han, W. Liao, J. Jia Calix[4]arene-Based {Co_{26}} Burr Puzzle: An Efficient Oxygen Reduction Catalyst ACS Appl. Nano Mater. 2 (2019) 4232-4237 10.1021/acsanm.9b00683

[134] I. V. Khariushin, A. S. Ovsyannikov, S.A. Baudron, J. S. Ward, A. Kiesilä, K. Rissanen, E. Kalenius, K. A. Kovalenko, V. P. Fedin, S. E. Solovieva, I. S. Antipin, V. Bulach, S. Ferlay Selective gas sorption by calix[4]arene-based porous octahedral M_{32} coordination cages Chem. Commun. 58 (2022) 13628-13631 10.1039/D2CC04510A

[135] W. Gong, D. D. Chu, H. Jiang, X. Chen, Y. Cui, Y. Liu Permanent porous hydrogen-bonded frameworks with two types of Brønsted acid sites for heterogeneous asymmetric catalysis Nat. Commun., 10 (2019) 600 10.1038/s41467-019-08416-6

[136] S. Wang, Y. Bi, X. Hang, X. Zhu, W. Liao A Calix[4]arene-based {Co_9} Coordination Triangle as an Efficient Heterogenous Catalyst *Z.* Anorg. Allg. Chem. 643 (2017) 160-165 10.1002/zaac.201600409

[137] S. Wang, X. Gao, X. Hang, X. Zhu, H. Han, W. Liao, W. Chen Ultrafine Pt Nanoclusters Confined in a Calix[4]arene-Based {Ni_{24}} Coordination Cage for High-Efficient Hydrogen Evolution Reaction J. Am. Chem. Soc. 138 (2016) 16236-16239 10.1021/jacs.6b11218

[138] M. Liu, S. Du, W. Liao A tetrahedral coordination cage based on p-tert-butylthiacalix[4]arene and 5-sulfoisophthalic acid Inorg. Chem. Comm. 41 (2014) 96-99 10.1016/j.inoche.2014.01.009

[139] Y. Yu, Z. Wang, Z. Li, X. Hang, Y. Bi, Assembly of {Co_{14}} nanoclusters from adenine-modified Co_4-thiacalix[4]arene units CrystEngComm 23 (2021) 4382-4388 10.1039/D1CE00440A

[140] C. Shi, M. Chen, X. Han, Y. Bi, L. Huang, K. Zhou, Z. Zheng Thiacalix[4]arene-supported Tetradecanuclear Cobalt Nanocage Cluster as Precursor to Synthesize CoO/Co_9S_8@CN Composite for Supercapacitor Application Inorg. Chem. Front. 5 (2018) 1329-1335 10.1039/C8QI00178B

[141] Y. Bi, S. Wang, M. Liu, S. Du, W. Liao A tetragonal prismatic {Co_{32}} nanocage based on thiacalix[4]arene Chem. Commun. 49 (2013) 6785-6787 10.1039/C3CC43347A

[142] X. Hang, S. Wang, H. Pang, Q. Xu A coordination cage hosting ultrafine and highly catalytically active gold nanoparticles Chem. Sci. 13 (2022) 461-468 10.1039/D1SC05407D

[143] X. Hang, S. Wang, T. Xue, X. Zhu, H. Han, W. Liao Calix[4]arene-Based {Ni_{14}} Seesaws: Active Chloride Anions to be Substituted by Isophthalic Acids Cryst. Growth Des. 16 (2016) 6696-6699 10.1021/acs.cgd.6b01072

[144] K. Su, F. Jiang, J. Qian, L. Chen, J. Pang, S. M. Bawaked, M. Mokhtar, S. A. AL-Thabaiti, M. Hong Stepwise Construction of Extra-Large Heterometallic Calix[4]arene- Based Cages Inorg. Chem. 54 (2015) 3183-3188 10.1021/ic502677g

[145] X. Hang, B. Liu, X. Zhu, S. Wang, H. Han, W. Liao, Y. Liu, C. Hu Discrete {Ni_{40}} Coordination Cage: A Calix[4]arene-Based Johnson-Type (J_{17}) Hexadecahedron J. Am. Chem. Soc. 138 (2016) 2969-2972 10.1021/jacs.6b00695

[146] D. Geng, X. Han, Y. Bi, Y. Qin, Q. Li, L. Huang, K. Zhou, L. Song, Z. Zheng Merohedral icosahedral M_{48} (M = Co^{II}, Ni^{II}) cage clusters supported by thiacalix[4]arene Chem. Sci. 9 (2018) 8535-8541 10.1039/C8SC03193B

[147] H. Han, L. Kan, P. Li, G. Zhang, K. Li, W. Liao, Y. Liu, W. Chen, C. T. Hu 4.8 nm Concave {M_{72}} (M=Co, Ni, Fe) metal-organic polyhedra capped by 18 calix[4]arenes Sci. China Chem. 64 (2021) 426-431 10.1007/s11426-020-9909-2

[148] (a) J. L. Atwood, L. J. Barbour, A. Jerga Storage of Methane and Freon by Interstitial van der Waals Confinement Science 296 (2002) 2367-2369 10.1126/science.1072252; (b) J. L. Atwood, L. J. Barbour, P. K. Thallapally, T. B. Wirsig A crystalline organic substrate absorbs methane under STP conditions Chem. Commun. (2005) 51-52 10.1039/B416752J; (c) P. K. Thallapally, L. Dobrzańska, T. R. Gingrich, T. B. Wirsig, L. J. Barbour, J. L. Atwood Acetylene Absorption and Binding in a Nonporous Crystal Lattice Angew. Chem. Int. Ed. 45 (2006) 6506-6509 10.1002/anie.200601391; (d) P. K. Thallapally, B. P. McGrail, J. L. Atwood Sorption of nitrogen oxides in a nonporous crystal Chem. Commun. (2007) 1521-1522 10.1039/B617340C; (e) G. S. Ananchenko, I. L. Moudrakovski, A. W. Coleman, J. A. Ripmeester A Channel-Free Soft-Walled Capsular Calix[4]arene Solid for Gas sorption Angew. Chem. Int. Ed. 47 (2008) 5616-5618 10.1002/anie.200800071

[149] A. J. Gosselin, A. A. Rowland, E. D. Bloch Permanently Microporous Metal-Organic Polyhedra Chem. Rev. 120 (2020) 8987-9014 10.1021/acs.chemrev.9b00803

[150] M. M. Deegan, G. R. Lorzing, K. J. Korman, C. A. Rowland, M. R. Dworzak, A. M. Antonio, E. D. Bloch Hydrogen Storage in Porous Cages ACS Mater. Au 3 (2023) 66-74 10.1021/acsmaterialsau.2c00051

[151] (a) H-Y. Lin, L-Y. Zhou, L. Xu Photocatalysis in Supramolecular Fluorescent Metallacycles and Metallacages Chem. As. J. 16 (2021) 3805-3816 10.1002/asia.202100942; (b) R. Saha, B. Mondal, P. S. Mukherjee Molecular Cavity for Catalysis and Formation of Metal Nanoparticles for Use in Catalysis Chem. Rev. 122 (2022) 12244-12307 10.1021/acs.chemrev.1c00811

[152] Y. Xue, X. Hang, J. Ding, B. Li, R. Zhu, H. Pang, Q. Xu Coord. Chem. Rev. 430 (2021) 213656 10.1016/j.ccr.2020.213656

[153] X. Hanga, Y. Bi Thiacalix[4]arene-supported molecular clusters for catalytic applications Dalton Trans. 50 (2021) 3749-3758 10.1039/D0DT04233A

[154] K. K. Liu, Z. J. Guan, M. Ke, Y. Fang, Bridging the Gap between Charge Storage Site and Transportation Pathway in Molecular-Cage-Based Flexible Electrodes ACS Central Science 9 (2023) 805-815 10.1021/acscentsci.3c00027

[155] D. Wang, M. Zhu, G. Zhao, B. Chen, Y. Bi Post-modified thiacalix[4]arene-based Ni16-NH_2 cluster by ferrocene for synergistic photothermal conversion property Inorganica Chimica Acta 555 (2023) 121587. 10.1016/j.ica.2023.121587

[156] T-P. Sheng, X-X. Fan, G-Z. Zheng, F-R. Dai, Z-N. Chen Cooperative Binding and Stepwise Encapsulation of Drug Molecules by Sulfonylcalix[4]arene-Based Metal-Organic Supercontainers Molecules 25 (2020) 2656 10.3390/molecules25112656

[157] Z. Xiao, H. Lin, H. F. Drake, J. Diaz, H-C. Zhou, J-P. Pellois Investigating the Cell Entry Mechanism, Disassembly, and Toxicity of the Nanocage PCC-1: Insights into Its Potential as a Drug Delivery Vehicle J. Am. Chem. Soc.145 (2023) 27690-2770 10.1021/jacs.3c09918

[158] Z. Lu, S. Wang, G.-L. Li, Z. Zhuo, H. Zhu, W. Wang, Y.-G. Huang, M. Hong Ultrastable Photoluminescence Enabled by 1D Rare-Earth Metal–Organic Frameworks Based on Double Thiacalix[4]arene-Capped Nodes, ACS Applied Materials & Interfaces 14 (2022), 37894-37903 10.1021/acsami.2c07910

[159] H. Wang, W.P. Liao A luminescent 2D Tb-calixarene aggregate: synthesis, structure and CH_4 separation from C_3H_8 and C_2H_2, J. Mol. Struct. 1293 (2023) 136226 10.1016/j.molstruc.2023.136226